Parallel and miniaturised Analysis
of
Protein-Protein Interactions in T-Cell Signal Transduction
by
Fluorescence Cross-Correlation Spectroscopy
and
Peptide Microarrays

Parallele und miniaturisierte Analyse von
Protein-Protein-Interaktionen in der T-Zell-Signaltransduktion
mittels Fluoreszenz-Kreuzkorrelations-Spektroskopie
und Peptidmikroarrays

DISSERTATION

der Fakultät für Chemie und Pharmazie
der Eberhard-Karls-Universität Tübingen
zur Erlangung des Grades eines Doktors
der Naturwissenschaften

2006

vorgelegt von

ODA STOEVESANDT

für meine Eltern!

Abbreviations

For some of the proteins, the origin of the abbreviation could not be deduced. In these cases, or if the full designation held little information on the function of the protein, some additional information is given.

cCBL	casitas B-lineage lymphoma proto-oncogene, E3 ubiquitin-protein ligase
CD28	T-cell-specific surface glycoprotein CD28
CD3ε	T-cell surface glycoprotein CD3ε-chain
CD3ζ	T-cell surface glycoprotein CD3ζ-chain
CFP	cyan fluorescent protein
CSK	cSRK kinase
FCCS	fluorescence cross-correlation spectroscopy
FCS	fluorescence correlation spectroscopy
FYB	FYN-binding protein; synonym: SLAP, SLP76 associated phosphoprotein
FYN	proto-oncogene tyrosine-protein kinase
GAB2	GRB2-associated binding protein 2
GADS	GRB2-related adapter protein downstream of SHC
GEM	glycosphingolipid-enriched membrane microdomain
GFP	green fluorescent protein
GRB2	growth factor receptor bound protein
ITAM	immunoreceptor tyrosine-based activation motif
ITK	synonym: TSK, T-cell-specific kinase
LAT	linker for activation of T-cells
LCK	lymphocyte cell-specific protein-tyrosine kinase
MHC	major histocompatibility complex
NCK	SH2/SH3 adapter protein
PAG	phosphoprotein associated with GEMs
PAK1	p21-activated kinase1, serine/threonine-protein kinase
PI3K p85	phosphatidyl inositol 3-kinase, regulatory subunit of 85 kDa
PLCγ1	phospolipase C gamma 1, 1-phosphatidylinositol-4,5-bisphosphate phosphodiesterase gamma 1
PSF	point spread function
PTB	phosphotyrosine-binding domain
polyP	proline-rich sequence motif
PV	pervanadate
pY	phosphotyrosyl residue

SH2	SRC-homology domain 2
SH3	SRC-homology domain 3
SHPTP2	SH domain containing protein tyrosine phosphatase 2
SLP76	SH2 domain containing leukocyte phosphoprotein of 76 kDa
SOS	son-of-sevenless, guanine-nucleotide excange factor for Ras in T-cells
VAV	guanine-nucleotide excange factor for Rho and adapter protein, named after the sixth letter of the Hebrew alphabet
WASP	Wiscott Aldrich syndrome protein
WH	WASP-homology domain
WIP	WASP-interacting protein
YFP	yellow fluorescent protein
ZAP70	zeta-associated protein-tyrosine kinase of 70 kDa

Danksagung

VI

1 Introduction

Cells are crowded with biomolecules [1] and physical interactions of these molecules constitute the basis of all life processes. Through genome sequencing and proteome analysis, comprehensive lists of all the molecular players involved in cellular processes are within reach, and one next pending task is to understand their functions and unravel their physical and functional interactions. It has been estimated from known structural and interaction data, that the total number of protein fold types is about 1000 [2] and the number of interaction types occurring between those folds in protein-protein-interaction networks is about 10000 [3]. The emerging field of proteome-wide analysis of interactions focuses on the question which protein-protein interactions are possible in principle [4], and on the generation of extensive interaction maps by techniques such as two-hybrid screens [5,6].

On a smaller, yet more immediately function-related scale, a question is, which interactions actually take place in the context of a specific cellular process. Systems biology investigates the behaviour and relationships of all of the elements in a particular biological system. The aim is to build a descriptive, and ultimatily predictive, computational model of the system that can be used to gain an in-depth understanding of perturbations (e.g. through protein malfunction, or pharmacological inhibitors) in the system.

Cellular signal transduction proceeds through cascades of enzymatic reactions and the formation and dissipation of molecular complexes. While the enzymatic reactions involved have been a subject of intense biochemical research for decades, our understanding of the composition and function of protein complexes is still less complete [7]. Traditionally, protein-protein interactions are investigated on a one-by-one basis through co-purification approaches like co-immunoprecipition, yielding detailed information on the occurrence of single interactions. One of their assets is, that, given good affinity reagents for co-purification, these methods collect information from an unmodified system – introduction of exogenous proteins with detection tags (e.g. tandem affinity purification tags [8]) is not necessary. However, they are blind for the surrounding interaction network in which the interaction under scrutiny is embedded. From a systems biological point of view, the reliance on endogenous proteins is desirable, but the size of data sets typically generated in classical co-purification is too small. Methods for the parallel analysis of molecular complexes are therefore a key to further our understanding of cellular signalling.

The aim of my thesis was to develop methods for the parallel analysis of complexes of endogenous proteins, and to employ them in the context of T-cell signal transduction.

2   Background

2.1   Signal transduction in T-lymphocytes

A common feature in the organisation and regulation of intracellular processes is the use of protein interaction domains. These functional modules direct the association of proteins with one another, and with non-proteinaceous cellular elements, such as phospholipids or nucleic acids. Notably, many of the domains mediate interactions with short, linear peptide motifs [9], which tend to reside in natively disordered protein regions [10]. For some of the domain classes, systematic screens have delineated preferred binding motifs and binding partners present in the cell, for example for SH3 domains[11], WW domains[12] and PDZ domains [13]. It is likely, that analysis of data sets from large-scale interaction screens will uncover more, maybe less widespread, short linear interaction motifs[14]. Domain-mediated interaction networks likely evolved through partial duplication and subsequent specialisation of modules, giving rise to structurally similar, but functionally different proteins and protein complexes [15].

The signal transduction cascade leading to T-cell activation is to a large extent triggered by protein-tyrosine kinases (PTKs). The molecular adapters recognising tyrosine phosphorylations (pY) are SRC-homology 2 domains (SH2) and phosphotyrosine-binding domains (PTB). Additionally to the inducible pY-dependent interactions, associations between SRC-homology 3 domains (SH3) and proline-rich (polyP) motifs stabilise complexes of signalling proteins. Both types of domains figure prominently in many proteins of the upstream signal transduction network in T-cells [16]. Figure 1 provides an overview the domain structure of some of the principal players involved.

2.1.1   SH2 and SH3 domains

SRC-homology domains were first described as sequences homologous to regions in the non-catalytic part of the cytoplasmic protein tyrosine kinase SRC [17,18].

SH2 domains comprise about 100 aminoacyl residues, folded into a conserved 3D structure consisting of two α-helices and six or seven β-strands in a continuous β-meander, forming the core of the domain [19]. SH2 domains bind to phosphotyrosyl residues in certain sequence contexts, thereby introducing switchable interactions in protein-kinase signalling networks. 325 human SH2 domains are catalogued in the InterPro database (www.ebi.ac.uk/interpro). Depending on their preferred consensus binding motif, usually determined by only few residues C-terminal with respect to the pY (positions +1, +2 and +3) SH2 domains are grouped into various classes (Table 1).

Table 1: *Various classes of SH2 and SH3 domain interacting motifs (according to www.elm.eu.org [20]). The IUPAC one letter code for amino acids is used. "." allows any aminoacyl residue in the position, [XYZ] bracketed allows any of the listed aminoacyl residues in the position.*

motif type	consensus	motif occurs for example in
GRB2-like SH2	pY . [EN]	LAT (pY191)
SHPTP2-, PLCγ1-like SH2	pY [IV] . [VILP]	LAT (pY132)
SRC-like SH2	pY E E I	FYN, SRC
tandem SH2, ITAM	[DE] . . pY . . [LI] . 6-12 pY . . [LI]	CD3ζ, CD3ε
Class I SH3	[RKY] . . P . . P	PI3Kp85α,
Class II SH3	P . . P . [KR]	PI3Kp85α, SOS1
Non-canonical Class I SH3	. . . [PV] . . P	
Non-canonical Class II SH3	K P . . [QK] . . .	SRC

Phosphopeptides of optimal sequence bind to SH2 domains with dissociation constants of ~50-500 nM. The interaction between SH2 domains and their substrates is additionally cooperatively stabilised by contacts with other surface regions of the protein surface. Some proteins contain two adjoining SH2 domains (a "tandem"-SH2 domain; e.g. present in ZAP70, SYK, PI3K-p85α, and SHPTP2; Figure 1), and bind to motifs containing two pY residues. While single SH2 domains usually display a preference of 20- to 50-fold for their biologically relevant ligand motifs over alternative motifs, tandem-SH2 domains benefit of an avidity effect and have 1000-10000 fold increased affinity towards their natural ligands [21] compared to single SH2 domains.

SH3 domains are small modules of about 50 – 60 aminoacyl residues in length. Their characteristic domain fold consists of five to six β-strands, forming two anti-parallel β-sheets. The linker regions in between the β-strands may contain short helical regions. 635 human SH3 domains are catalogued in the InterPro database. SH3 domains bind to polyP sequence motifs that form a left-handed polyproline type II helix. Both ligand orientations with respect to the SH3 domain are possible, depending on the position of the positive residue in the polyP motif [22] (canonical class I and II SH3 motifs, Table 1). Additionally, non-canonical SH3-binding motifs exist. A non-P residue, often R, can form part of the binding core by contacting the SH3 domain. Dissociation constants are usually in the micromolar range. The binding affinity and specificity can be increased by interactions involving loops on the SH3 domain. Additionally, methylation of arginine residues adjacent to polyP motifs has been described as a regulatory mechanism for SH3 domain binding [23].

2.1.2   Upstream events and molecular players in T-cell signalling

T-cells can be activated by binding of T-cell receptor (TCR)/CD3-complexes to agonistic MHC-peptide complexes on antigen-presenting cells (APC). In addition to the contact between TCR/CD3 and MHC/peptide, accessory membrane molecules on T-cells and APCs interact, stabilise the cell-cell contact and provide additional stimuli for cellular signalling. Prominent among these is the co-stimulus provided by the T-cell surface glycoprotein CD28 and its ligands on APCs, CD80 and CD86 (also known as B7.1 and B7.2). The events initiated by interaction of TCR/CD3 and CD28 with their APC ligands involve overlapping sets of signalling molecules [24].

The **TCR/CD3** complex comprises the clonotypic TCR α and β chains which contact the MHC/peptide complex and the invariant CD3 γ, ε, δ and ζ chains . The highly diverse sequence and binding specificity of the α and β chains arise through combinatorial genetic rearrangement, with some junctional flexibility and possible addition of nucleotides to the rearranged sequence. The CD3 chains, typically occurring in dimers of γε, εδ and ζζ, contain tyrosine-phosphorylation sites in their intracellular portion. The critical tyrosines are found in consensus motifs of 20 – 25 aminoacyl residues, so called immunoreceptor tyrosine-based activatory motifs (ITAMs, Table 1, p.3).

The CD3-**ITAM**s are the starting point of a cascade of tyrosine-phoshorylations, induced protein interactions and further activation of kinases and other enzymes generating second messengers. In resting cells, protein tyrosine phosphatases (PTPases) have a capacity several orders of magnitude higher than that of protein tyrosine kinases (PTKs), holding activation through phosphorylation at bay [25]. TCR-engagement by MHC-peptide complex shifts the equilibrium between PTK and PTPase activities through several mechanisms.

The TCR-CD3 complex is accompanied by either CD4 or CD8 co-receptors recognising membrane-proximal regions of the class II or class I MHC molecules, respectively. The cytoplasmic portion of CD4 or CD8 interacts with the SRC-family kinase **LCK** (lymphocyte cell-specific protein-tyrosine kinase) [26] via short motifs containing two cysteines [27]. LCK is acylated and partitions to glycosphingolipid-enriched membrane microdomains (GEMs). Upon TCR engament, LCK is brought into proximity of CD3 subunits and phosphorylates their ITAMs [28]. LCK itself is subject to regulatory phosphorylation events. CD45 is a transmembrane PTPase with an overall deactivating effect on LCK through dephosphorylation of pY394 (although CD45 also dephosphorylates the inhibitory pY505) [29]. The extracellular domain of CD45 is bulky enough to exclude the enzyme from regions of tight T-cell APC contact, thus relieving LCK-inhibition through spatial segregation [30]. In resting cells, LCK-activity is additionally downregulated by phosphorylation of Y505 through CSK [31]. CSK binds the lipid-raft residing, constitutively tyrosine-phosphorylated transmembrane adapter PAG

(phosphoprotein associated with GEM) [32]. Upon TCR-engagement, PAG is dephosphorylated, CSK dissociates from PAG and ceases to inhibit LCK.

One further substrate of LCK is the SYK-family PTK **ZAP70** (ζ-associated protein of 70 kDa). ZAP70 contains two SH2 domains in tandem and is named for its capacity to bind to ITAMs of the CD3 complex phosphorylated by LCK. Most notably CD3ζ ITAM 1 [33], but also CD3ε [34] are bound by ZAP70. *In vitro* affinities for binding of ZAP-70 to bisphosphorylated CD3-ITAM peptides are in the lower nanomolar range [21]. After recruitment to phospho-CD3, ZAP70 is activated through phosphorylation of Y492 and Y493 in the kinase activation loop by LCK [35] and autophosphorylation [36]. Phosphorylated Y319 of ZAP70 interacts with the SH2 domain of LCK, contributing to LCK-dependent activation of ZAP70 [37]. In contrast, phosphorylation of ZAP70 on Y292 has a negative regulatory effect by forming a site for recruitment of the E3-ubiquitin ligase **CBL** (casitas B-lineage lymphoma proto-oncogene) via its PTB domain [38,39]. The PTB domain is composed of different subdomains comprising a calcium-binding EF hand and a divergent SH2 domain [40]. In this case, ZAP70 acts as an adapter between CD3ζ and the negative regulator CBL, promoting the ubiquitinylation of CD3ζ [41] and termination of TCR-signalling.

ZAP70 itself is a PTK and phosphorylates several adapter molecules playing critical roles in T-cell signalling, among them the transmembrane protein **LAT** (linker for activation of T-cells) [42] and the cytoplasmic adapter protein SLP76 (SH2 domain containing leukocyte phosphoprotein of 76) [43].

LAT is a palmitoylated transmembrane protein, localised preferentially in GEMs [44], and therefore in proximity to the TCR/CD3 complex. Upon TCR engagement, LAT is phosphorylated by ZAP70 on several Y residues, among them Y132, 191 and 226, within less than a minute [45]. The resulting pY motifs represent different classes of SH2-binding motifs (Table 1, p. 3) and recruit various SH2 domain containing proteins. Prominent among them are the phospholipase Cγ1 (PLCγ1) associating with LATpY132 and the adapter proteins GADS or GRB associating with LATpY191 [46,47].

GADS (Grb2-related adapter downstream of Shc) is an SH3-SH2-SH3 adapter protein. The c-terminal SH3 domain of GADS associates constitutively with a polyP motif in SLP76 [48]. Phosphorylation-dependent recruitment of GADS to LAT therefore gives rise to a tetrameric complex of PLCγ1, LAT, GADS and SLP, which is additionally stabilised by interaction between the SH3 domain of PLCγ1 with a further polyP motif in SLP76 [49]. Together, these proteins form the core of the so-called "LAT-signalosome" which acts as a scaffold for the association of further proteins, such as VAV and ITK [50,51].

The SH3-SH2-SH3 adapter protein **GRB2** (growth factor receptor bound protein) interacts via both of its SH3 domains with the Ras guanine nucleotide excange factor SOS [52]. GRB2 additionally associates via its SH2 domain with another adapter, SHC, which in turn binds to phosphorylated ITAMs of CD3, thus leading to Ras-activation [53].
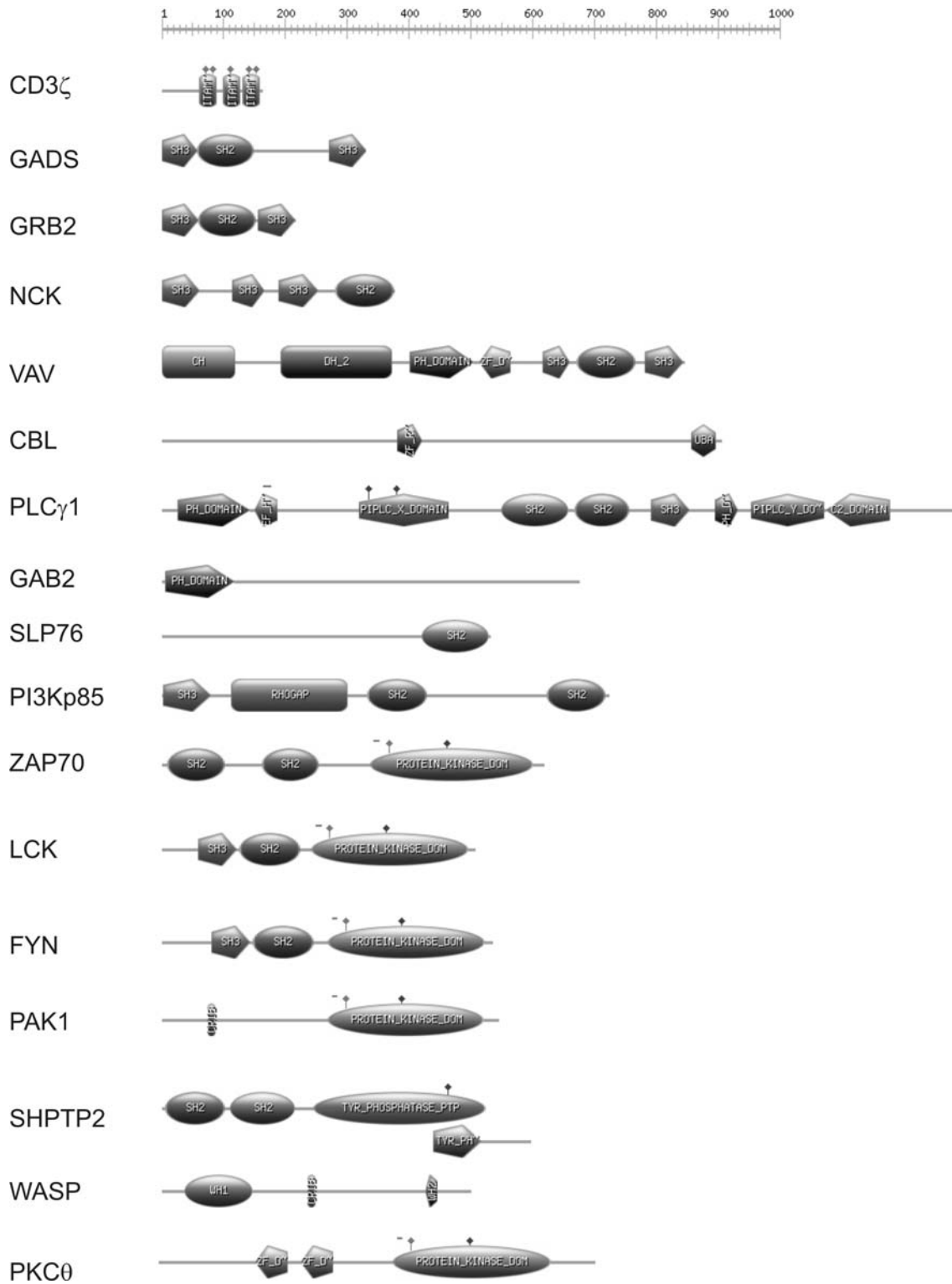
Figure 1: *The domain structure of some proteins involved in T-cell signal transduction. Domain schemes are adapted from ProSite (54), based on the information provided in the Swiss-Prot database (55). SH2 and SH3 domains figure prominently. The ruler is scaled in amino-acyl residues.*

Association of **PLCγ1** with LAT increases the concentration of PLCγ1 in the vicinity of its substrate, the membrane lipid phosphatidylinositol-4, 5-bisphosphate (PIP2). PLCγ1 is activated by phosphorylation of Y783, presumably through ITK, a PTK of the TEC family [45]. Moreover, PLCγ1 contains a calcium-binding EF-hand domain, involving calcium in the regulation of the activity of PLCγ1. Active PLCγ1 hydrolyses PIP2, generating the second messenger molecules inositol-1,4,5-trisphosphate (IP3) and diacylglycerol (DAG).

IP3 increases the cytoplasmic Ca^{2+} concentration by acting on ion channels in the ER and the plasma membrane. The increased Ca^{2+}-level activates, among other proteins, protein kinase C θ (**PKCθ**). PKC θ is additionally recruited to the plasma membrane by interaction of its Zinc-finger domains with DAG, and is both bound and phosphorylated by LCK [56]. RasGRP, another Ras guanine nucleotide excange factor, also interacts with DAG in the membrane, and is presumably phosphorylated by PKCθ [57]. In mature T-cells, PKCθ is essential for the NFkB-dependent induction of IL2-expression upon TCR-crosslinking [58].

SLP76 is a cytoplasmic adapter protein, containing regulatory tyrosine phosphorylation sites, a polyP region (harbouring the interaction sites for the SH3 domains of GADS and PLCγ1) and a C-terminal SH2 domain. SLP76 is tyrosine-phosphorylated by ZAP70. Phopho-SLP76 interacts with NCK, an adapter protein, and VAV, a guanine-nucleotide exchange factor (GEF) for Rho-GTPases, providing a link between TCR-stimulation and reorganisaton of the actin cytoskeleton [59]. A phosphorylation-dependent trimolecular complex of SLP76, VAV and ITK has been described[50,51], which localises ITK to the LAT-signalosome. The SH2 domain of SLP76 mediates interaction with the FYN-binding potein (FYB) [60]. FYB is a cytoplasmic adapter protein, named after its capacity to bind the SRC-family protein tyrosine kinase FYN, which has been repoted to be a key regulator of the microtubule cytoskeleton in T-cells [61]. Furthermore, SLP76 phosphorylated at tyrosines 113 or 128 interacts with the SH2 domain of PI3K p85 [62].

CD28 is a disulfide-linked homodimeric single-pass transmembrane protein expressed on most peripheral T-cells, which acts costimulatory upon engagement by CD80 or CD86 on APCs. Like the TCR/CD3 complex, CD28 is not a receptor-tyrosine-kinase. Tyrosine residues in the cytoplasmic tail of CD28 are phosphorylated upon CD28 engagement, presumably by LCK [63] associating via its SH3 domain with polyP motif surrounding residues around 187-190 [64]. Conversely, CD28 has been decribed to sustain autophosphorylation and activation of LCK [65]. Additionally, PTK of the TEC-family relocate to CD28 upon CD28-crosslinking and associate via their SH3 domains with polyP motifs of CD28 [66]. Phosphorylation of tyrosine 173 of CD28 results in recruitment of SH2-containing proteins, such as PI3K [67], and the GRB2-SOS complex [68].

Phosphoinoside-3-kinases **(PI3K)** of the class IA are heterodimers of a 85kD regulatory and a 110kD catalytic subunit. The regulatory subunit contains a tandem SH2 domain, which recruits the heterodimer to tyrosine-phosphorylated membrane receptors,

such as CD28. The catalytic subunit then phosphorylates the membrane lipid phosphatidylinositol-(4,5)-bisphosphate (PIP2), generating phosphatidylinositol-(3,4,5)-trisphosphate (PIP3). PIP3 is bound by pleckstrin-homology (PH) domains of various proteins, among them TEC kinases, which have been implicated in the phosphorylation-dependent activation of PLCγ1 [69].

GAB2 is an adapter protein predominantly involved in the negative regulation of T-cell signalling [70], possessing a PH domain likely responsible for its localisation to the plasma membrane upon production of PIP3 by PI3K. Upon CD28 crosslinking, GAB2 is tyrosine phosphorylated and associates with the SH-domain containing protein tyrosine phosphatase 2 (SHPTP2) [71]. Via an atypical SH3 binding motif, GAB2 can bind to SH3 domains of GADS or GRB2 [72] and thus mediate the dephosphorylation and inactivation of molecules in the LAT-signalosome by SHPTP2 [70].

2.2   Fluorescence and confocal fluorescence detection

2.2.1   Fluorescence

Luminescence is the emission of light by a molecule relaxing from an electronically excited state. In photoluminescence, the molecule has reached the excited state by absorption of a photon. In fluorescence, photon emission takes place between electronic states of the same spin state (e.g. S_1 to S_0). Such transitions occur with typical lifetimes of the excited state of 10^{-8} s [73]. In phosphorescence, photon emission occurs between electronic states of the opposite spin state (e.g. T_1 to S_0). As these transitions are disfavoured by quantum mechanical rules, they occur with a low likelihood and the lifetime of the excited state in phosphorescence is considerably longer than in fluorescence (10^{-3}s up to s) [73]. Both processes have in common, that the wavelength of the emitted photon is longer than the wavelength of the originally absorbed photon. This is due to nonradiative dissipation of some part of the energy of the excited state, usually through collisions with neighbouring molecules. Other processes of nonradiative energy transfer are intersystem crossing, by which triplet states are reached, and internal conversions, in which a vibrational state from an electronically excited state couples with a vibrational state of a lower electronic state [74]. The red-shift of fluorescence emission relative to the excitation is the basis of fluorescence detection. By using appropriate filters, scattered or reflected excitation light is blocked before the respective detector is reached, and only light emitted by fuorescence is allowed to pass.

Numerous fluorophores are employed as probes in the molecular and cellular life sciences. The increasing use of lasers for fluorescence excitation (as in laser scanning

microscopes, microarray scanners and flow cytometres) constitutes a preference for fluorophores with excitation near 488 nm (Argon-laser; e.g. fluorescein), 543 nm (Helium-Neon-laser; e.g. rhodamin, Cy3) and 633 nm (Helium-Neon-laser; e.g. Cy5). Some fluorophores (e.g. propidium iodide) intercalate directly with DNA and are used as nuclear trackers or viability markers. However, most fluorophores are covalently attached to biomolecules of choice by employing a reactive derivative of the fluorophore (e.g. fluorescein isothiocyanate, N-hydroxysuccinimide esters).

Over the last decade, fluorescent proteins have become an indispensable tool for cell biological analysis [75]. Most fluorescent proteins in use today are derivatives of the green fluorescent protein (GFP) of the jellyfish *Aequorea Victoria*. This original GFP has been adapted to laboratory requirements by introducing numerous mutations, conferring enhanced and faster folding, increased pH and ion tolerance, and, not least, different spectral characteristics [76,77]. The spectral range of available fluorescent proteins has been further expanded to long wavelengths by proteins of the DsRed-family, derived originally from corals of the species *Discosoma* [78].

2.2.2 Confocal fluorescence detection

The beampath of a widefield epifluorescence microscope is largely analogous to the beampath of a classical light microscope. Mercury lamps are usually employed for excitation of fluorescence, as their spectrum covers the near UV range as well as the visible range of the electromagnetic spectrum. In contrast to transmission illumination in classical light microscopy using a condensor, the excitation light in epifluorescence is introduced through the objective, which simultaneously collects the fluorescence light emanating from the sample. Filter sets comprising an excitation filter, a dichroic mirror and an emission filter are used. All fluorophores within the field of vision of the objective contribute simultaneously to the fluorescent image of the microscopic specimen, which can be viewed through the eyepieces of the microscope. Nowadays, the image is usually detected by the light-sensitive chip of a CCD camera.

This optical setup conserves one of the disadvantages of classical light microscopy: In addition to light from the focal plane, out-of-focus information reaches the detector. This disadvantage is circumvented by confocal optics (Figure 2). The decisive difference in the beampath of a confocal microscope is a pinhole placed in a plane confocal to the object plane. The pinhole aperture allows only light from the optically conjugated point on the object plane to pass through and reach the detector. A laser focussed through the objective to a diffraction limited point is used for excitation. Fluorescence originating from fluorophores in the illuminated cones of the focussed laser, but outside of the focal plane, is to a large extent blocked by the pinhole. However, confocal detection comes at the price of analysing only the fluorescence within the confocal volume element; i.e. one pixel at a

time, instead of a whole image. Therefore, confocal images are generated by scanning the focal plane in a pixel by pixel fashion. In confocal laser scanning microscopes, this is accomplished by a set of mirrors deflecting the laser beam in x and y direction. In confocal microarray scanners, different modi of x-y-scanning are used, either the optics move in one dimension, while the slide is moved in the other, or the slide is moved in both dimensions relative to the fixed optics.

The diameter of the pinhole aperture determines the degree of confocality of the acquired images. In the ideal case, the pinhole is limited to a point, and detection is limited to one point in the confocal plane. The image of an ideal point is described by the point spread function (PSF), which relates the point to the intensity distribution in the image space. The total PSF of ideal confocal laser optics is a convolution of the illumination PSF and the detection PSF. In reality, the pinhole is opened to the diameter of the first maximum of the PSF in the xy-plane (Airy disk)[79].
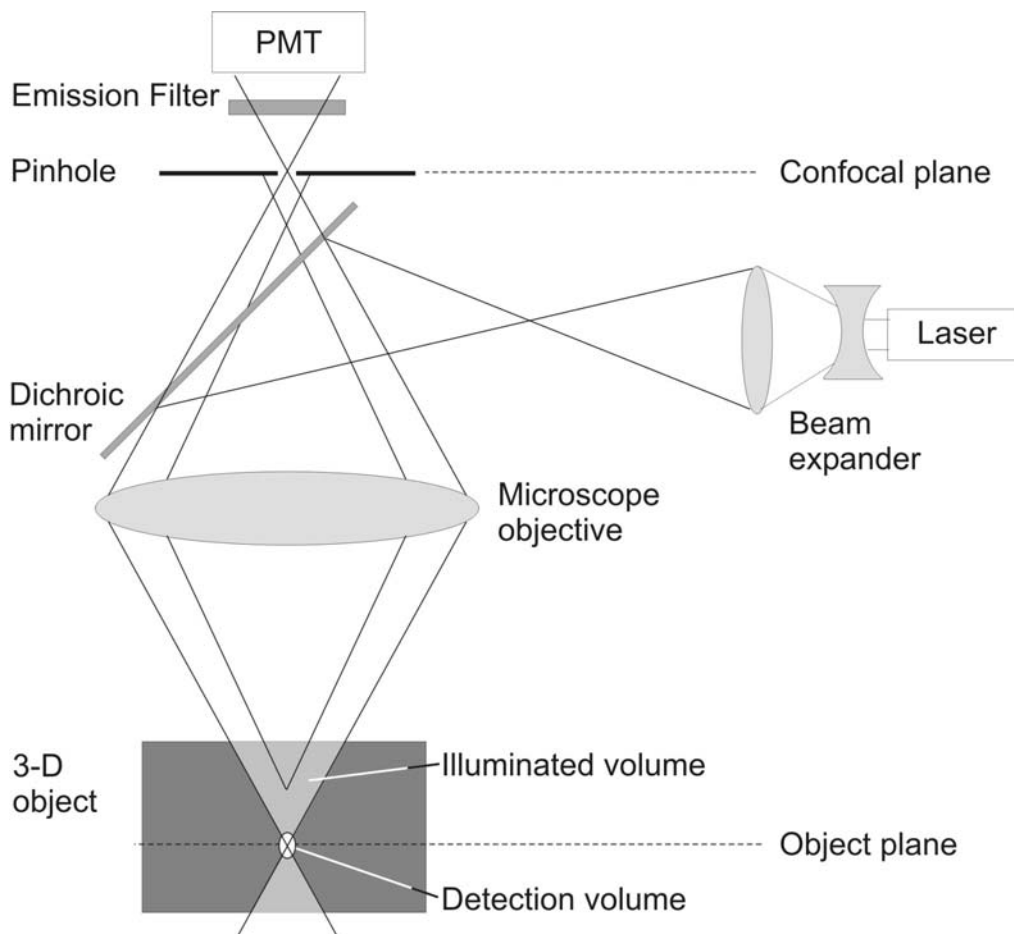
Figure 2: *Principle of confocal fluorescence detection (modified from [79])*

2.3 Fluorescence correlation and cross correlation spectroscopy

2.3.1 Basics of fluorescence auto- and cross-correlation spectroscopy

Autocorrelation is the comparison of a series of values with itself, usually in the time- or space-domain. In Fluorescence Correlation Spectroscopy (FCS), the temporal fluorescence fluctuations detected from fluorophores moving through a laser illuminated confocal detection volume [80] are analyzed for their self-similarity after the lag time τ. Analysis of the autocorrelation curve then uncovers time constants of processes underlying the fluorescence fluctuation and average numbers of molecules in the detection volume. In order to enable correlation analysis of the fluorescence fluctuations, concentrations of labelled probe molecules should ideally be in the range of 10 nM. At too high concentrations (> 500 nM), fluctuation amplitudes are too low to be discriminated from noise. FCS requires only microliter amounts of sample. Automated, serial measurements of samples in multiwell plates are easily accomplished. Per well, fluorescence fluctuations are sampled for seconds up to minutes. An overview of FCS is given by Figure 3.

The autocorrelation function $G(\tau)$ of the fluorescence fluctuation $F(t)$ is:

$$G(\tau) = 1 + \frac{\langle \delta F(t) \rangle \cdot \langle \delta F(t + \tau) \rangle}{\langle F(t) \rangle^2} \qquad \text{Eq. 1}$$

$\delta F(t)$ is the difference of the fluctuation and its temporal mean:

$$\delta F(t) = F(t) - \langle F \rangle \qquad \text{Eq. 2}$$

With the mean fluorescence intensity over the measurement time t_m:

$$\langle F \rangle = \frac{1}{t_m} \int_0^{t_m} F(t)dt \qquad \text{Eq. 3}$$

In order to interpret the autocorrelation function $G(\tau)$ calculated from the fluorescence fluctuation signal, a mathematical model of $\delta F(t)$ is used. This model comprises both the optical characteristics of the confocal illumination and detection system and the molecular basis of the fluorescence fluctuation:
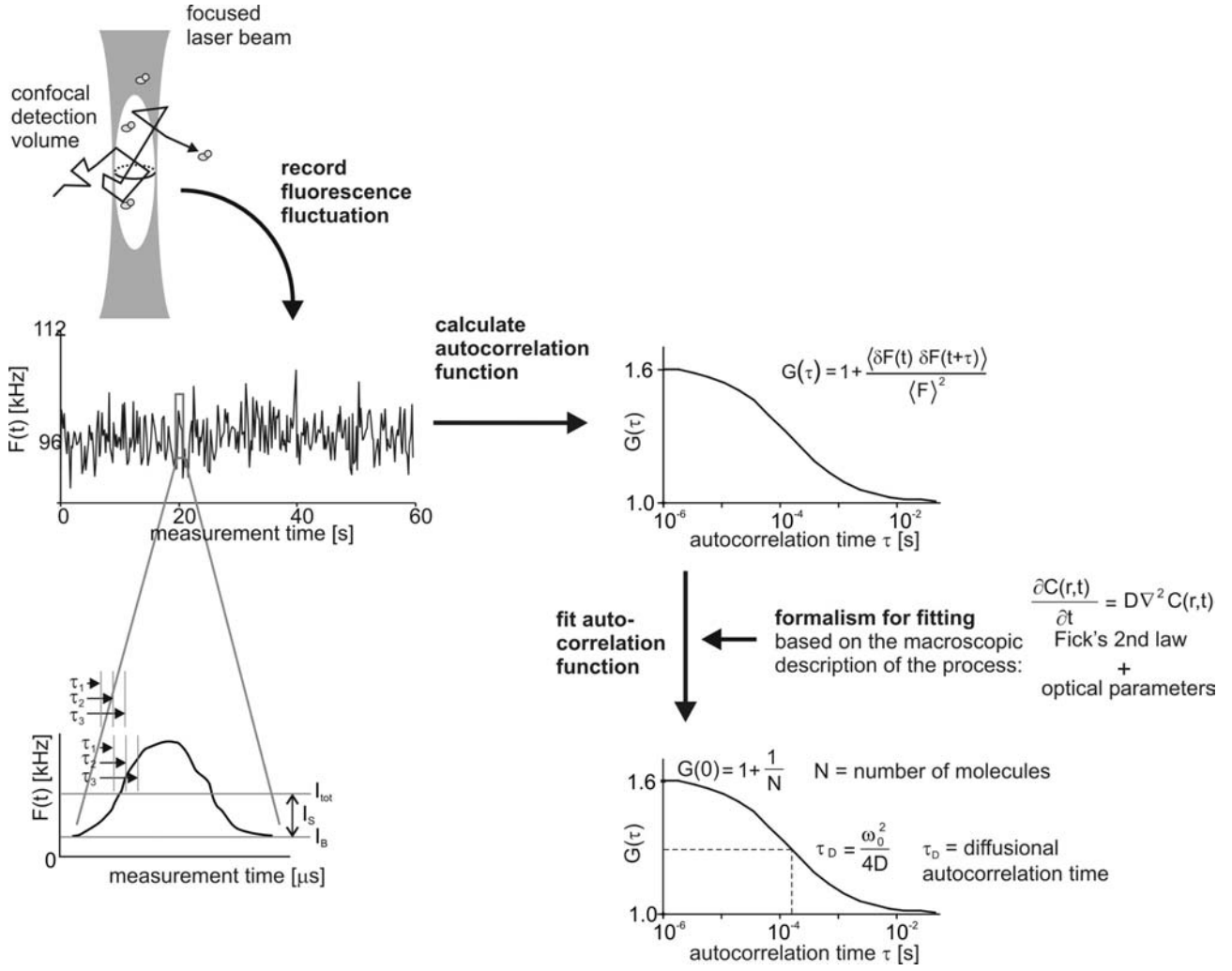
Figure 3: *Schematic overview of the principle of fluorescence correlation spectroscopy (FCS) measurement (from [81])*

$$\delta F(t) = \kappa \int_V I_{ex}(\underline{r}) \cdot S(\underline{r}) \cdot \delta(\sigma \cdot q \cdot c(\underline{r}, t))$$

Eq. 4

In Eq. 4, κ is the overall detection efficiency of the instrument, $I_{ex}(r)$ is the spatial distribution of the excitation light with I_0 as maximum, $S(r)$ is the collection intensity function describing the spatial detection efficiency of the pinhole-objective combination used, and $\delta(\sigma q c(r,t)$ describes the dynamics of the fluorophore on the single-particle level in terms of fluctuations in the molecular absorption cross-section σ, the quantum yield q, and the local particle concentration $c(r,t)$ [82].

The confocal detection volume V_{det} is not sharply limited, but rather its profile corresponds to the convolution $(I_{ex}(r)/I_0) * S(r)$. In an approximation, the confocal V_{det} can be described by Gaussian distributions both in the axial and lateral dimension[80]:

$$V_{det} = e^{-2\frac{x^2+y^2}{\omega_{xy}^2}} \cdot e^{-\frac{x^2}{\omega_z^2}}$$

Eq. 5

For practical reasons, the 3-dimensional exponential decay given by Eq. 5 is replaced by an effective detection volume V_{eff} enclosed by the isocontours of e^{-2}-fold detection efficiency relative to the centre of the distribution[83]:

$$V_{eff} = \pi^{3/2} \omega_{xy}^3 S$$

Eq. 6

S denotes the instrument-specific structure parameter:

$$S = \frac{\omega_z}{\omega_{xy}}$$

Eq. 7

where ω_z and ω_{xy} are the radii of the detection volume along the optical axis and in the optical plane, defined by the isocontour of e^{-2} detection efficiency relative to the center of the confocal detection volume.

Fluctuations in the local concentration of excitable fluorophore C(r,t) (Eq. 4) may be due to various processes, from 3-dimensional Brownian diffusion in solutions to directed transport phenomena in cells. Additionally, transitions into 'dark states' of the fluorophores, e.g. by intersystem crossings or protonation have to be taken into account. In all systems analyzed in this thesis, unobstructed translational diffusion was assumed, according to Fick's second law:

$$\frac{\partial C(x,t)}{\partial t} = D\frac{\partial^2 C(x,t)}{\partial x^2}$$

Eq. 8

D is the diffusion coefficient, usually expressed in the unit $cm^2\ s^{-1}$.

Implementing diffusion and transient dark states, the normalised fluorescence autocorrelation function reads:

$$G(\tau) = 1 + \frac{1}{V_{eff} \cdot \langle C \rangle} \cdot \frac{1}{1+\left(\tau/\tau_D\right)} \cdot \frac{1}{\sqrt{1+\tau/S^2 \cdot \tau_D}} \cdot \left(1 + \frac{T}{1-T} \cdot e^{-\frac{\tau}{\tau_T}}\right) \cdot \left(1 + \frac{R}{1-R} \cdot e^{-\frac{\tau}{\tau_R}}\right)$$

Eq. 9

τ_D is the mean dwelling time of a molecule crossing the confocal observation volume by lateral diffusion. T and R are the fractions of molecules in a dark state due to triplet

transition or a first-order reaction (e.g. protonation, as occurs for YFP[84]). Correspondingly, τ_T and τ_R are the decay times of such dark states.

The relationship between D and τ_D is [85]:

$$D = \frac{\omega_{xy}^2}{4\tau_D} \qquad \text{Eq. 10}$$

The term $V_{eff} \cdot \langle C \rangle$ in Eq. 9 corresponds to the mean particle number N in the detection volume. Thus, the autocorrelation amplitude $G_0(\tau=0)$ is inversely related to the concentration of diffusing fluorophores in the sample (Figure 3). If a calibration substance with a known diffusion coefficient D_{cal} is used, the size of V_{eff} and hence the concentration of fluorophore-labelled particles can be calculated from Eq. 6, Eq. 10 and the measured lateral diffusion time τ_{Dcal} of the calibrant:

$$c = \frac{N}{N_A\ V_{eff}} = \frac{N}{N_A\ \pi^{3/2}\ \omega_{xy}^3\ S} = \frac{N}{N_A\ S\ (4\ \pi\ D_{cal}\ \tau_{D,cal})^{3/2}} \qquad \text{Eq. 11}$$

Examples for diffusion coefficients of fluorophores often used for calibration are $2.8 *10^{-6}$ $cm^2\ s^{-1}$ for rhodamine-6-g, $3.16 *10^{-6}\ cm^2\ s^{-1}$ for Cy-5 [86]. The elegance of this approach is, that no external concentration standard, established by another method, is needed to determine concentrations by FCS. Of course, it is also possible to determine the particle number N for a calibrant of known concentration, and calculate concentrations of fluorescent analytes accordingly form their particle numbers.

The relation of the diffusion coefficient D to the hydrodynamic radius of the diffusing particles is described by the Stokes-Einstein equation:

$$r_h = \frac{kT}{6\pi\eta D} \qquad \text{Eq. 12}$$

k is the Boltzmann constant, T is the temperature, η is the viscosity of the medium. Approximate molecular weights M are calculated according to:

$$M = \tfrac{4}{3}\pi\rho N_A r_h^3 \qquad \text{Eq. 13}$$

ρ is the mean density of the diffusing particles (for globular proteins, $\rho \approx 1.2$ g cm^{-3} [87]) N_A is Avogadro's constant.

Fluorecence cross correlation spectroscopy (FCCS) is an extension of the concept of FCS (Figure 4). Typically, two superpositioned lasers are used for excitation. The fluorescence fluctuations $F_1(t)$ and $F_2(t)$ caused by the diffusion of the two spectrally

distinct fluorophores 1 and 2 through the detection volume are detected separately by two detectors with (sub)microsecond resolution. Suitable pairs of fluorophores employed in FCCS are distinguished by minimal overlap between the emission-spectrum of the shorter wavelength fluorophore and the excitation spectrum of the longer-wavelength fluorophore. This is in contrast to detection of interactions based on fluorescence resonance energy transfer (FRET), where spatial proximity of fluorophores with overlapping emission-and excitation spectra is the basis of detection[88] .

Concerted diffusion of different fluorophores due to physical linkage results in simultaneous contributions to both fluorescence fluctuations[83]. Information on the presence of such concerted fluctuations is extracted from the fluorescence signals by temporal cross-correlation analysis according to:

$$G_{12}(\tau) = 1 + \frac{\langle \delta F_1(t) \rangle \cdot \langle \delta F_2(t+\tau) \rangle}{\langle F_1(t) \rangle \cdot \langle F_2(t) \rangle} \qquad \text{Eq. 14}$$

In the ideal case of equal size and complete overlap of the detection volumes, and complete spectral separation of the signals of both fluorophores by adequate filter sets, the cross-correlation function $G_{12}(\tau)$ reads [83]:

$$G_{12}(\tau) = 1 + \frac{\langle C_{12} \rangle}{V_{eff}(\langle C_1 \rangle + \langle C_{12} \rangle) \cdot (\langle C_2 \rangle + \langle C_{12} \rangle)} \cdot \frac{1}{(1 + \frac{\tau}{\tau_D})\sqrt{1 + \frac{\tau}{S^2 \tau_D}}} \qquad \text{Eq. 15}$$

C_1 and C_2 designate concentrations of the singly labelled and C_{12} of the doubly labelled species, respectively. The temporal decay of $G_{12}(\tau)$ is governed only by the diffusion properties of the doubly labelled species. In the real case, some crosstalk of the shorter-wavelength fluorophore into the detection channel for the longer-wavelength fluorophore can not be avoided. At $\tau=0$, the amplitude of the cross-correlation function is:

$$G_{12}(0) = 1 + \frac{\langle C_{12} \rangle}{V_{eff}(\langle C_1 \rangle + \langle C_{12} \rangle) \cdot (\langle C_2 \rangle + \langle C_{12} \rangle)} \qquad \text{Eq. 16}$$

$$= 1 + \frac{1}{V_{eff}} \cdot \frac{\langle C_{12} \rangle}{\langle C_{1total} \rangle \cdot \langle C_{2total} \rangle} = 1 + \frac{N_{12}}{N_{1total} \cdot N_{2total}}$$

Parameters with index "total" designate the sum of both singly and doubly labelled species for fluorophore 1 or 2, respectively. N_{1total} and N_{2total} are derived from the autocorrelation functions acquired for both separate channels. In contrast to autocorrelation, the amplitude of the cross-correlation function is directly proportional to the fraction of doubly labelled particles (Figure 4 C).
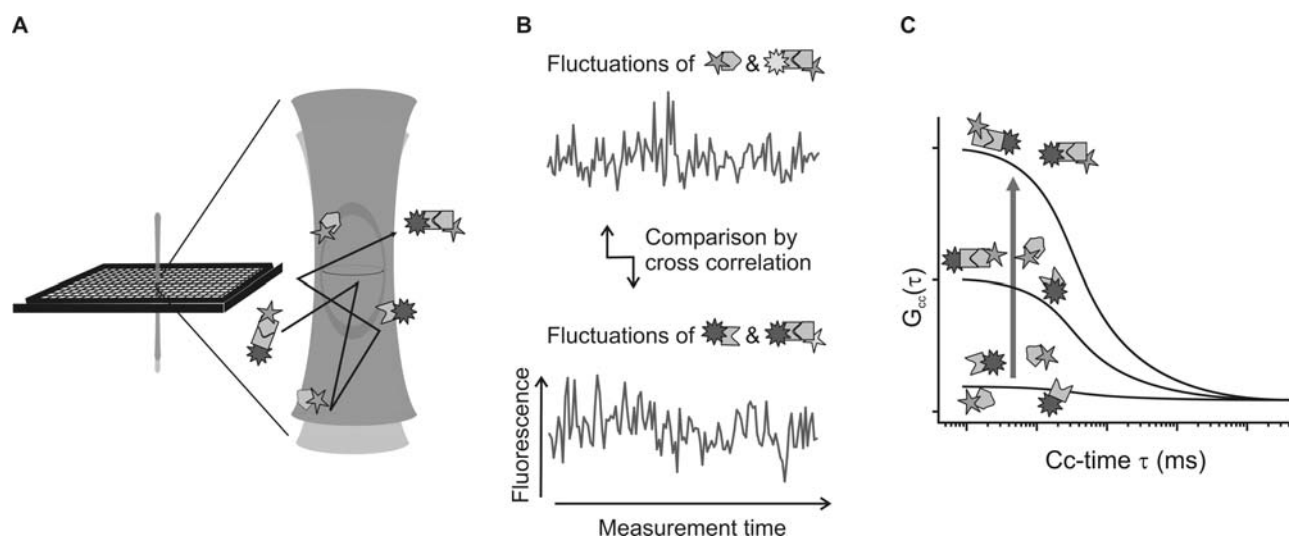
***Figure 4:** Schematic of Fluorescence Cross Correlation Spectroscopy: A) Molecules labelled with two different fluorophores diffuse through a confocal detection volume. B) The resulting fluctuations of the fluorescence of both fluorophores are detected with (sub)microsecond resolution and are cross-correlated. C) The fraction of particles carrying both fluorophores is proportional to the height of the amplitude of the cross-correlation function $G_{cc}(\tau)$.*

In the ideal case of complete overlap of equally-sized detection volumes and 100% of doubly labelled particles in the sample, the cross-correlation curve and both auto-correlation curves are identical.

Both FCS and FCCS are techniques predestined for the detection of molecular interactions. In FCS, interactions of a fluorophore-labelled molecule are detected based on the changes of its autocorrelation diffusion time τ_D due to mass gain upon binding. As diffusion coefficients are proportional to the cubic root of the molecular weight (Eq. 12 and Eq. 13), a detectable increase of the autocorrelation diffusion time requires substancial mass increase. Therefore, FCS is primarily employed to detect interactions of labelled, small ligands with much larger receptors. In this case, the binding event creates a labelled species, i.e. the ligand-receptor complex, with a much larger molecular weight compared to the ligand alone. Accordingly, FCS has for example been successfully employed in high-throughput screening of drug candidates [89]. In contrast, FCCS can be employed to monitor interactions of partners of similar molecular weight, making it an ideal technique for the detection of (bio-) macromolecular interactions. Applications include detection of nucleic acid hybridisation [90] and protein-protein interactions. However, due to the proportionality of autocorrelation amplitude and fraction of doubly-labelled particles (Eq. 16), FCCS is not suited for the detection of rare interactions.

2.3.2 Intracellular applications of FCS and FCCS

As the confocal measurement volume has approximately the size and proportions of a coliforme bacterium, FCS and FCCS measurements can be also carried out in live, eukaryotic cells. Positioning of the measurement volume in a cell is enabled by integration of the optics used for FCS and FCCS into an optical microscope, either equipped with epifluorescence detection or a confocal laser scanning microscopy module. Interpretation of the diffusional characteristics observed by intracellular FCS is complicated by the inhomogenous intracellular environment. Intracellular molecule numbers can be determined from the autocorrelation amplitude.

One basic requirement for analysis by FCS is that the fluorescent molecules cross the detection volume in a time considerably shorter than the duration of an FCS measurement. In the cytoplasm and nucleus, interactions giving rise to diffusible complexes have been monitored by FCS[91] and FCCS[92]. By contrast, membrane association of the fluorescent molecules under scrutiny can impede FCS and FCCS. Measuring the binding of fluorescently labelled small-molecule ligands to membrane-bound receptors [93,94] has been demonstrated. While recruitment of a GFP-labelled signalling protein to a receptor was obvious from an increased fraction of slowly diffusing components, the variation of diffusion constants over a wide range prohibited a more detailed analysis of the molecular state [95]. Finally, receptor clustering in membranes has been reported to immobilise proteins beyond the timescale measurable by FCS [96].

In addition, the need for fluorescent readouts imposes limitations on the application of FCS and FCCS, particularly so for the measurement in living cells. For the pairwise identification of binding partners, two specific labels conferring properties that can be monitored by FCS or FCCS are required. In most cases, interaction partners monitored by FCS-based techniques are directly covalently labelled. Protein interactions can be detected by expression of the interaction partners as fusion proteins with spectrally different fluorescent proteins [97,98,99]. Alternatively, chemically labelled fluorescent molecules have been introduced into cells by electroporation [92] or receptor-mediated endocytosis [100].

In addition to FCS and FCCS, a range of other fluorescence-based techniques has been applied to the analysis of protein complexes in living cells. These *in vivo* approaches are all based on recombinant versions of the proteins of interest, which carry tags for reporting on the interaction. In a system inspired by two-hybrid methods, these tags correspond to complementary fragments of fluorescent proteins, which on interaction of their fusion parners recombine into a fluorescent species [101,102]. Fluorescence resonance energy transfer (FRET) has been more widely used, however, this technique reports rather on the proximity of molecules than on molecular interactions [103]. For drug discovery, systems based on cellular bioluminescence resonance energy transfer (BRET) [104] have been proposed for the idenfication of compounds interfering with complex formation.

However, due to the need for recombinant reporter proteins, all these *in vivo* detection systems are restricted to the protein complexes for which they were developed, they cannot be easily generalised, and considerable efforts are required for the generation and validation of suitable fusion proteins and expression levels.

2.4 Microarrays for the parallelised analysis of proteins

2.4.1 Basic concepts and different formats of arrays

Microarrays have revolutionised the detection of biomolecules by introducing the highly parallel incubation of sample on a multitude of miniaturised probes. Microarrays typically consist of $10^2 - 10^5$ probes arranged in a regular, spatially addressable pattern on a solid two-dimensional support. Barely ten years ago a fledgling technique for nucleic acid detection [105,106,107], microarray development now rapidly moves forward to tackle questions related to the detection and analyis of proteins and their functions [108,109]. An overall aim is to better understand the expression and function of large, or eventually proteome-wide [110], sets of proteins.

Some of the methodology and technical equipment can be transferred from nucleic acid to protein microarrays. However, compared to nucleic acids, proteins are a chemically highly heterogeneous group of individuals, and their functionality often depends critically on the integrity of their structure. These properties make the use of parallel array techniques for proteins a challenge, as working conditions have to be identified that accommodate all used proteins at once.

Different array formats have been developed. A general distinction can be made beween capture arrays and reverse arrays. Capture arrays consist of immobilised binding molecules, e.g. antibodies or peptides, that pull down their protein targets from the incubation solution containing analyte. Antibody capture arrays can therefore be viewed as a miniaturised and parallelised variant of immunoaffinity purification. Reverse arrays, by contrast, are arrays of immobilised samples, e.g. patient sera or cell lysates, which are incubated with detection reagents (again, typically antibodies).

For both formats, binding of a macromolecule from the incubation solution to the binding partner on the array surface is the crucial step. It has been debated, whether microspots of molecules act as mass-sensing [111] or as concentration-sensing [112] devices for their binding partners in solution. In the first case, binding of ligand to the microspot would be dependent on the volume (and hence the total ligand mass) of the incubation solution. In the second case, known as ambient analyte theory, the assumption is that the concentration of the ligand in the incubation solution is not changed perceptibly by

binding of molecules to the microspot, and hence the incubation volume has no influence. In the framework of the ambient analyte theory, it has been shown, that mass-transport of the macromolecules in solution to the surface is the rate-limiting step in microspot immunoassays, slowing down binding reactions by several orders of magnitude compared to well-stirred bulk solutions [113].

The strategy of immobilisation of probes on the array substrate crucially influences their functionality. Chemically reactive surfaces, e.g. epoxysilane reacting with thiol- or amino-groups, may result in random orientation, and possibly partially denatured and nonfunctional proteins. Directional immobilisation via protein tags (e.g. His-tags on Ni-NTA-surfaces [110]) results in uniform orientation of the capture molecules on the array surface and is presumably better suited to preserve their structure and function. Thin polymer gels, so called hydrogels, provide an aqueous environment for deposited proteins and, due to their 3-dimensionality, allow deposition of relatively large substance amounts.

If peptides are used as capture molecules on an array, conservation of structure is less critical than for full-length proteins. Peptides can be synthesised *in situ* as microspots on glass slides using photolithographic approaches [114], or as macrospots on membranes through SPOT synthesis [115]. Alternatively, peptides synthesised by conventional solid phase chemistry can be attached to microarray substrates, e.g. through reaction of thiol- and amino-moieties with epoxy-activated glass slides.

Protein arrays are usually generated from overexpressed and purified proteins [110], often making availability of large sets of proteins a limiting bottleneck for protein array applications. Circumventing this problem, cell-free expression of proteins with tags for direct immobilisation on a tag-binding surface [116] has been employed to express and immobilise proteins *in-situ* on cDNA microarrays [117].

Detection of binding events on arrays is usually based on fluorescence. Either, analyte molecules are labelled directly with fluorophores. Amine-reactive dyes reacting via their succinimidyl ester moieties with primary amines of proteins are commonly used. Strategies analogous to the two-colour-ratio experiments with DNA-arrays exist, where proteins in two samples to be compared are directly chemically labelled with different fluorophores and then incubated on the same array [118]. The ratio of both fluorescence signals on each spot of the array corresponds to the relative amounts of the bound protein present in the samples, and taken together the the experiment allows to determine overall diffential translation profiles. Alternatively, proteins in just one sample are biotinylated, and then detected on the array by fluorescently labelled streptavidin [110]. The advantage of this strategy is that all analytes bound to the array can be detected with just one reagent. However, in both detection strategies, signals are determined by just one binding event to the capture molecule. Signals due to unspecific binding of analytes to arrayed capture molecules or crossreactivity may occurr, and cannot be easily told apart from signals of *bona fide* interaction partners.

To circumvent this problem, dual-level recognition of analytes is preferable, making erroneous identification of proteins much more unlikely. Analytes in the sample are captured by a binder immobilised on the array, and detection is based on a second recognition event by another binder. In most cases, the resulting protocol is essentially a miniaturised and multiplexed adaptation of a classical antibody sandwich assay. The first set of immobilised antibodies captures their target proteins from the analyte mixture. The antibodies in a second set (which have to recognise other epitopes) are either labelled with biotin, again allowing detection by fluorophore-labelled streptavidin, or are detected by fluorophore-labelled secondary antibodies. Although multiplexing is an attractive option for the parallel detection of multiple analytes, there is a general consensus that, due to low-level cross reactivity even of highly specific antibodies, multiplex sandwich assays are limited to the parallel detection of about 50 analytes [119].

For readout of fluorescence on arrays, both confocal and non-confocal microarray scanners are used. Special array formats also allow the coupling of excitation light into a planar waveguide, and the excitation of fluorescence by the evanescent field.

2.4.2 Brief overview of applications

Microarrays have been applied to a wide range of questions in the analysis of large protein sets.

In analogy to the applications of DNA arrays for transcriptional profiling [120], antibody arrays are used for translational profiling [121,122] of biological and clinical samples. For example, patient sera and sera of healthy control donors were directly labelled with different fluorophores and applied to antibody microarrays, in order to identify potential prostate cancer biomarkers based on their differential expression in health and disease [118].

Sandwich-assays based on antibody microarrays and a second set of detection antibodies have been used for the multiplex detection and quantitation of cytokine and chemokine levels in biological samples (reviewed in [123]).

In reverse-capture approaches, protein microarrays comprising auto-antigens for tumors or autoimmune disorders are used to screen for the presence of autoreactive antibodies [124,125,126].

A microarray comprising 80% of the proteins of the yeast proteome has been presented [110]. 5800 open reading frames were cloned, and their encoded proteins were overexpressed, purified and printed in microarray format. When the arrays were screened for binding of calmodulin and phospholipids, many hitherto unknown binding partners were identified, demonstrating the potential of protein microarrays for the analysis binary interactions in biomolecular interaction networks.

In the context of signalling-dependent changes, antibody microarrays were used to detect and quantify tyrosine kinase signalling [127]. Pan-specific capture antbodies were

used together with differentiall labelled phospho-specific and pan-specific detection antibodies.

In summary, microarrays are used to detect the presence of biomolecules, or modified biomolecules, of interest and quantify their levels. However, biological function is not only determined by the presence or absence of molecular players, but also by their interaction state. The formation of protein complexes in cellular signalling is a prominent example. Given the complexity of signalling networks, the application of methods for the parallel detection of interaction events seems evident. In this respect, microarrays provide an intriguing basis, but conceptual advances are required to turn arrays into devices for the parallel detection of signalling-dependent protein-protein interactions.

3   General Materials and Methods

3.1   Basic buffers

Phosphate-buffered saline (PBS)

   1.5 mM KH_2PO_4, 8.1 mM Na_2HPO_4, 137 mM NaCl, 2.7 mM KCl (pH 7.4)

PBS-Tween

   PBS, 0.05 % (v/v) Tween-20

HEPES buffered saline (HBS)

   10 mM HEPES, 135 mM NaCl, 5 mM KCl, 1 mM $MgCl_2$, 1.8 mM $CaCl_2$ (pH 7.4)

HBS-BSA/Glucose

   HBS, 5 mM Glucose, 0.1% (w/v) BSA

Lysis buffer

   1% Triton X100, 20 mM Tris, 1mM EDTA, 150 mM NaCl, 50 mM n-octyl β-D-glucopyranoside (Fluka, Taufkirchen, Germany) (pH 7.5). 1mM Na_3VO_4 and 1x Protease Inhibitor Cocktail (Complete Protease Inhibitor Cocktail tablets; Roche, Mannheim, Germany) were added directly before use. β-D-glucopyranoside ensures the efficient extraction of proteins residing in membrane rafts[128]. If this is not a concern, the reagent may be omitted.

Antibody dilution buffer for FCCS (AD-buffer)

   PBS, 0.1% (w/v) BSA

SDS page running buffer (5x)

   250 mM TrisHCl, 1.9 M glycin, 0.5% SDS (pH approx. 8.6, no adjustment)

Resolving gel buffer (4x)

   1.5 M Tris-HCl (pH 8.8), 4 mM EDTA

Stacking gel buffer (4x)

   0.5 M Tris-HCl (pH 6.8), 4 mM EDTA

Resolving gel mix, 12.5% acrylamide

2.1 ml ddH$_2$O, 1.55 ml 40% acrylamide/N,N´-methylene-bisacrylamide (37.5:1, BioRad), 1.25 ml resolving gel buffer (4x), 50 μl 10% (w/v) SDS, 50 μl 10% (w/v) APS, 5 μl TEMED.

Stacking gel mix, 4% acrylamide

1.6 ml ddH$_2$O, 0.25 ml 40% acrylamide/N,N´-methylene-bisacrylamide (37.5:1), 0.625 ml stacking gel buffer (4x), 25 μl 10% (w/v) SDS, 40 μl 10% (w/v) APS, 4 μl TEMED.

SDS-PAGE sample buffer (5x)

250 mM Tris-HCl (pH 6.8), 500 mM DTT, 0.5% bromephenol blue, 50% (v/v) glycerol, 10% (w/v) SDS

Blotting buffer

192 mM glycine, 25 mM Tris-HCl, 20 % (v/v) methanol (pH 8.3)

Alkaline phosphatase buffer (5x)

500 mM Tris-HCl, 500 mM NaCl, 25 mM MgCl$_2$ (pH 9.5)

Reagent for alkaline posphatase detection

90 mg/ml nitroblue tetrazolium in 70% DMF, 45 mg/ml 5-Bromo-4-chloro-3-indolyl-phosphate in ddH$_2$O; storage at -20°C°; use at 20 μl each per 5 ml 1x alkaline phosphatase buffer

Array blocking buffer

PBS with 1% (w/v) Top Block (Fluka)

Array wash buffer: PBS-Tween/BSA

PBS, 0.05% (w/v) BSA, 0.05% (v/v) Tween-20. Array wash buffer was also used for dilution of antibodies for incubation on the arrays.

3.2 Peptides

Peptides were supplied by EMC microcollections, Tübingen. All peptides contained an N-terminal cysteine residue with free amino-terminus for efficient immobilisation on epoxy-activated surfaces. Table 2 lists the peptides that were used in this work. Peptide designations are derived from the protein containing the peptide sequence; names for phospho-tyrosine (pY) peptides additionally contain the number of the pY residue within the protein (according to Swiss-Prot, www.expasy.org), names for other peptides contain the number of the first residue in the peptide.

Table 2: *Peptides used in this thesis. pY designates phosphotyrosyl residues. Peptide designations in parenthesis correspond to the name used for the peptide during synthesis and analytics.*

Peptide	Sequence	Source	Interaction Partner and binding domain
CD3zpY72/83 (KK 37)	C-AhxNQL(pY)NELNLGRREE(pY)DVL-CONH₂ [129]	CD3ζ ITAM1 69-86	ZAP70 SH2
SigpY437 (KK80)	CGEEREIQ(pY)APLSFHKG-CONH₂ [130]	Siglec-7 ITIM 430-445	SHP-1/SHP-2 SH2
LATpY132 (KK83)	CEDEDDYHNPG(pY)LVVLPDSTP-CONH₂ [46,131]	LAT-Y-132 121-141	PLCγ1 SH2
LATpY191 (KK87)	CEASLDGSRE(pY)VNVSQEL-CONH₂ [131,47]	LAT-Y-191 181-198	VAV, GADS, GRB2, PLCγ1 SH2
LATpY226 (KK89)	CEVEEEGAPD(pY)ENLQELN-CONH₂ [47,132]	LAT-Y-226 217-233	GADS, GRB2, VAV SH2
SLP228 (WH4)	CAKLPAPSIDRSTKPPLDRS-CONH₂ [133]	SLP76 228-246	GADS c-term. SH3
WIP446 (WH6)	CEDEWESRFYFHPISDLPPP-CONH₂ [134]	WIP 446-464	WASP WH1
PAG421 (WH10)	CSDLQQGRDITRL-COOH [135]	PAG 421-432	EBP-50 PDZ
ZAPpY319 (WH21)	CVYESP(pY)SDPEELKD-CONH₂ [37]	ZAP70 Y-319 314-327	LCK SH2
ZAPpY296 (WH25)	CIDTLNSDG(pY)TPEPARIT-CONH₂ [38]	ZAP70 Y-296 284-300	cCBL PTB
PAK6 (WH29)	CLDIQDKPPAPPMRNT-CONH₂ [136]	hPAK1 6-20	NCK SH3
SLP179 (OS3)	CSGKTPQQPPVPPQRPMAAL	SLP76 179-197	PLC SH3
FYB pY595 (OS4)	CEDDQEV(pY)DDVAEQD-NH2	FYB 589-602	FYN, SLP76 SH2
FYB pY625 (OS6)	CDDDI(pY)DGIEEED-NH2	FYB 621-632	FYN2 SH
FYB pY651 (OS7)	CLDMGDEV(pY)DDVDTSDF-NH2	FYB 644-659	SLP76 SH2
LCK pY505 (OS8)	CVLEDFFTATEGQ(pY)QPQP	LCK pY505	LCK SH2
SHPTP1pY564 (KK93)	CSKHKEDV(pY)ENLHTKNK-NH2	SHPTP1	LCK SH2
GAB2-509 (KK94)	CQPPPVNRNLKPDRKAKPTPLD-NH2	GAB2	GRB2 SH3
GAB2 pY614 (KK95)	CKSTGSVD(pY)LALDFQPS-NH2	GAB2 pY614	SHPTP1 SH2
CD28pY191 (KK96)	CSRLLHSD(pY)MNMTPRRP-NH2 [137]	CD28pY191	GRB2, PI3K SH2
cCBL pY699 (KK98)	CEGEEDTE(pY)MTPSSRPL-NH2 [138]	cCBL pY699	VAV SH2
PLCg pY (83KK108)	CEGRNPGF(pY)VEANPMPT-NH2	PLCγ1 pY 783	PLCγ1 SH2
PI3K84 (KK109)	CPTPKPRPPRPLPVAPGSSKT-NH2	PI3K p85α 84-104	FYN SH3
CD28 pY202 (KK114)	CTRKHYQP(pY)APPRDFAA	CD28 pY202	GRB2 SH2

3.3 Antibodies

Antibodies for detection of proteins both on microarrays and in FCS and FCCS had to recognise their target proteins in a non-denatured state. Therefore, antibodies certified for immunoprecipitation were chosen if available. For detection by secondary antibodies, pairs of primary antibodies used together in one experiment were chosen so that one antibody was from mouse and the other one from rabbit. Used primary antibodies are listed in Table 3.

Table 3*: Primary antibodies used for FCCS or mass-tag FCS (FCS) or peptide microarrays (MA).*

Target protein	Type of ab	Application	Supplier
PLCγ1	Rabbit polyclonal	FCS, MA	Santa Cruz
LAT	Mouse IgG1, clone 11B.12	FCS, MA	Upstate
SLP76	Mouse IgG2a, clone 2B2.98	FCS, MA	USBiological
GADS	Rabbit polyclonal	FCS, MA	Upstate
SHPTP2	Rabbit polyclonal	MA	Santa Cruz
CD28	Mouse IgG1, clone CD28.2		Pharmingen
cCBL	Mouse IgG1, clone 17	MA	BectonDickinson
GRB2	Rabbit polyclonal	FCS, MA	Santa Cruz
LCK	Mouse IgG2b, clone 3A5	MA	Upstate
NCK	Rabbit polyclonal	MA	US Biologicals
ZAP70	Mouse IgG2a, clone 29	FCS, MA	BectonDickinson
GAB1	Rabbit polyclonal	MA	Santa Cruz
FYB	Mouse IgG1, clone 5	MA	BectonDickinson
FYN	Mouse IgG1	MA	Santa Cruz
WASP	Mouse IgG1	MA	Santa Cruz
VAV	Rabbit polyclonal	MA	Santa Cruz
pLAT(226)	Rabbit polyclonal	MA	Upstate
PI3K	Rabbit polyclonal	MA	Transduction Labs
pPLCγ1(783)	Rabbit polyclonal	MA	Cell Signalling
CD3ε	Biotinylated hamster IgG1, clone 2C11	FCS, MA	BectonDickinson
CD3ζ	Mouse IgG1, clone 6B10.2	FCS, MA	Santa Cruz
CD3ε	hamster IgG1, clone 2C11	FCS, MA	BectonDickinson
phospoY	Mouse IgG1; # 9411	MA	Cell Signalling

Secondary reagents were Cy5-labelled streptavidin (Dianova, Hamburg), Alexa488- and Alexa633-labelled goat-anti-mouse and goat-anti-rabbit antibodies (highly cross-absorbed, Molecular Probes, Leyden, The Netherlands), Alexa647 labelled IgG2a Fab

fragments (Zenon system, Molecular Probes), Cy5-labelled goat anti-hamster antibodies (Dianova), Cy5-labelled goat anti-mouse antibodies (Dianova) and Protein G or streptavidin nanoparticles of 50nm diameter (µMACS MicroBeads, Miltenyi Biotec, Bergisch Gladbach, Germany).

3.4 Cell culture, stimulation and lysis

Human Jurkat T leukemia cells, Jurkat cells lacking PLCγ1 (J.gamma1[139], ATCC # CRL-2678) and Jurkat cells expressing kinase-dead LCK (J.CaM1.6[140], ATCC # CRL-2063, a kind gift of Claus Belka, Tübingen) were kept in RPMI supplemented with 10% fetal calf serum at 37°C and 5% CO_2.

Mouse 3A9 T-hybridoma cells and derivatives transfected with a fusion protein of ZAP70 and the yellow fluorescent protein (YFP), or both free YFP and a fusion protein of the CD3ζ-chain with cyan fluorescent protein (CFP) were cultured in DMEM supplemented with 10 % fetal calf serum, 100 µM sodium pyruvate, non-essential amino acids, and 200 µM L-glutamine. The generation of the transfected cell lines has been described elsewhere[141] .

The broad-range phosphatase inhibitor sodium pervanadate was generated in a freshly prepared mixture of equal volumes of 10 mM Na_3VO_4 and 10 mM H_2O_2 (corresponding to 1:1000 (v/v) dilution) in HBS. The solution was incubated at room temperature for 15 min and used immediately at a tenfold dilution[142]. For activation, cells suspended in HBS/BSA/Glucose were incubated with pervanadate for 20 min at 37 °C.

For TCR-mediated stimulation, 10^7 cells per ml were resuspended in ice-cold HBS/BSA/glucose containing 10 µg/ml of the anti-CD3 antibody (OKT-3, G. Jung, Institute for Immunology, University of Tübingen) or the isotype control (mouse IgG2a, Sigma) and incubated on ice for 10 min. Then, the crosslinking secondary antibody (goat anti-mouse IgG, Calbiochem), was added to a final concentration of 20 µg/ml and the samples were immediately transferred into a 37°C water bath for timespans between 2 and 30 min. Stimulation was stopped by adding an excess of ice-cold HBS and placing the samples on ice. To remove remaining unbound antibody, cells were washed with ice-cold HBS.

Cell lysates were prepared by suspension of cells in lysis buffer. For microarray experiments, routinely 2 * 10^7 cells per 1 ml of lysis buffer were used, corresponding to 10^6 cells per 50 µl lysate user for each array. For FCCS and mass-tag FCS, $10^7 – 5*10^7$ cells per 1 ml of lysis buffer were used. After lysis on ice for 30 min, the crude lysates were clarified by centrifugation at 20,000 x g for 15 min. Total protein concentration of lysates was determined by a standard protein assay (BioRad, Munich, Germany).

For competition experiments, peptides were added upon lysis to the indicated final concentrations.

3.5 Immunoprecipitation, SDS-page and western blotting

Samples for immunoprecipitation were prepared as described for mass-tag FCS (see 4.1.1), scaled up by a factor of 6.5. After centrifugation (14,000 × g, 4°C, 10 min) the pellets were washed twice with lysis buffer, and once with PBS, followed by resuspension in 1x sample buffer and heating to 95°C for 5 min.

SDS-PAGE of lysates or immunoprecipitation samples was carried out according to the procedure described by Laemmli[143]. The gel was blotted on a PVDF membrane (Millipore, Schwalbach, Germany). After blocking with 5 % nonfat dry milk powder in PBS-Tween, the blot was developed using primary and cognate alkaline phosphatase-conjugated secondary antibody (Sigma, Munich, Germany) and NBT-BCIP substrate. Western bands were quantified by scanning the blots and integrating mean signal intensity and area of the bands.

3.6 FCS of ZAP70-YFP in cell lysates

A ConfoCor2-module, coupled to an Axiovert 100 M inverted microscope stand, equipped with a C-Apochromat 40-fold water-immersion objective, NA 1.2 (Carl Zeiss, Jena, Germany) was used. YFP was excited at 514 nm by an argon ion laser and detected using an infrared-blocking 535-590 nm bandpass filter. Rhodamine-6-G was used as a calibrant for pinhole adjustment and for determination of the structure parameter S. Each lysate sample was kept on ice until measurement. 20 μl per sample were measured in a 384-well glass bottom plate (175 μm glass thickness; M-plates, cat.-no. 60200, MMI, Glattbrugg, Switzerland).

Routinely, 10 measurements of 15 s duration each were taken per sample. Autocorrelations of YFP were fitted between 10 μs and 1 s with a formalism accounting for one diffusing species and the protonation-dependent blinking of YFP [84].

$$G(\tau) = 1 + \frac{1}{N} \cdot \frac{1}{1 + \left(\tau/\tau_D\right)} \cdot \frac{1}{\sqrt{1 + \tau/S^2 \cdot \tau_D}} \cdot \left(1 + \frac{R}{1-R} \cdot e^{-\frac{\tau}{\tau_R}}\right) \qquad \text{Eq. 17}$$

This fit was carried out in the ConfoCor2 software (version 2.8), using the implemented fit function for one diffusing species and triplet transitions (comprising an exponential term analogous to that in Eq. 17). For YFP, the output triplet time constant was reinterpreted as protonation-fluctuation time constant.

ω_{xy} was determined according to Eq. 10 from the calibration measurement of rhodamine-6-G (D = 2.8 10^{-6} cm^2 s^{-1}), enabling further calculation of V$_{eff}$ (Eq. 6). With these parameters, the concentration c (Eq. 11), the diffusion coefficient D (Eq. 10), and the approximate hydrodynamic radius r$_h$ (Eq. 12) and molecular weight M (Eq. 13) of the YFP-containing species in the samples were calculated.

3.7 Cellular FCS measurements

For cellular FCS-measurements, 8-well chamber slides (NUNC, Wiesbaden, Germany) were coated for 1 hour with 100 µl poly-L-lysine solution (0.01%, MW 70-150 kDa, Sigma). Coated chambers were washed twice with HBS. 3A9 cells expressing ZAP70-YFP were suspended in HBS/BSA/Glucose at cell densities of 10^6 per ml. Optionally, pre-incubated pervanadate solution was added (see 3.4). 200 µl cell suspension were used per chamber.

Instrument settings for the ConfoCor2 were as described for the measurement in lysates (see 3.6). Additionally, the epifluorescence unit and CCD camera (SensiCam, PCO, Kehlheim, Germany) of the Axiovert 100 M microscope were used for imaging of the cells. In order to determine the position of the FCS-laser beam within the field of vision, a slide covered with a dried solution of rhodamine-6-G was focused, and subsequently submitted to bleaching by the laser. By comparison of the epifluorescent images taken of the surface before and after bleaching, the xy-position of the laser focus could be determined with an approximate lateral precision of 2 µm. For cellular measurements, cells were moved to the xy-position of the laser by the moving the microscope stage. Positioning of the laser focus along the optical axis z was performed by scanning the fluorescence count rate profile in z-direction in the ConfoCor software. Profiles displayed a distinct increase in fluorescence count rate upon entering the cell, slightly decreased count rate while traversing the nucleus, and again increased count rates before leaving the cell. 15 measurements of 10 s each were carried out per cell. The first of this measurements was routinely excluded from analysis by curve fitting, due to non-negligible photobleaching of immobile molecules.

4 Methods developed during the thesis

A considerable part of the laboratory work carried out for this thesis was the development and optimisation of methods for the detection of interactions of endogenous proteins from crude cell lysates. This chapter contains concise descriptions of these methods *per se*, in order to facilitate reproduction of experiments and avoid overfreighting of the results capters.

4.1 Protein complex detection by mass-tag FCS and FCCS

Parts of this chapter were originally written for a protocol [144] published in addition to the original paper describing this method [145].

4.1.1 Sample preparation

For the sake of general applicability, this protocol describes the detection of the interaction of protein X with protein Y. anti-X and anti-Y are the primary unlabelled antibodies, anti-anti-X and anti-anti-Y are the secondary reagents. The following options A and B for sample composition list the reagent need for per FCCS sample. For the detection of most interactions described in chapters 5.2.2 and 5.2.2.3, option A, employing two bivalent secondary antibodies, was used. Option B was used if excessive formation of immunocomplexes between one primary and the cognate secondary antibody occurred, as was the case for anti-SLP76 and goat-anti-mouse-Alexa488. In that case, the bivalent secondary reagent was replaced by Alexa647-labelled Fab fragments (Zenon, Molecular Probes/Invitrogen). Option C describes how mass-tag FCS samples probing for ZAP70-CD3ε/ζ interactions were prepared.

Antibodies were prediluted in AD-buffer. If multiple samples probing for the same interaction and hence using the same set of antibodies were prepared, master mixes were created of the pair of primary antibodies and the pair of secondary antibodies. Incorporation of matching primary and secondary antibodies into the same 'master mix' was avoided, as their still relatively high concentration might have promoted the formation of large crosslinked complexes (see troubleshooting, Table 4, p. 32).

Option A:

anti-X (25 µg/ml stock)	1.6 µl
anti-Y (25 µg/ml stock)	1.6 µl
clarified cell lysate	20 µl
anti-anti-X-Alexa488 (25 µg/ml stock)	1.6 µl

anti-anti-Y-Alexa633 (25 µg/ml stock)   1.6 µl

For each antibody combination, a control sample was prepared as above, but cell lysate was replaced by lysis buffer.

The final concentration of each antibody in samples prepared according to option A was 10 nM (assuming MW 150 kDa). This is in the ideal concentration range for fluorescence cross-correlation analysis. Equimolarity of primary and secondary binders minimises the presence of primary binders without indirect label or of free fluorophore-labelled secondary binders (confer Table 11, p. 86). Both would decrease the fraction of doubly labelled particles, and hence the cross-correlation amplitude. The control sample was necessary to assess any interactions of the binders themselves (see troubleshooting, Table 4, p. 32).

Option B:

anti-X (100 µg/ml stock)   0.4 µl
cognate Fab-Alexa 647 (200 µg/ml stock, as supplied)   0.4 µl
were mixed and incubated for 15 min at 37°C, then chilled on ice and diluted with:
AD-buffer   2.4 µl

Lysate, anti-Y, and anti-anti-Y were added as above in option A, and controls were created accordingly.

The labelling ratio of Fab:primary antibody was 6:1, corresponding to the maximal ratio recommended by the manufacturer for the Zenon-labelling system. Lower ratios were tested but proved less suitable. In contrast to the manufacturer's instructions for labelling of primary antibody with Fab-fragments, preincubation for 5 min at RT was not sufficient.

Option C:

Mass-tag FCS was only employed for the detection of the interaction between ZAP70 and phosphorylated CD3ε or CD3ζ. Both ZAP70-YFP and endogenous ZAP70 were used. In mass-tag FCS, all reagents that may give rise to large, slowly diffusing molecular aggregates must be avoided. Therefore, again monovalent labelled Fab-fragments were employed instead of bivalent secondary antibodies. For endogenous ZAP70, sample setup was as follows:

anti-ZAP70 (100 µg/ml stock)   0.4 µl
cognate Fab-Alexa 647 (200 µg/ml stock, as supplied)   0.4 µl
were mixed and incubated for 15 min at 37°C, then chilled on ice. Then was added:
AD-buffer   1 µl
clarified cell lysate   20 µl

| biotinylated anti-CD3ε (75 µg/ml stock) | 1.6 µl |
| streptavidin-nanobeads (as supplied) | 3 µl |

In lysates containing ZAP70-YFP, the endogenous fluorophore was used, anti-ZAP70 and the secondary Fab-fragments were omitted, and anti-CD3ζ or anti-CD3ε and ProteinG-nanobeads were employed at 3-fold lower concentrations.

Samples were set up in separate reaction tubes and incubated on ice for 16 h. Setup directly in the measurement carrier was avoided, as prolonged exposure to room temperature (i.e. for the last samples that were measured in a multiwell plate) was observed to influence measurement results.

4.1.2 FCS and FCCS measurement and data evaluation

For measurements, the same intrumental hardware as described in chapter 3.6 (p. 27) was used. Alexa488 was excited by the 488nm line of an argon ion laser and detected using an infrared-blocking 500-550 nm bandpass filter. Alexa633, Alexa647 and Cy5 were excited by a 633 nm helium neon laser and detected using a 650 nm longpass filter. A dichroic beam splitter at 610 nm separated fluorescence from Alexa488 and the respective red fluorophore. After warming up the lasers, the calibration of the instrument for cross-correlation measurement in the relevant channels was checked[83]. Each sample was kept on ice until immediately prior to measurement. For measurement, samples were transferred into a 384-well glass bottom plate (175 µm glass thickness; M-plates, cat.-no. 60200, MMI, Glattbrugg, Switzerland) already mounted on the microscope stage.

Measurement parameters were optimised using the respective control samples. For FCCS-measurements, excitation powers of both lasers were adjusted to yield comparable counts-per-molecule for the red and green particles. At the same time, laser powers were adjusted to yield fluorescence excitation near saturation, in order to optimise the signal-to-noise ratio by ensuring optimum specific signal from the fluorophores over background noise resulting e.g. from cell lysate constituents with low autofluorescence

10 measurements of 15 s duration each were recorded for all experimental conditions (see troubleshooting, Table 4, p. 32). The fluorescence fluctuations were correlated on-line. The software of the ConfoCor2 was used for fitting the auto- and cross-correlation functions. Fit functions for cross-correlation functions accounted for one diffusing species. All 10 individual cross correlation functions were fitted separately.

Table 4: *Troubleshooting for protein complex detection by FCCS and indirect immunolabelling.*

Problem	Possible reason	Solution
No cross-correlation is detected, although the proteins are known to interact.	a) The concentration of the target complex in the lysate is higher than the concentration of the antibodies for labelling. Consequently, only a very small fraction of doubly labelled particles is formed. b) The concentration of the target complex in the lysate is too low to give rise to a detectable fraction of doubly labelled particles. c) The interaction of the proteins masks an epitope required for antibody recognition.	a) Prepare a less concentrated lysate[145]. b)Prepare a more concentrated lysate. c) Use an alternative antibody.
High cross-correlation amplitudes already in control sample.	Some of the reagents crossreact.	Identify the culprit by cross-correlation measurements of samples • containing no primary antibodies (secondaries interact) • containing only either one primary antibody (one of the secondaries cross reacts with the included primary)
Particle numbers derived from autocorrelations in red and green channels differ strongly and the autocorrelation function of the fluorophore in excess indicates the presence of a fast-diffusing species.	Free fluorophore is present in the stock solutions of the secondary reagents.	Use a different secondary reagent, or try to separate the labelled reagent from the free fluorophore by size exclusion chromatography.
Presence of relatively few, very slowly diffusing and bright particles, resulting in an inhomogeneous set of cross-correlation amplitudes in repeated measurements. (see Table 2).	Excessive formation of immuno-complexes between individual primary and secondary anti-bodies. Some primary anti-bodies may have individual epitopes that are more ractive with the (usually polyclonal) secondaries.	Use monovalent secondary reagents (e.g. Fab fragments) instead of bivalent secondary.
The total measurement time per sample may need to be optimised.	If the fraction of doubly labelled particles in the sample is very low, longer total measurement times may be needed to stabilise the mean cross-correlation amplitude. If the fraction of doubly labelled particles is high, shorter measurement times per sample will be sufficient.	Use e.g. 10 x 30s. Use e.g. 10 x 7 s.

The amplitude of the cross-correlation function was the only fitted parameter used for further analysis. Means and standard deviations of cross-correlation amplitudes and t-tests for comparison of the means were calculated in Excel (Microsoft). For combination of data from multiple independent experiments, individual data sets were internally normalised to one experimental condition.

Autocorrelation functions from mass-tag FCS were compared after normalisation to an amplitude of 1. In order to rapidly assess the presence of slowly diffusing particles from the autocorrelation functions, a fitting formalism accounting for only one diffusing species was sufficient.

4.1.3 Anticipated results for FCCS

Sample data for the detection of the pervanadate-induced interaction of PLCγ1 with LAT and the titration with the inhibitory peptide LATpY132 (also shown in Figure 31, p. 80) is presented in Table 5. Cross-correlation amplitudes increase from a minimum of 1.001 (no interaction). No cross-correlation is detected in the lysis buffer control (control) and in the lysate of resting cells (resting). The mean cross-correlation amplitude is significantly higher in the lysate of PV-stimulated cells (+PV) than in the lysate of resting cells and decreases again upon titration of the inhibitory LATpY132 peptide (PV + various concentrations). Statistical analysis is performed by one-tailed Student's t-tests assuming unequal variances. Table 6 lists the mean autocorrelation amplitudes from the red and green channel determined in the same experiments.

Sample data comparing labelling by whole bivalent secondary antibodies (according to option A) and labelling by Fab-fragments (option B) is shown in Table 7. The pervanadate-dependent formation of the SLP76-PLCγ1 interaction is detected. In both setups, the increase in cross-correlation amplitudes upon PV-stimulation is obvious and significant. However, in the sample containing labelled IgG as a secondary binder for anti-SLP76, the individual values in the set of 10 measured cross-correlation amplitudes vary widely. This is due to the occurrence of large immunocomplexes which introduce irregularities into the fluorescence fluctuation that stochastically affect the cross-correlation amplitude. In the samples using labelled monovalent Fab-fragments as secondary binders for anti-SLP76, cross-correlation amplitudes of individual measurements vary less.

Table 5: *Cross-correlation amplitudes of the interaction of PLCγ1 with LAT. Indirect immunolabelling was performed using anti-LAT (mouse monoclonal IgG1), goat anti-mouse IgG-Alexa488, anti-PLCγ (rabbit polyclonal IgG), goat anti-rabbit IgG-Alexa633. Samples were lysis buffer (control), lysate of resting cells (resting), lysate of PV-stimulated cells (PV), lysate of PV stimulated cells with titration of inhibitory peptide (PV + various concentrations)*

repeated 15s measurements	control	resting	PV	PV + 50 nM	PV + 100 nM	PV + 200 nM	PV + 500 nM	PV + 1 μM	PV + 10 μM
1	1.006	1.003	1.014	1.012	1.008	1.015	1.007	1.001	1.001
2	1.001	1.009	1.017	1.018	1.019	1.007	1.008	1.003	1.001
3	1.001	1.003	1.012	1.001	1.008	1.008	1.012	1.002	1.001
4	1.010	1.001	1.012	1.018	1.013	1.009	1.017	1.006	1.005
5	1.001	1.001	1.010	1.016	1.011	1.018	1.018	1.001	1.001
6	1.001	1.008	1.014	1.017	1.003	1.015	1.008	1.030	1.001
7	1.001	1.001	1.017	1.039	1.013	1.024	1.014	1.001	1.001
8	1.001	1.001	1.032	1.011	1.011	1.006	1.001	1.006	1.001
9	1.001	1.001	1.012	1.037	1.014	1.023	1.012	1.012	1.001
10	1.001	1.006	1.046	1.034	1.014	1.029	1.006	1.001	1.001
mean	**1.002**	**1.003**	**1.019**	**1.020**	**1.011**	**1.015**	**1.010**	**1.006**	**1.001**
stdv	**0.003**	**0.003**	**0.011**	**0.012**	**0.004**	**0.008**	**0.005**	**0.009**	**0.001**
p-value of t-test versus control		2.4 E-1	7.1 E-4						
p-value of t-test versus resting			1.1 E-3	9.2 E-4	1.1 E-4	4.5 E-4	1.5 E-3	1.8 E-1	4.3 E-2

Table 6: *Means and standard deviations of autocorrelation amplitudes for the same titration experiment as in Table 5.*

Channel	control	resting	PV	PV + 50 nM	PV + 100 nM	PV + 200nM	PV + 500nM	PV + 1μM	PV + 10μM
633 nm mean	1.15	1.15	1.16	1.15	1.17	1.18	1.17	1.17	1.16
stdv	0.01	0.00	0.01	0.01	0.01	0.01	0.00	0.00	0.01
488 nm mean	1.84	1.83	1.75	1.89	1.74	1.81	1.76	1.82	1.75
stdv	0.09	0.12	0.10	0.21	0.09	0.14	0.06	0.08	0.11

Table 7: *Cross-correlation amplitudes for the pervanadate-dependent PLCγ1-SLP-76 interaction. Indirect immunolabelling were perforemd using anti-PLCγ1 (rabbit polyclonal IgG), goat anti-rabbit IgG-Alexa488, anti-SLP-76 (mouse monoclonal IgG 2a) and either goat anti-mouse IgG-Alexa633 or goat anti-mouseIgG 2a Fab-Alexa647. Samples were lysis buffer (control), lysate of resting cells (resting), lysate of PV-stimulated cells (+PV).*

	anti-mouseIgG IgG-Alexa633			anti-mouseIgG2a Fab-Alexa647		
repeated 15-s measurements	control	resting	+ PV	control	resting	+ PV
1	1.001	1.006	1.425	1.006	1.007	1.069
2	1.001	1.039	2.134	1.005	1.005	1.043
3	1.002	1.004	1.035	1.006	1.010	1.025
4	1.009	1.026	1.425	1.001	1.008	1.037
5	1.005	1.007	1.377	1.006	1.012	1.022
6	1.001	1.010	1.076	1.003	1.011	1.022
7	1.001	1.012	1.286	1.008	1.012	1.051
8	1.006	1.005	1.472	1.004	1.018	1.043
9	1.008	1.003	1.231	1.007	1.007	1.031
10	1.006	1.006	1.401	1.004	1.010	1.061
mean	**1.004**	**1.012**	**1.386**	**1.005**	**1.010**	**1.040**
stdv	**0.003**	**0.011**	**0.287**	**0.002**	**0.003**	**0.015**
p-value of t-test versus control		3.4 E-2	1.6 E-3		1.0 E-3	3.3 E-5
p-value of t-test versus resting			1.8 E-3			9.4 E-5

4.2   Protein complex detection on peptide microarrays

Susann Wolf and Wilfred Hummel advanced the procedures for the generation and incubation of peptide microarrays in their diploma theses [146,147].

4.2.1   Generation of peptide arrays

In early stages of the work, cover slips were used as array substrates, and surface functionalisation was carried out in-house [148]. In brief, cover slips (BK7, type 1, 12 mm diameter; Marienfeld, Lauda-Königshofen, Germany) were cleaned by sonication in an aqueous solution of Extran MA01 (Merck, Darmstadt, Germany)/water (1:4, v/v) for 5 min followed by 20 min of sonication in piranha solution, a freshly prepared mixture of 6 volumes H_2SO_4 with 5 volumes of 30 % (v/v) H_2O_2. For silanisation cover slips were covered with 40 µl of (3-glycidyloxypropyl)trimethoxysilane (Fluka), placed in an airtight container, and incubated at room temperature for 6 h, followed by rinsing with acetone. Immediately after silanisation, four arrays of 3*3 peptides were spotted with 300 µm centre-to-centre spacing onto the dry cover slips.

Later on, 16 identical arrays of up to 9*9 spots per array were spotted on epoxy-activated glass slides (Nexterion Slide E, Schott, Jena) with a fluorescein labelled control peptide for orientation. Per peptide, duplicate spots of 1.2 nl each were spotted with a centre-to-centre spacing of 500 μm [147].

For spotting, peptides were freshly diluted from 3 mM DMF stock solutions to a spotting concentration of 100 μM in 0.1 M phosphate buffer (pH 8.0). A GeSiM NP2.0 nanopipettor (GeSiM, Dresden, Germany) was used, maintaining 70% air humidity in the spotter casing and cooling the target support to 15 °C. After the spotting process, slides were left in the closed spotter casing for 30 min. Afterwards, slides were covered with O,O'-bis(2-aminopropyl) polyethylene glycol 800 (Fluka) and incubated at 70 °C for 16 h to quench the remaining reactive epoxy groups. After cooling, slides were rinsed with deionised water, dried under airstream, and stored at 4°C.

4.2.2 Incubation and scanning of peptide arrays

Cover slips with peptide arrays were mounted in a custom-made open measurement chamber with the coated surface up, allowing incubation directly on the stage of the confocal laser scanning microscope (Carl Zeiss, Göttingen, Germany). 100 μl of cell lysate or antibody solutions were used for incubation on each cover slip. After addition to the cover slip, the solution was mixed by pipetting up and down several times. Incubation was carried out for 3 min for the lysates and for 15 min for antibodies. Antibodies were diluted to 5 μg/ml for anti-ZAP70, to 15 μg/ml for anti-phosphotyrosine and to 2.8 μg/ml for Cy-5 labelled goat-anti-mouse-antibody in PBS-Tween/BSA. Between each incubation step, arrays were washed twice with PBS-Tween. Images of the arrays in the last washing buffer were acquired at a resolution of 512 x 512 pixels using a Plan-Neofluar 10 x 0.3 NA objective. YFP was excited with the 514 nm line of an argon-ion laser and detected using a BP530-600 nm band pass filter, Cy5 was excited with the 633 nm line of a helium neon laser and detected using an LP650 nm long pass filter.

For peptide arrays on slides, slides were washed with lysis buffer and dd H_2O and dried by air-stream. A 16-well clip-on frame (ProPlate Multiarray System, Molecular Probes, Eugene, Oregon) was sandwiched to with the slide to create a separate incubation chamber for each array. Arrays were blocked with 1% Top-Block (Fluka) in PBS for 1 h and washed with PBS-Tween/BSA. Originally, arrays were incubated with 200 μl cell lysate per chamber at 4°C for 1 h [147]. In oder to minimise sample consumption, lysate incubation volumes were decreased to 50 μl, after a pilot experiment had shown that signals were independent of the lysate volume, in accordance with the ambient analyte theory[112] (Figure 5).
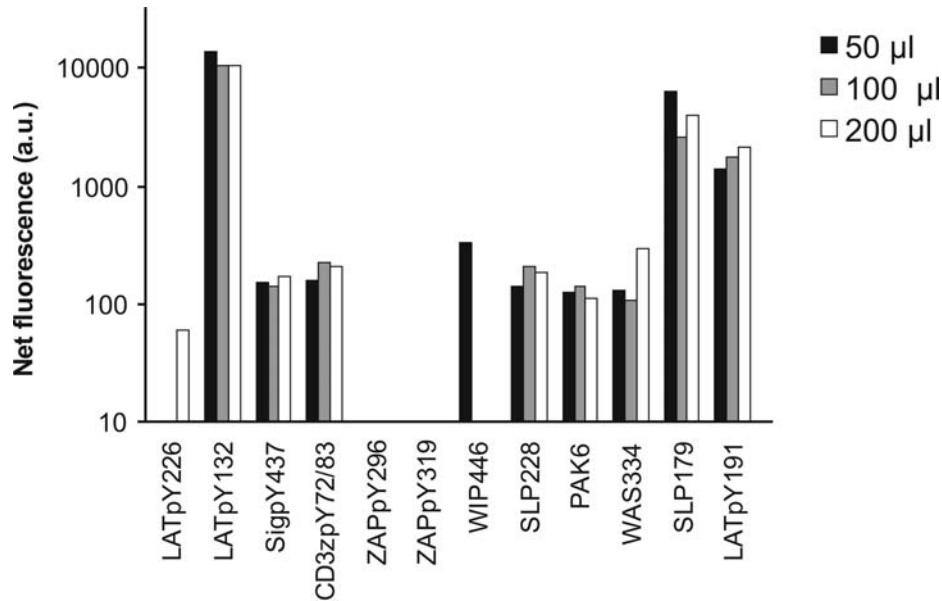
Figure 5: *Net fluorescence of anti-PLCγ1 immunostaining on peptide arrays after incubation with lysate of PV-stimulated Jurkat cells. Different volumes of lysate were used per array, either 50 μl, 100 μl or 200 μl.*

After lysate incubation, the arrays were washed with PBS-Tween/BSA, incubated with 2 μg/ml primary antibody at room temperature for 15 min, washed again with PBS-Tween/BSA, and incubated with 1 μg/ml secondary antibody at room temperature for 10 min [146]. Per array, two primary antibodies were used, one from mouse, one from rabbit. Secondary antibodies were goat-anti-mouse-Alexa546 and goat-anti-rabbit-Alexa633 (Molecular Probes/Invitrogen). For each primary antibody used, a negative control was carried out by immunostaining on an array without prior lysate incubation (Figure 6). Subsequent to staining, arrays were washed with PBS-Tween/BSA, rinsed with dd H_2O, and dried by an air-stream [147]. Dried slides were scanned on a confocal microarray scanner (ScanArray, Perkin Elmer, Rodgau-Jügesheim, Germany) with a lateral resolution of 10 μm, equipped with a 543 nm and a 633 nm laser. Sequential scans for Alexa546 and Alexa633 were taken to record both channels.

4.2.3 Data analysis

For evaluation of arrays on coverslips scanned wet on the LSM, the functionalised spots and the surrounding background were defined as separate areas-of-interest and the mean intensity within the respective area-of-interest was determined using Image Pro Plus 4.5 (Media Cybernetics Inc., Silver Spring, USA). The net fluorescence *F* was calculated by subtracting the mean intensity of the background from the mean intensity of the respective spot. The net fluorescence over equally functionalised spots was averaged [149].
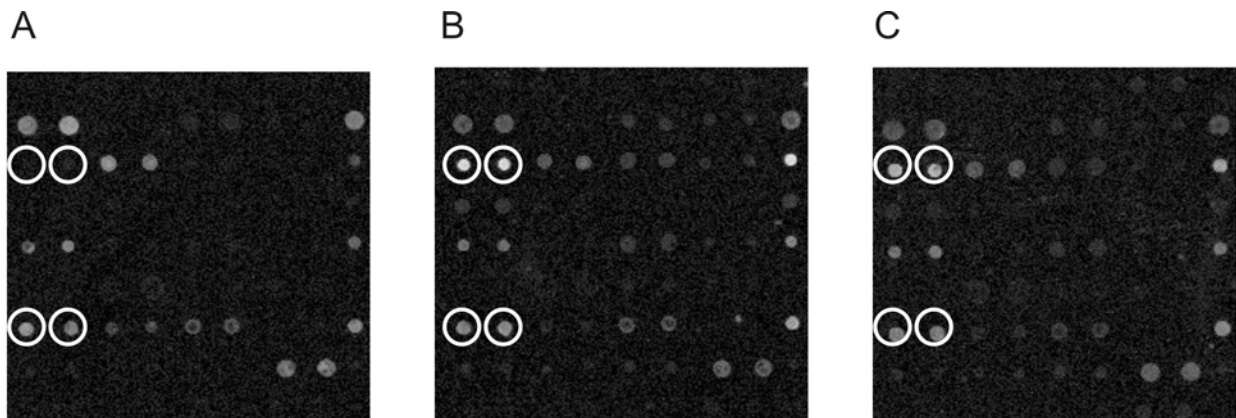
Figure 6: *Peptide microarrays incubated with mouse anti-ZAP70 and anti-mouseIgG-Alexa546 after incubation with A) BSA in lysis buffer (Control array), B) lysate of resting Jurkat cells, C) lysate of PV-stimulated Jurkat cells. Upper pairs of circles: immobilised phospho-ITAM-peptide CD3 pY72/83. Lower pair of circles: polyproline motif peptide UBP403. To correct for signals resulting from crossreactivity of the anti-ZAP70 antibody, respective spot intensities were calculated: B – A and C – A. While low crossreactivity with spotted peptides was observed for most antibodies, the depicted anti-ZAP70 displayed particularly strong and promiscuous crossreactivity.*

For evaluation of slides scanned on the array scanner, resulting 16 bit greyscale tif files were further processed using ArrayProPlus (Media Cybernetics). In order to remove detector shot noise and speckles originating from dust on the arrays, images were first filtered using the 'despeckle' function which replaces pixels deviating by more than a certain value from their neighbouring pixels with the median of the neighbourhood. A filter kernel of 7x7 pixels and a threshold of 15 were used. Images were then overlayed with array grids, using fixed cell diameters of 30 pixels. The local background of each cell was defined as a ring of 3 pixel width, with an offset of 3 pixels around the cell. Net values were calculated by subtracting the local background from the cell content. Cells were identified by a description file with identical names for duplicate spots on the same subarray. The output data table contained net average values for cells with identical names.

Data tables were copied into Excel (Microsoft) for further processing. First, negative net values (as occasionally resulted from unspecific binding around the spot area functionalised with peptide) were set to 0. From signals of each peptide spot and incubation condition, the respective signal of the antibody control was subtracted (Figure 6). If a negative value was the result, it was set to 1, in order to enable further batch calculations. Corrected signal intensities of the stimulated conditions were divided by the corrected signal intensity of the unstimulated condition from respective peptide spots, if at least one of the values was above a certain threshold. Theses thresholds were employed in

order to filter out error-prone ratios resulting from division of one small value by another. Thresholds were established empirically (Figure 7): Various threshold values were set, e.g. at 10, 100 and 1000, defining intensity ranges from 10 to 100, 100 to 1000 and larger than 1000. Ratios of signal intensities on corresponding peptide spots were calculated and assigned to an intensity range, depending on the value of the higher of both signals in the ratio. While ratios assigned to the intensity-range 10-100 proved unreproducible between repeated experiments, ratios assigned to the intensity range 100-1000 were reproducible in many cases. Ratios assigned to intensity range >1000 were highly reproducible (Figure 7). For PV-stimulation experiments, a threshold of 100 was used, for antibody-stimulation, a threshold of 50 was used.

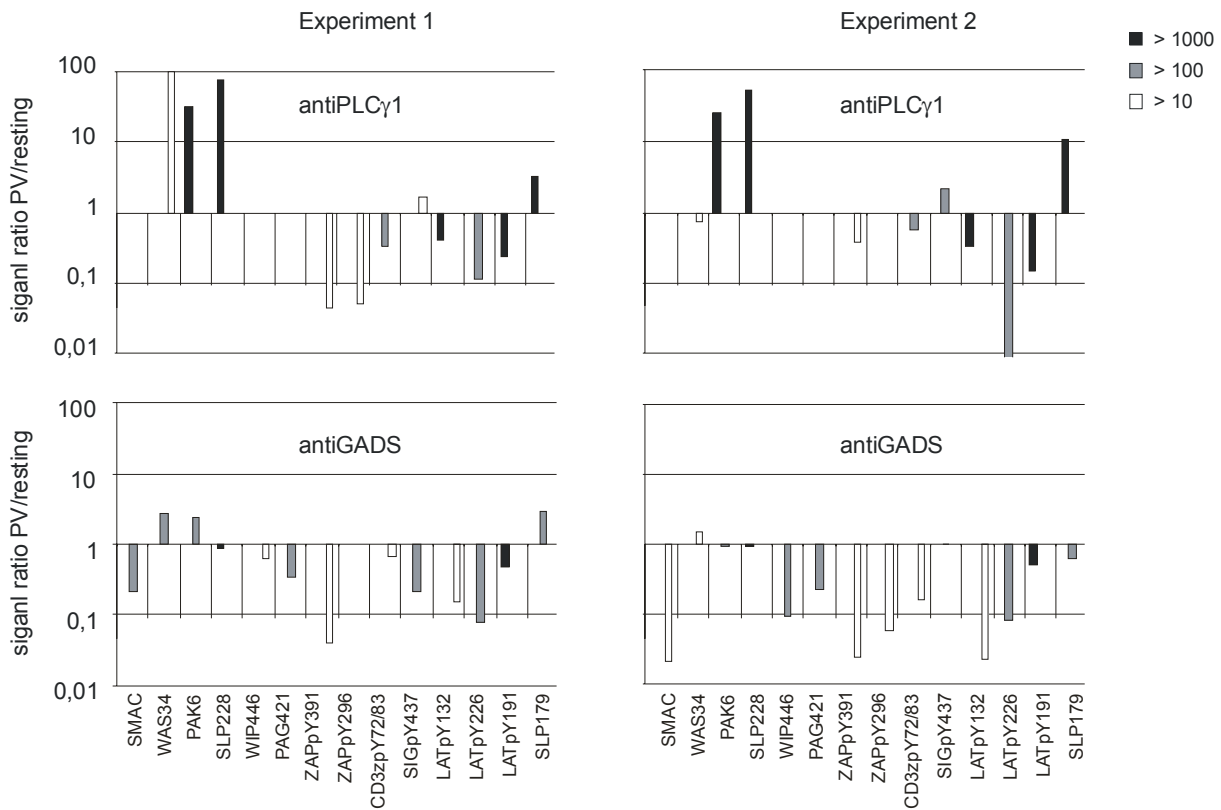***Figure 7****: Establishment of signal intensity treshholds for the evaluation of microarray data. Ratios of signals from lysates of PV-stimulated versus resting Jurkat cells are depicted in various colours, if either the numerator or the denominator of the ratio exceeded a certain threshold: Black: one of the signals > 1000; grey: one of the signals > 100 but < 1000; white: one of the signals >10 but < 100.*

5 Results and Discussion

5.1 Peptide microarrays for the detection of protein interactions in cellular signal transduction

The experiments presented in chapter 5.1.1 were carried out together with Martin Elbs and Karsten Köhler, and the content of this chapter is derived from a published manuscript [149]. The experiments presented in 5.1.3 were carried out with Karsten Köhler, and the content of chapter 5.1.3 is derived from an unpublished manuscript written together with Karsten Köhler.

5.1.1 Pilot experiments

5.1.1.1 Detection of changes in the availability of binding domains

We realised that microarrays of peptides corresponding to protein interaction motifs [9] may provide a specific means for detecting the signalling-dependent masking or unmasking of binding sites. If, inside a cell, a protein engages in a molecular interaction, the binding domain involved in this interaction is masked. Complex formation should therefore decrease the amount of protein available for binding to the microarray after lysis (Figure 8). Peptide arrays have been employed already to profile the structural requirements of the binding of protein domains [12,11]. For interaction motifs involving posttranslational modifications, such as phosphorylation, peptide microarrays are advantageous compared to protein microarrays. Amino acids carrying posttranslational modifications can be incorporated in a site-specific manner by organic synthesis procedures. For the detection of protein-peptide interactions, purified recombinant proteins as well as crude cell lysates [150] have served as the source for protein.

In order to validate our concept, the activation dependent interaction of the tyrosine kinase 70 kDa ζ-associated protein (ZAP70) with the T-cell receptor (TCR)-associated CD3ζ-chain, was selected as a model system [151]. ZAP70 consists of an N-terminal tandem SH2 domain and a C-terminal tyrosine kinase domain (Figure 1, p. 6). In resting cells, this protein is located throughout the cell [152]. Crosslinking of the TCRs by MHC-peptide complexes on an antigen-presenting cell leads to the phosphorylation of several tyrosine residues within immunoreceptor tyrosine-based activation motifs (ITAM) of the CD3ζ-chain [28].
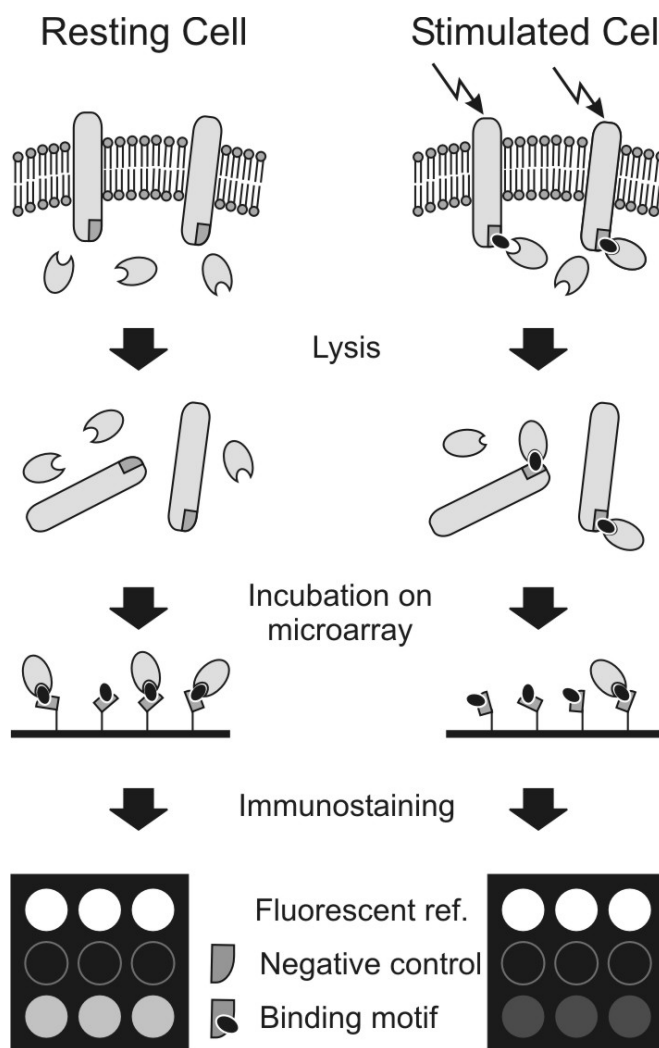
Figure 8: *Schematic of the application of peptide microarrays for detecting the masking of binding sites. Peptide microarrays are generated from peptides that correspond to motifs interacting with binding domains of signalling proteins. Recruitment of a protein into a complex masks a binding site on the protein, which is therefore no longer available for interaction with the microarray. Consequently, those proteins engaging in a molecular interaction will yield weak signals on the microarray. The binding of proteins may be detected in parallel by immunofluorescence, employing cocktails of primary antibodies. The pattern of proteins bound to the microarray reflects the pattern of molecular interactions inside the cells.*

The bis-phosphorylated CD3ζ ITAM peptide motif acts as a high-affinity docking site for the tandem SH2 domain of ZAP70 and recruits ZAP70 to the plasma membrane. Using plasmon resonance spectroscopy, an apparent dissociation constant of 2.0 ± 0.5 nM was reported for this interaction [21]. Once incorporated into the TCR complex, ZAP70 becomes phosphorylated and fully activated and initiates a series of downstream signalling events [36].

Because of its relevance for the propagation of the TCR signal, the bis-phosphorylated CD3ζ ITAM motif (pITAM) was selected to probe for the masking of signalling domains using a peptide microarray approach (Figure 8). The non-phosphorylated counterpart (ITAM) served as a control for the specificity of binding. Both peptides were synthesised as peptide amides with an N-terminal cysteine residue for the covalent immobilisation on epoxy-activated surfaces. Ahx served as a spacer. Fluo-Ahx-KAA was employed as a control for surface chemistry and spotting. This peptide was immobilised via the ε-amino group of the lysine side-chain. Microarrays of the peptides were generated on cover slips by nanopipetting subnanoliter volumes of solutions of the peptides. In initial experiments, ZAP70-containing cell lysates were prepared from 3A9 mouse T-hybridoma cells stably overexpressing a ZAP70-YFP fusion protein as well as a fusion protein of the ZAP70-binding CD3ζ-chain with the cyan fluorescent protein (CD3ζ-CFP). Binding of the ZAP70 fusion protein to the microarray was detected using a confocal microscope by recording the YFP fluorescence or after indirect immunofluorescence staining.

For microarrays incubated with lysis buffer, only the fluorescence of the fluorescein-labelled control peptide could be detected. When microarrays were incubated with lysate from resting cells expressing ZAP70-YFP, the pITAM spots showed a bright fluorescence, indicating an interaction of the peptide with the ZAP70 tandem SH2 domains, whereas the ITAM spots remained dark (Figure 9 A, B). The specificity of the binding of ZAP70-YFP to the pITAM was further confirmed by preincubation of the lysate with 1 μM of free pITAM peptide to block available SH2 domains. Here, only the reference spots were visible (not shown).

In comparison to lysates of resting cells, for lysates of cells treated with the tyrosine phosphatase inhibitor sodium pervanadate, binding of ZAP70-YFP was strongly reduced. The pITAM-associated net fluorescence was only about one quarter to one third of that detected for lysates of resting cells (Figure 9 C). Inhibition of tyrosine phosphatases leads to a strong phosphorylation of the transmembrane protein CD3ζ by protein tyrosine kinases. On the whole-cell level the effect of pervanadate was apparent by the recruitment of ZAP70-YFP to the plasma membrane (Figure 10). The observed decrease in the microarray-bound signal is therefore consistent with the activation-dependent masking of the ZAP70 SH2 domains and reduction of protein available for binding. A comparable reduction in signal was also observed when ZAP70-YFP binding was detected by indirect immunofluorescence using an anti-ZAP70 primary and a Cy5-labelled secondary antibody (Figure 9 D, E).
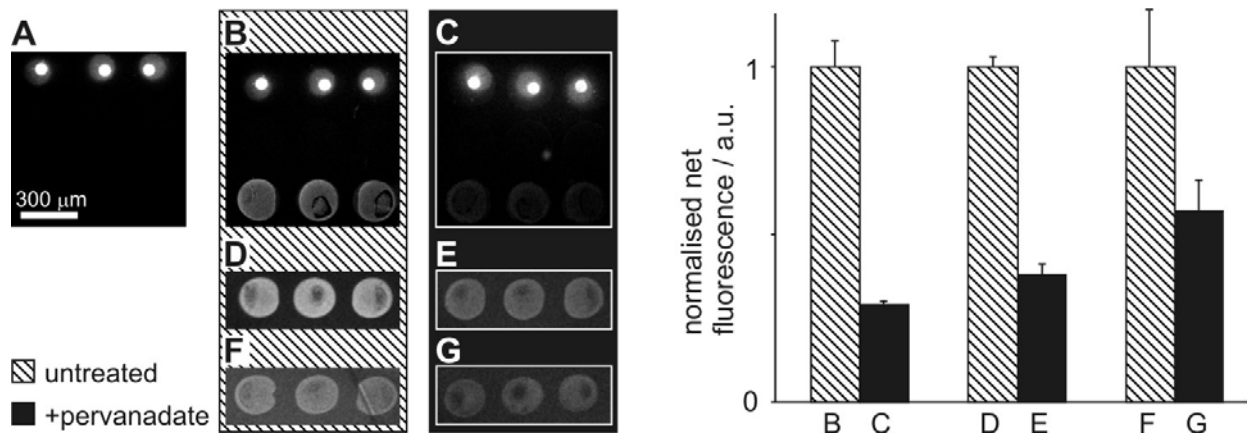
Figure 9: *Activation-dependent binding of ZAP70 to peptide microarrays. All microarrays contained spots of a fluorescein labelled peptide, serving as a control for the surface chemistry (upper row in A–C), the unphosphorylated ITAM-peptide (middle row in A–C) and the bisphophorylated pITAM-peptide (lower row in A–C). (D–G) show the pITAM spots only. Microarrays were scanned by confocal fluorescence microscopy. (A) Microarray incubated with lysis buffer. Microarrays in (B, D, F) were incubated with lysates of resting cells, those in (C, E, G) with corresponding lysates of cells treated with sodium pervanadate. (B, C) Binding of ZAP70-YFP detected by YFP-fluorescence, (D, E) binding of ZAP70-YFP after indirect immunostaining for ZAP70 using Cy5-fluorescence. (F, G) Indirect immunostaining of endogenous ZAP70. The image contrast of each set of images (A–C; D, E; F, G) was optimised separately. The graph depicts the mean intensity of the background-corrected fluorescence of each set of spots, normalised to the untreated condition for each experiment. Error bars reflect the mean deviation of the mean for each condition.*

Figure 10: *Pervanadate-dependent cellular redistribution of ZAP70-YFP. In resting cells, ZAP70-YFP was evenly distributed (A). After incubation with pervanadate, ZAP70-YFP was recruited to the membrane-proximal region (B). Cell images were acquired with a sampling rate of 1024 x 1024 pixels using a C-Apochromat 63 x 1.2 NA water immersion objective*
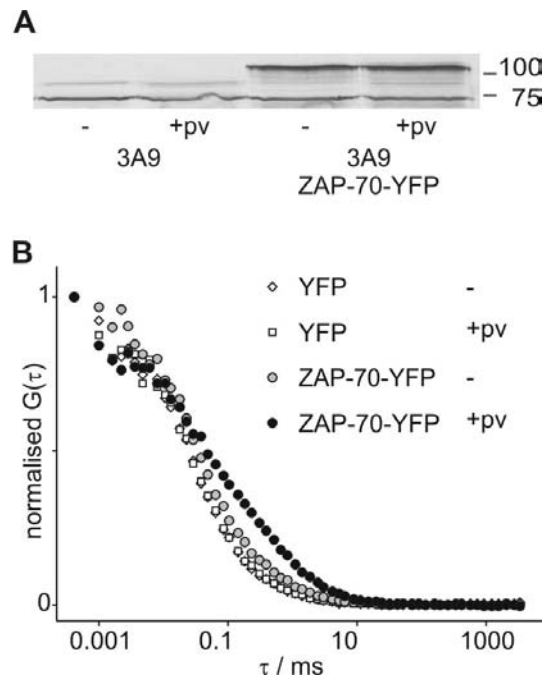
Figure 11: (A) Cellular content of ZAP70 and ZAP70-YFP before and after pervanadate treatment. Lysates of untransfected cells and cells overexpressing ZAP70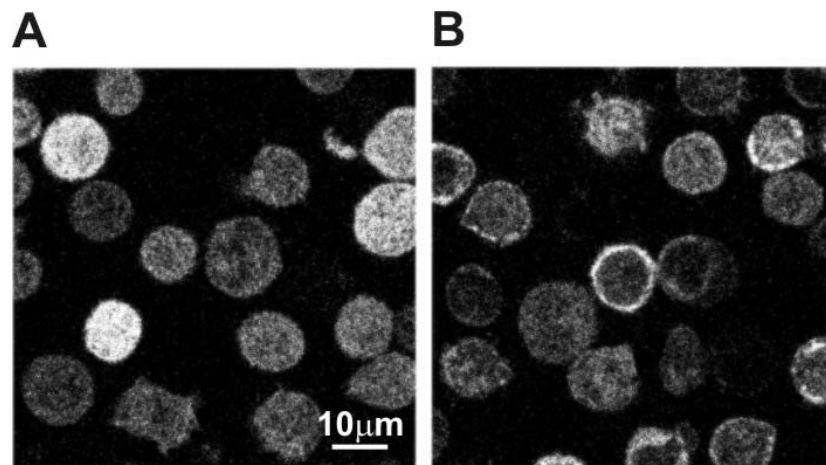-YFP and CD3ζ-CFP, both treated with pervanadate or left untreated, were probed by western blot analysis for ZAP70. Equal amounts of protein were loaded in each lane. Endogenous ZAP70 runs at an apparent molecular weight of 70 kDa, ZAP70-YFP at approximately 100 kDa. (B) Validation of ZAP70 complex formation upon pervanadate treatment by fluorescence correlation spectroscopy (FCS). Autocorrelation functions were determined from lysates of cells overexpressing ZAP70-YFP and CD3ζ-CFP, treated with pervanadate or left untreated. The amplitudes of the autocorrelation functions were normalised to unity. As a control, FCS measurements were performed in lysates of pervanadate treated or resting cells expressing free YFP.

Up to this point, the microarrays had succeeded in detecting an activation-dependent reduction of protein binding using cells in which both binding partners were overexpressed. Western blot analysis revealed that the level of ZAP70-YFP fusion protein was about 2.5 times the level of endogenous protein in non-transfected cells (Figure 11). In order to test whether the microarray approach was sensitive enough to detect the masking of binding sites in lysates of cells expressing endogenous amounts of both proteins, untransfected cells were employed. Binding of ZAP70 could be detected by immunofluorescence. Again, pervanadate treatment led to a significant reduction in the signal (Figure 9 F, G).

To exclude a pervanadate-dependent degradation of total protein or specifically of ZAP70 as the cause of the reduced binding, lysates of pervanadate treated and resting cells were analysed for protein content and ZAP70 levels. Neither the total

protein content (data not shown) nor the ZAP70 content were influenced by pervanadate (Figure 11 A). Fluorescence correlation spectroscopy (FCS) in lysates of ZAP70-YFP expressing cells was employed to further substantiate that the reduction in binding reflected recruitment of ZAP70 into molecular complexes. FCS derives information on diffusion constants of fluorescent particles by the analysis of temporal fluctuations of a fluorescence signal [80,153]. The decay time of the autocorrelation function reflects the size of the fluorescent particle. In a close approximation, the diffusion constant of a particle is inversely related to the cubic root of its mass (Eq. 10, Eq. 12, Eq. 13, p. 14). The intrinsic fluorophore YFP allows the sensitive detection of fusion proteins by FCS. Autocorrelation functions of ZAP70-YFP could be derived from fluorescence fluctuations recorded in crude cell lysates of pervanadate treated and resting cells. For pervanadate treated cells the autocorrelation curve was shifted towards longer autocorrelation times. The observed shift corresponded to a decrease of the diffusion constant by 45% and a sixfold increase in mass of the fluorescent particle, consistent with the recruitment of ZAP70-YFP into high-molecular weight complexes (Figure 11 B). No such change was observed for cells expressing free YFP instead of ZAP70-YFP.

5.1.1.2 Determination of free and occupied binding sites of ZAP70

Although a marked reduction of the pITAM-bound fluorescence was consistently found after pervanadate treatment, the reduction was stronger for cells overexpressing the fusion protein (Figure 9). This observation could either be due to the fact that the transfected cells also overexpressed the CD3ζ-chain or inherent to the detection method, i. e. YFP-fluorescence versus indirect immunofluorescence. In order to resolve this question we next asked to which degree the changes in signal on the microarray correlated with the availability of binding sites of ZAP70 in the cell lysate. Given such a correlation, microarray-based analyses would yield a quantitative measure of changes in molecular interactions in cellular signalling.

In a first step, we took advantage of the ability of FCS to directly determine the concentration of fluorescent molecules. Lysates of resting cells expressing ZAP70-YFP were prepared at different cell densities, ranging from 2 to 50 x 10^6 cells per ml lysate. The total protein content increased linearly with the cell density. The same was found for the ZAP70-YFP concentration, determined by FCS. By autocorrelation analysis, concentrations of the fusion protein in the cell lysates between 4 and 85 nM were derived. Moreover, the net fluorescence of ZAP70-YFP bound to pITAM spots on the microarrays was directly proportional to the concentration of ZAP70-YFP in the examined range (Figure 12 A, B).
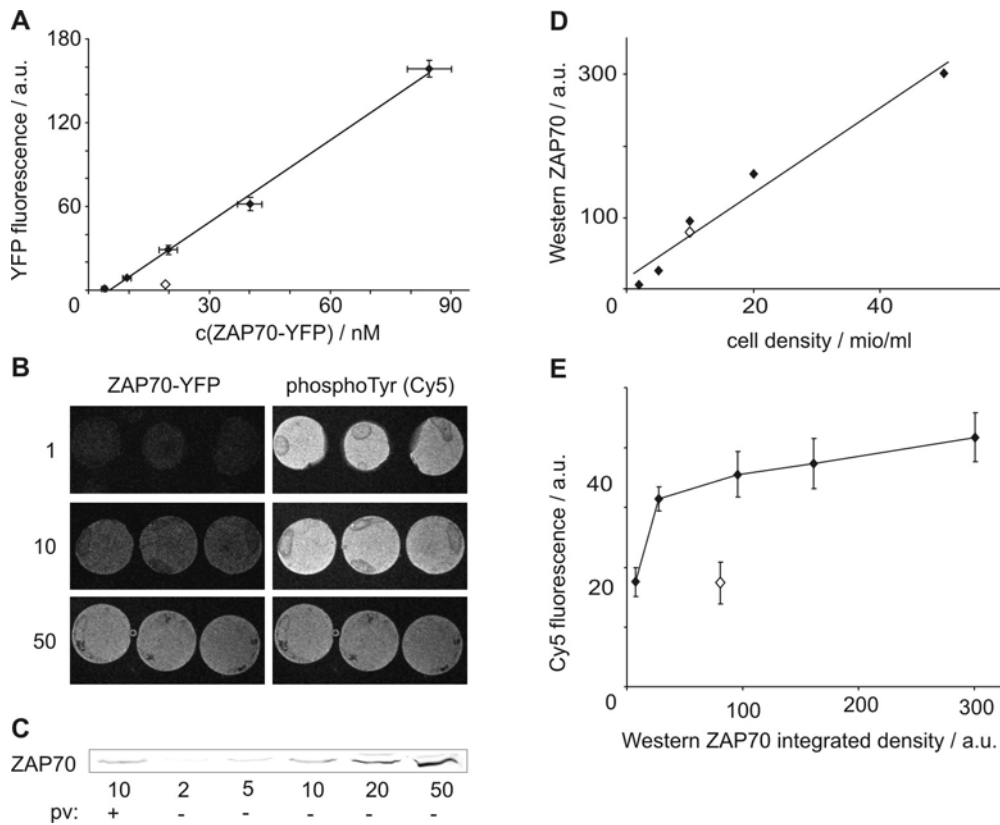
***Figure* 12**: *Relation between the concentration of ZAP70 in the lysates of resting cells and array-bound fluorescence on pITAM spots after incubation on microarrays. (A) Lysates of resting cells expressing ZAP70-YFP were prepared at cell densities of 2, 5, 10, 20 and 50 x 10⁶ cells / ml lysate (black diamonds). The concentration of ZAP70-YFP was determined by FCS. Array-bound fluorescence of ZAP70-YFP increased linearly over the concentration range tested. Binding of ZAP70-YFP from a pervanadate treated lysate prepared at 10 x 10⁶ cells / ml was strongly reduced (open diamond). (B) pITAM spots on arrays incubated with lysates of 1, 10 and 50 x 10⁶ cells / ml displayed an increasing fluorescence intensity of ZAP70-YFP, while indirect immunostaining against phosphotyrosine using a Cy5-labelled secondary antibody revealed that pITAM was not saturated by ZAP70-YFP. (C) Western blot analysis of endogenous ZAP70 from lysates of untransfected cells prepared at cell densities from 2 to 50 x 10⁶ cells / ml. Equal volumes of lysate were loaded. Pervanadate treatment of the cells prior to lysis is denoted by pv. (D) ZAP70 western bands shown in (C) were quantitated by integrating their density and area. The ZAP70 content inceased linearly with the density of cells in the lysate. (E) Aliquots of the lysates depicted in (D) were incubated on arrays and the arrays indirectly immunostained for ZAP70. A correlation between ZAP70-content as determined by western blotting and intensity of the immunostaining on the array was established for lysates of resting cells (black diamonds). An array incubated with lysate from pervanadate treated cells (open diamond) showed a clear reduction of immunostaining. Error bars represent the mean deviation from the mean.*

Figure 13: *Western blot against ZAP70 after immunoprecipitation with anti-CD3ζ. Two cell lines were used, 3A9 cells, and 3A9 cells overexpressing ZAP70-YFP (3A9+ZY). Cells were either resting (-) or treated with pervanadate (+) before lysis. Expected molecular weights are 70 kD for ZAP 70 and 99 kD for ZAP70-YFP.*
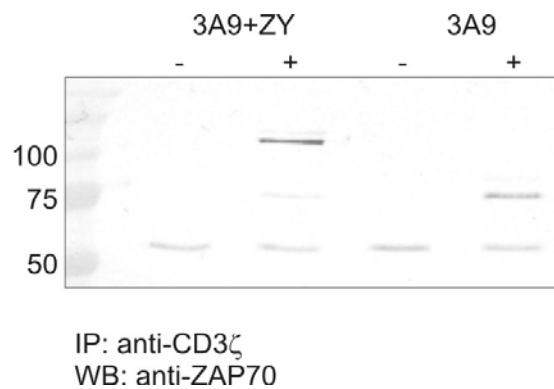
This calibration curve provided the basis to determine the decrease in the concentration of available binding sites upon treatment with pervanadate. In a lysate of 1×10^7 resting cells / ml the concentration of ZAP70-YFP was 19.9 ± 2.2 nM. From the reduction of the array-bound fluorescence after pervanadate treatment a reduction of unbound ZAP70-YFP to 7.1 ± 0.4 nM was calculated for a lysate of corresponding cell density (Figure 12 A). In order to confirm that the concentration determined by FCS corresponded to the concentration of ZAP70-YFP with available binding sites, we performed an immunoprecipitation of the CD3ζ-chain. Only after pervanadate treatment, ZAP70 and ZAP70-YFP coprecipitated with the CD3ζ-chain. In resting cells, no interaction with the CD3ζ-chain was detectable(Figure 13).

At this point we were concerned, that the activation-dependent change in the level of microarray-bound ZAP70 and ZAP70-YFP could also have arisen from a competition of ZAP70 with other proteins in the lysate for which an activation-dependent unmasking of binding sites had occurred. Such a competition would take place if binding of protein to the peptide spots was close to saturation. The linear dependence of array-bound fluorescence and ZAP70-YFP concentration to lysate densities of up to 5×10^7 cells / ml, five times the density employed for the quantification of activation-dependent changes, indicated that binding of ZAP70 to the microarray was clearly below saturation (Figure 12 A). The capacity of the spots for binding protein was further analysed by detection of remaining free pITAM after incubation with lysate. Here, we took advantage of the detectability of the pITAM peptide by indirect immunostaining, using anti-phosphotyrosine primary and Cy5-labelled secondary antibodies. With increasing lysate concentration, Cy5-fluorescence decreased by one half (Figure 12 B), demonstrating that pITAM peptide

was not a limiting factor for detecting activation-dependent changes in the masking of binding sites.

Next, we intended to demonstrate that calibration curves can provide quantitative information on the masking of binding sites for endogeneous protein, as well. Lysates of untransfected resting cells were prepared at cell densities up to 5 x 10^7 per ml lysate. The ZAP70 content of the lysates as determined by western blot analysis scaled linearly with the cell density (Figure 12 C, D). Again, the microarray-bound fluorescence after indirect immunostaining correlated positively with the ZAP70 content. In contrast to the fluorescence of the ZAP70-YFP fusion protein, the correlation was non-linear (Figure 12 E). In the lysates of cells expressing ZAP70-YFP, the fusion protein was overexpressed by 2.5-fold in addition to the endogenous protein (Figure 11) and the arrays were still not saturated at the highest lysate concentration tested. Therefore, the non-linear increase of immunofluorescence staining for endogenous ZAP70 most likely was not due to saturation.

Rather, the immunostaining of bound ZAP70 had not reached equilibrium under the incubation conditions used [113]. However, as long as incubation times are carefully controlled, antigen-antibody interactions can be used for quantitative detection in nonequilibrium assays [154]. Especially for protein-peptide interactions with lower affinity, dissociation of bound protein after removal of the cell lysate would preclude a prolonged incubation to reach equilibrium. Even though the interaction of ZAP70 with the pITAM peptide is of rather high affinity, we intended to validate the method for conditions appropriate for interactions of lower affinity, therefore using short incubation times with primary and secondary antibody. The observed decrease in array-bound fluorescence for lysate from pervanadate treated cells corresponded to an 80% decrease of endogenous ZAP70 with unmasked SH2 domains.

Finally, we calculated absolute numbers of available ZAP70-YFP or ZAP70 molecules per cell both in resting and in pervanadate treated cells by combining the information obtained from (i) determining the concentration of ZAP70-YFP in lysates of resting cells by FCS, (ii) the relative pervanadate-dependent reduction of free binding sites derived from the calibration curves, and (iii) the level of overexpression of fusion protein versus endogenous protein (Table 8). The total number of available ZAP70 molecules (ZAP70-YFP and ZAP70) in cells overexpressing the fusion protein could either be determined experimentally by western blot analysis or estimated from the overexpression level of the fusion protein.

Table 8: Pervanadate-dependent changes in the number of ZAP70 molecules with unmasked SH2 domains per cell. Numbers given relate to ZAP70-YFP for cells overexpressing the fusion protein and to endogenous ZAP70 for untransfected cells.

	ZAP70-YFP with unmasked SH2 domains		endogenous ZAP70 with unmasked SH2 domains
	concentration / nM	molecules per cell	molecules per cell
resting cells	19.9 ± 2.2 [a]	$(1.20 \pm 0.13) \times 10^6$	4.8×10^5 [c]
PV treated cells	7.1 ± 0.4 [b]	$(0.43 \pm 0.02) \times 10^6$	1.0×10^5 [d]

[a] directly determined by fluorescence correlation spectroscopy (FCS)

[b] calculated from array-bound fluorescence using the calibration curve of array-bound fluorescence versus ZAP70-YFP concentration (Figure 12)

[c] estimated from the 2.5-fold overexpression of ZAP70-YFP over endogenous ZAP70 as determined by western blotting (Figure 11)

[d] estimated from array-bound fluorescence using the calibration curve of indirect immunostaining for array-bound ZAP70 versus integrated western band (Figure 12)

5.1.1.3   Discussion

The detection of the signalling-dependent masking of binding sites represents a valuable new protocol for the application of peptide microarrays in the analysis of cellular signalling processes. The protocol provides a significant shortcut to the detection of molecular interactions in comparison to established techniques such as coimmunoprecipitation. While the identity of the binding partner in the complex is not resolved, the parallel detection of binding events using microarrays functionalised with a multitude of peptides will provide a detailed description of the functional state of signalling proteins inside a cell. Given a repertoire of peptides that act as specific sensors for individual signalling proteins, each spot of a microarray may specifically report on the availability of a specific binding site.

Moreover, through acquisition of calibration curves, e. g. by western blot analysis, quantitative information on the fraction of a protein recruited into a molecular complex is obtained. If cells expressing a fusion protein with a fluorescent protein are available, combination of the microarray-based approach with fluorescence correlation spectroscopy yields absolute figures on the change of available binding sites both in cells overexpressing the fusion protein and, through comparison of expression levels by western blotting, also in cells only expressing the endogenous protein.

The affinity range of protein-peptide interactions detectable by this technique will have to be determined. Interactions have to withstand multiple washing steps on the array in order to remain detectable. Compared to other interactions of proteins with peptide motifs, the interaction of the tandem ZAP70 SH2 domains with the bisposphorylated pITAM peptide is of rather high affinity. However, the applicability of peptide microarrays for the profiling of interactions with dissociation constants in the upper nanomolar to lower micromolar has already been demonstrated [11,12]. In principle, protein microarrays might be used to monitor the masking of binding sites in a similar way. However, peptides as capture molecules afford a simple way to incorporate posttranslational modifications, which may be critical for binding.

The results obtained for the interaction of ZAP70 with immobilised pITAM peptide encouraged the compilation of a collection of peptides with binding specificities for different proteins of the T-cell signal transduction cascade for further experiments.

5.1.2 Additional interactions, 2-Colour detection

As our pilot experiments revealed, phosphotyrosine motifs derived from SH2 domain binding sites are attractive probes for the detection of the interaction status of a domain in a microarray format. To accordingly extend this detection principle, a number of pY peptides, as well as polyP motifs binding to SH3 domains, were chosen, based on the literature (Table 2, p. 24).

In all further experiments, the human T-cell leukemia cell line Jurkat (or signalling-deficient derivatives of Jurkat) were used. Although these cells lack the lipid phosphatases SHIP and PTEN and have high levels of phosphatidylinositol 3,4,5-trisphosphate [155], Jurkat cells are a widely used model for signal transduction in T-cells. Lysates of Jurkat cells were incubated on the peptide arrays and binding of the adapter proteins GADS and GRB2, of the scaffolding proteins LAT and SLP76, and of the signal transduction enzymes (most also with adapter functions) LCK, ZAP, cCBL, PLCγ1, PI3K-p85, VAV, and SHPTP2 was investigated by indirect immunofluorescence.

16 identical peptide arrays were nanospotted per glass slide. A 16-well clip on frame allowed the incubation of individual arrays with different cell lysates and indirect immunostaining for bound proteins with different primary antibodies. In order to augment the number of proteins detectable per slide, in each well two proteins were detected simultaneously, using primary antibodies from mouse and rabbit and species-specific distinctly labelled secondary antibodies (Figure 14 A, B).
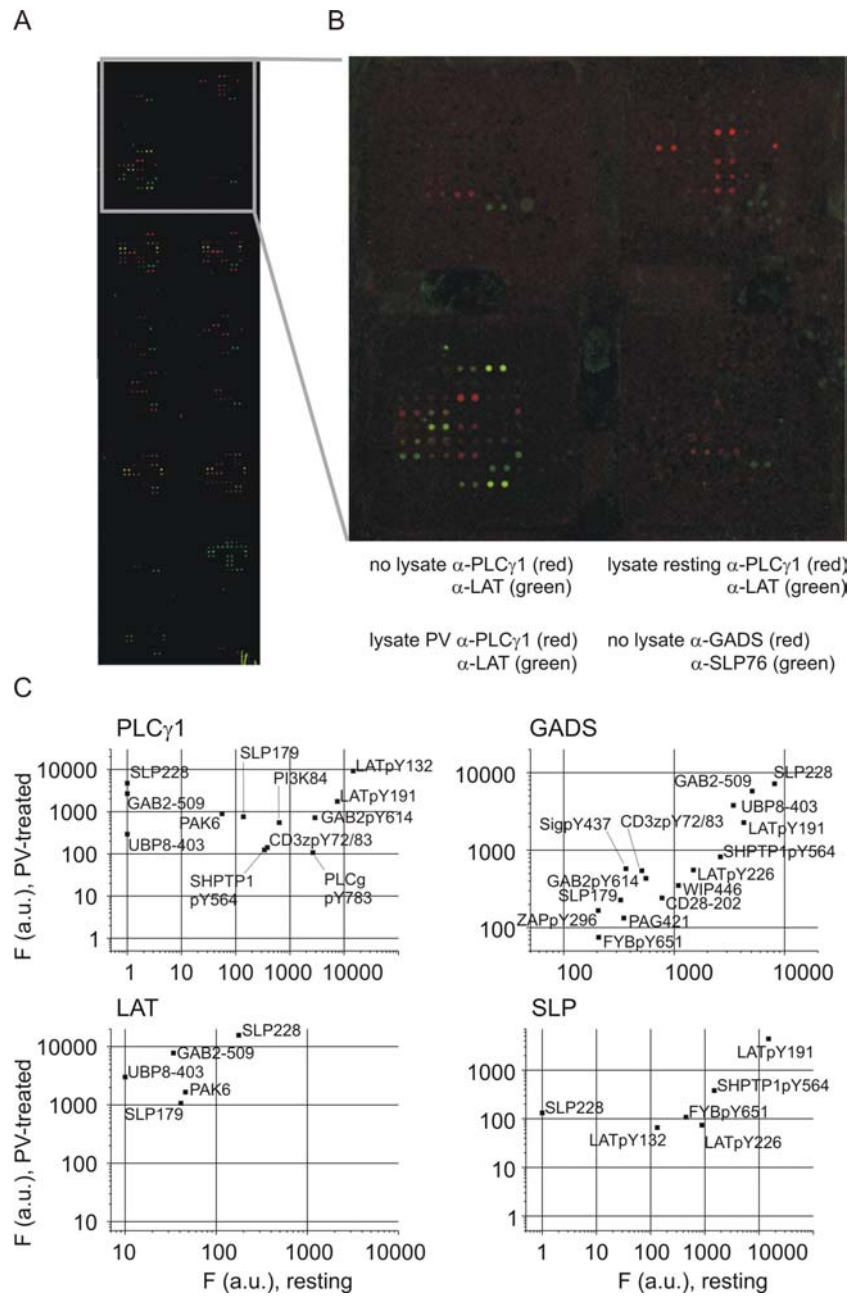
Figure 14: A) One coverslip holding 16 identical peptide microarrays, incubated with cell lysates and different antibodies for immunostaining. Each subarray was incubated with lysate of 10^6 Jurkat cells. Green: secondary immunostaining with anti-mouse-Alexa546; red: secondary immunostaining with anti-rabbit-Alexa633. B) Detailed view of the arrays used for determining background binding of anti-PLCγ1 and anti-LAT antibodies, and binding of PLCγ1 and LAT from resting and pervandate (PV) treated cells. Additionally, the background control for anti-GADS and anti-SLP76 is shown. C) Fluorescence intensities F derived for resting and PV treated condition were corrected for background binding of antibodies. Median values of 5 experiments are shown, if a minimum of 4 out of 5 experiments produced a signal above threshold for either one of the stimulated or unstimulated condition (see Materials and Methods).
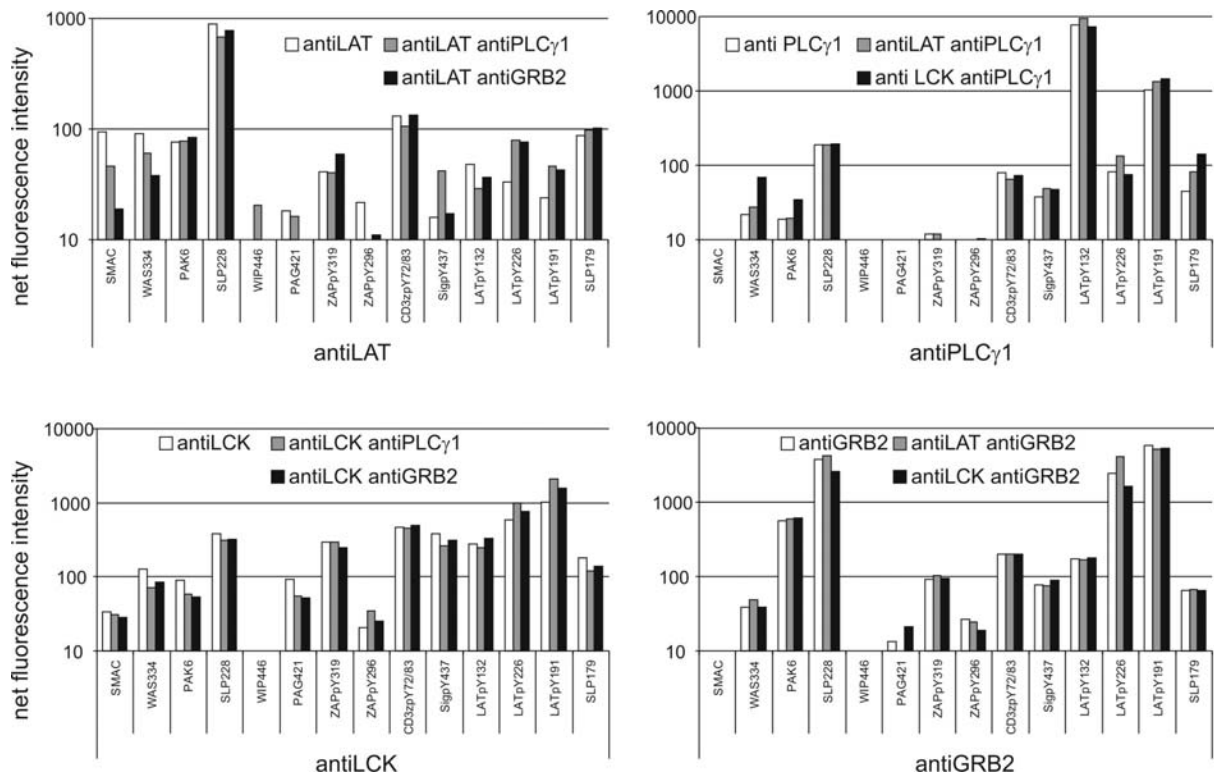
Figure 15: *Two-analyte two-colour detection on peptide microarrays in comparison to one-analyte one-colour detection. Lysates from resting Jurkat cells were employed. Secondary immunostaining was performed with goat anti-mouseIgG-Alexa546 against antibodies from mouse (antiLAT and antiLCK) and anti-rabbitIgG-Alexa633 against antibodies from rabbit (antiPLCγ1 and antiGRB2). Each panel shows signals obtained for binding of one protein to the array (labels below the panel) obtained in one-colour immunostaining (white columns) or in two-colour immunostaining in the presence of further antibodies (grey and black columns).*

The possibility of mutual influence of the signals (as might result from steric hindrance of antibody binding, or from crosstalk of fluorophores) was taken into account. In a pilot experiment, immunostaining signals obtained for proteins from Jurkat cell lysates with various combinations of two mouse antibodies (anti-LAT and anti-LCK) and two rabbit antibodies (anti-PLCγ1 and anti-GRB2) were compared with signals from incubations with individual antibodies alone. For all tested antibodies, the presence of further antibodies showed no influence on the detection on all immobilised peptides (Figure 15). Therefore, further experiments were carried out using two detection antibodies per array, thus increasing the information gain from each slide by a factor of two.

Judged by the intensity of immunostaining on the array, proteins showed a strong preference for peptides representing binding motifs for the respective domain

subtype of the protein, notably peptides derived from known binding partners (Figure 14 C). For example, PLCγ1 contains an SHP/PLC type SH2 and correspondingly its signal on the peptide LATpY132 (SHP/PLC motif) was about twice as intense as on LATpY191 (GRB2/SFK/PLC motif) and nondetectable on LATpY226 (GRB2/SFK motif). The signal of GADS on the peptide SLP228 (atypical SH3 motif [133]) was about 300fold higher than on SLP179 (type2 SH3 motif).

5.1.3 Dissection of signalling complexes on peptide microarrays

5.1.3.1 Phosphorylation-dependent changes in interaction profiles

To initiate signal transduction by protein phosphorylation, we employed the phosphatase inhibitor pervanadate[142]. Lysates of resting or pervanadate-treated Jurkat cells were incubated on separate arrays (Figure 14 B, C) and ratios of signals from corresponding peptides were calculated (Figure 16 A).

For interactions of SH2-proteins on pY peptides representing known binding partners, pervanadate induced a moderate signal decrease, as for GADS, GRB2, and PLCγ1 on the respective LATpY motifs. This decrease was in line with our previously demonstrated concept, that phosphorylation-dependent complex formation masks binding sites of proteins and therefore reduces binding to cognate immobilized phosphopeptides[149]. Remarkably, for GRB2 an increase was observed on SIGpY437, representing an pY-motif subtype of the PLC/SHP subtype. For proteins directly binding to cognate polyP-motifs through SH3 domains, we observed only moderate signal changes, as for example for PLCγ1 binding to SLP179 or Grb2 binding to GAB2-509 [72]. In most cases, these changes were minor signal increases. In addition, most proteins lacking SH3 domains were also detected on the SH3-binding polyP peptides (Figure 16 A), suggesting that they were recruited to the array in a complex with a direct binding partner for an immobilized polyP peptide. Remarkably, signal increases for these proteins were much stronger than those of proteins for which direct binding was possible. Signals for which the subtype preference of the respective domain was violated could also originate from the binding of complexes rather than from direct interactions. For example, LAT, which has no interaction domains at all, displayed a stimulation-dependent median 74-fold increase of binding of on the polyP peptide SLP228. This binding could be mediated by an SH2/SH3 adapter like GADS or GRB2, which were also detectable, albeit with moderate median signal changes.
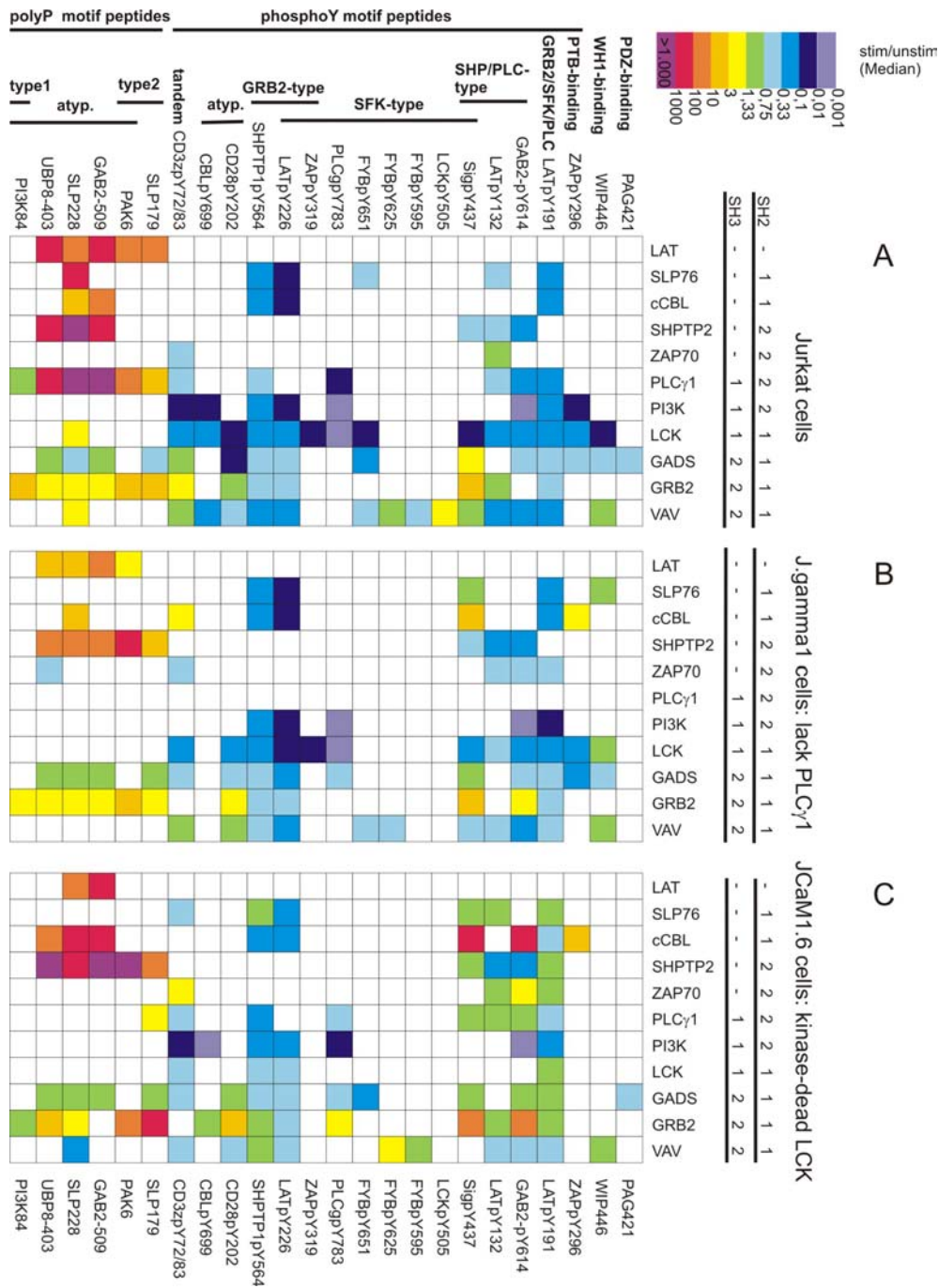
Figure 16: *Changes in protein signal intensity on the peptide microarray upon treatment of Jurkat cells and derivative cell lines with sodium pervanadate. Peptides (horiontal) are plotted against proteins probed by immunostaining (vertical). Next to the proteins, their numbers of SH2 and SH3 domains are listed. Ratios of background-corrected fluorescence intensities were calculated for PV-treated to resting cells. A) Jurkat cells. The median ratio of 5 experiments is shown, if a minimum of 4 out of 5 experiments produced a signal above threshold (see Materials and Methods). B) J.gamma1 cells and C) JCaM1.6 cells. The median ratio of 4 experiments is shown, if a minimum of 3 out of 4 experiments produced a signal above threshold.*

The LAT-interactor PLCγ1 was detected on SLP228 with a median increase upon stimulation of 4400. Likewise, the increase of the GRB2 signal on SIGpY437 could be explained by a phosphorylation-dependent interaction between GRB2 and SHPTP2, and binding of SHPTP2 to SIGpY437. On LATpY191, the median signal of GADS decreased to 0.7, while the medain signals of the GADS-interactor SLP76 and the SLP76-interactor PLCγ1 decreased to 0.2 of the unstimuated control (Figure 16 A). Similar tendencies were found for GRB2 (0.7) and its binder CBL (0.3), which contains a PTB domain [38], unlikely to mediate direct interactions with LATpY191.

The absolute signal intensities provided further evidence for the binding of protein complexes to the arrays (Figure 14 C). For lysates of resting cells, immunostaining for PLCγ1 was intense on SLP179 and PAK6 and negligible on SLP228 and GAB2-509. For lysates of pervanadate-treated cells, signals on SLP228 and GAB2-509 were stronger than signals on SLP179 and PAK6. If a mere change in the availability of the SH3 domain of PLCγ1 was the reason for a signal increase, then the signal should increase uniformly on all peptides. The reversal in the order of signal intensities therefore suggests that a portion of PLCγ1 was contained in complexes recruited to the array via the SH3 domain of another protein.

5.1.3.2 Dissection of complex architectures by peptide competition and titration

Next we sought to confirm experimentally the binding of complexes on the array and to obtain information on the architecture of these complexes. On the SLP228 peptide spot, we detected GADS, LAT, and PLCγ1 (Figure 17 A). If the proteins were bound as a complex, then incubation with peptides corresponding to individual motif should selectively remove either one, two or all three proteins from the array We had shown previously, that the PLCγ1-LAT interaction was competed by incubation of lysates with the LATpY132 peptide and less effectively with LATpY191[145]. Peptide concentrations for competition on the arrays were chosen accordingly. The signals of GADS, LAT and PLCγ1 were all sensitive to SLP228. Upon addition of LATpY191, the signals of LAT and PLCγ1 decreased, while the signal of GADS was not affected. In contrast to the LAT signal, the PLCγ1-signal was also sensitive to the LATpY132 peptide. Taken together, this suggested the following order of binding: SLP228 directly bound GADS, the SH2 of GADS bound LAT via LATpY191, LAT bound the SH2 of PLCγ1 via LATpY132 [131]. Moreover, these results confirm that the binding of PLCγ1 to SLP228 is indirect.

Peptide competition of the signals of GADS, SLP76 and PLCγ1 on the immobilized peptide LATpY191 enabled the dissection of the same set of interactions from yet another perspective (Figure 17 B): All proteins contain SH2

domains. Therefore, instead of binding as a complex, these proteins might bind the peptide independently. Detection of GADS, SLP76 and PLCγ1 was all sensitive to LATpY191. However, only SLP76 and PLCγ1 were sensitive to SLP228. PLCγ1 was also sensitive to SLP179, even though this peptide had some effect on all three proteins. Finally, the sensitivity of PLCγ1 to LATpY132 may suggest that further SH2-interactions stabilize the complex. In contrast to the LAT-containing complex described above, all three proteins were detected on LATpY191 also upon incubation of lysates of resting cells. Inhibitory peptides had similar effect in lysates of resting and pervanadate-treated cells (Figure 17 B), indicating the existence of a preformed complex of GADS, SLP76 and PLCγ1. However, the effect of all disrupting peptides on PLCγ1 was weaker in lysates from resting cells, suggesting that direct binding of PLCγ1 to immobilized LATpY191 accounted for a larger part of the signal than after stimulation.

Titration with the peptides LATpY132 and LATpY191 yielded further information on the organisation of signalling complexes through comparison of titration curves obtained (i) for several proteins on the same array spot, or (ii) for one protein on a range of arrayed peptides (Figure 17 C). (i) For LAT and PLCγ1 on the SLP228 spot, signal losses upon addition of LATpY191 occurred with the same concentration dependence, while for LATpY132 only PLCγ1 dissociated, supporting the binding order inferred from the simple peptide competition experiment (Figure 17 A). (ii) Upon titration with LATpY132, PLCγ1 fully dissociated from GAB2-509 and SLP228 (atypical SH3-binding motifs), but only partially from PAK6 and SLP179 (type 2 SH3-binding motifs), suggesting different modes of PLCγ1 binding. On SLP228, indirect binding of PLCγ1 as a part of a large complex can be assumed as shown by the competition experiment (Figure 17 A). SLP179 represents a favoured binding motif of the PLCγ1 SH3 domain. Still, titration with pY-peptides decreased the signal of PLCγ1, suggesting a role for the SH2-domain of PLCγ1 in the stabilisation of binding to the array.
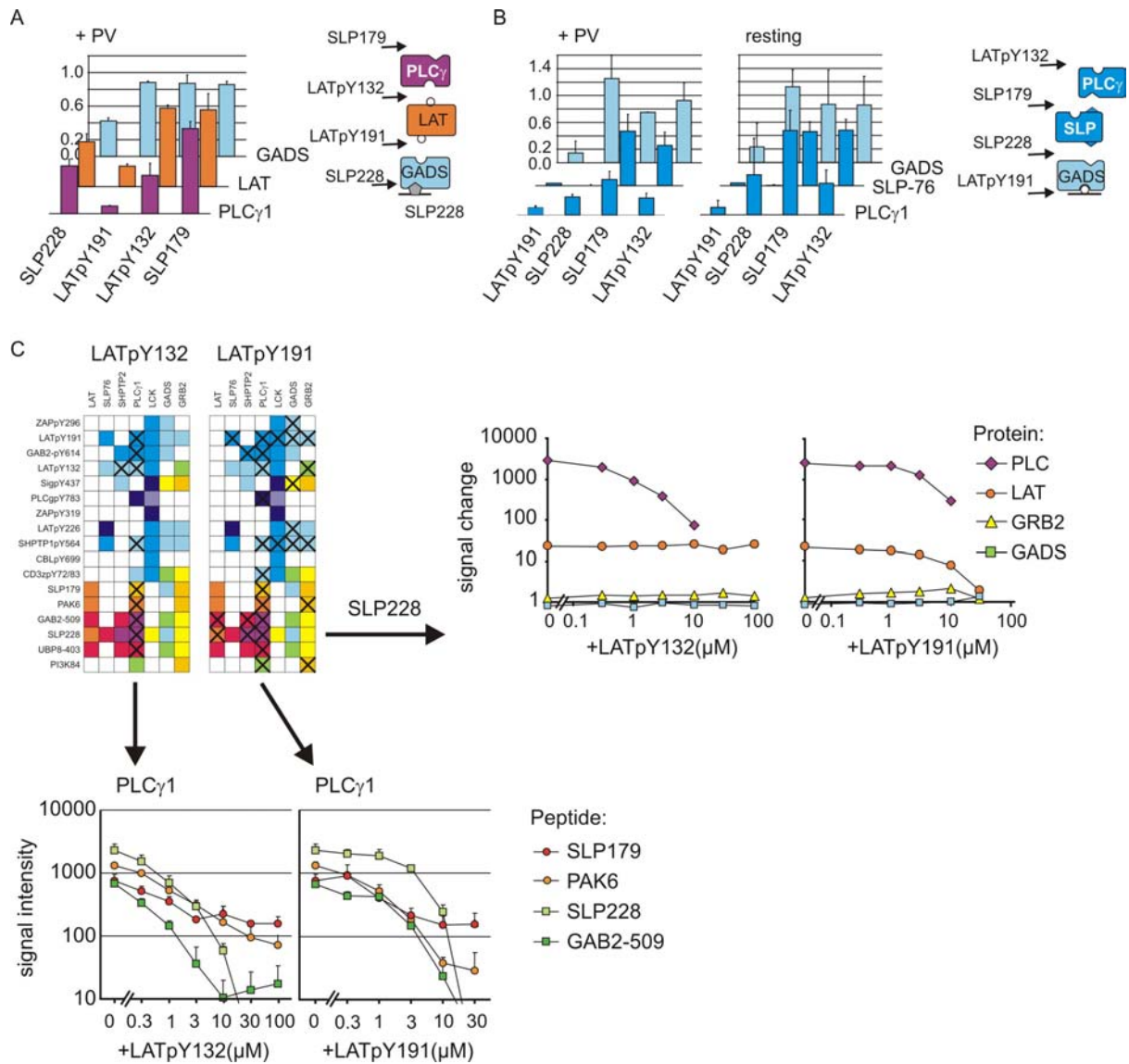
Figure 17: *Effects of competing peptides on the detection of proteins on the peptide array. Resting or pervanadate-treated (PV) Jurkat T-cells were lysed in the presence of the competitor peptides. A) Relative signal changes for PLCγ1, LAT, GADS on SLP228 for lysates of PV treated cells with and without addition of peptides LATpY191 (20 μM), LATpY132 (0.5 μM), SLP228 (20 μM), SLP179 (20 μM). Means and mean deviations from the mean of two independent experiments. B) Relative signal changes in the presence of competing peptides on spot LATpY191. Peptide concentrations as in A. Means and mean deviations from the mean of two independent experiments. C) Titration of lysates of PV-treated cells with peptides LATpY132 and LATpY191. Overview of protein signals affected by peptide, with a signal decrease of more than 50%, indicated by X (upper left). Relative signal changes between lysates of PV-treated cells with varying peptide concentration and resting cells on peptide spot SLP228, from one representative experiment (upper right). Influence of peptide titration on the signal intensity of PLCγ1 on diffent peptide spots, means and standard deviation from the mean of two experiments (lower panels).*

5.1.3.3   Effect of single protein deficiencies on the interactions network

The titration experiments had revealed the significance of individual interaction motifs for the functional organisation of the network. Next, we examined the impact of a loss of a multidomain protein on the organisation of the network, using the PLCγ1-deficient Jurkat-derivative JGamma1 [139].

Loss of PLCγ1 affected the formation of various complexes, notably on the preferential PLCγ1-interacting peptides. SLP76 on LATpY132 and LAT on SLP179 became undetectable, supporting the role of PLCγ1 for their recruitment in Jurkat cells (Figure 16 B). To analyze the role of PLCγ1 in complex formation, ratios of signal intensities from JGamma1 to Jurkat lysates were calculated for resting and stimulated cells (Figure 18). For proteins supposed to bind directly to immobilised peptides (e.g. GADS and GRB2 on LATpY191 and SLP228), only marginal changes were observed. However, PLCγ1-deficiency strongly inhibited phosphorylation-dependent recruitment of LAT to polyP peptides. Furthermore, in JGamma1-lysates, SHPTP2-signals on polyP-peptides were increased compared to WT Jurkat lysates, with no significant differences of SHPTP2 expression detected by Western Blot (not shown). As the SH2-domains of SHPTP2 and PLCγ1 share a common consensus motif, the lack of competing PLCγ1 may enable increased binding of SHPTP2.

The Jurkat derivative cell line JCAM 1.6 displays no LCK activity, due to a mutation affecting the kinase domain of LCK [140]. JCaM1.6 cells were used as a model for generally impaired TCR-downstream signalling capacity. For JCAM1.6 cells (Figure 16 C), the predominant signal decrease observed on pY peptides for Jurkat cells (Figure 16 A) was largely missing, agreeing with the role of LCK in starting a phosphorylation cascade. Effects were observed for ZAP70, a binding partner of activation motifs phosphorylated by LCK, and for proteins further downstream the kinase cascade, such as the ZAP70 substrates SLP76 and LAT. PLCγ1 became undetectable on most polyP peptides, likely due to missing phosphorylated LAT and SLP76 as mediators of binding. By contrast, pervanadate-dependent recruitment of SHPTP2 to polyP peptides was not affected. This suggests LCK independent, but phosphorylation-dependent formation of a complex between SHPTP2 and an SH3-SH2 adaptor protein.
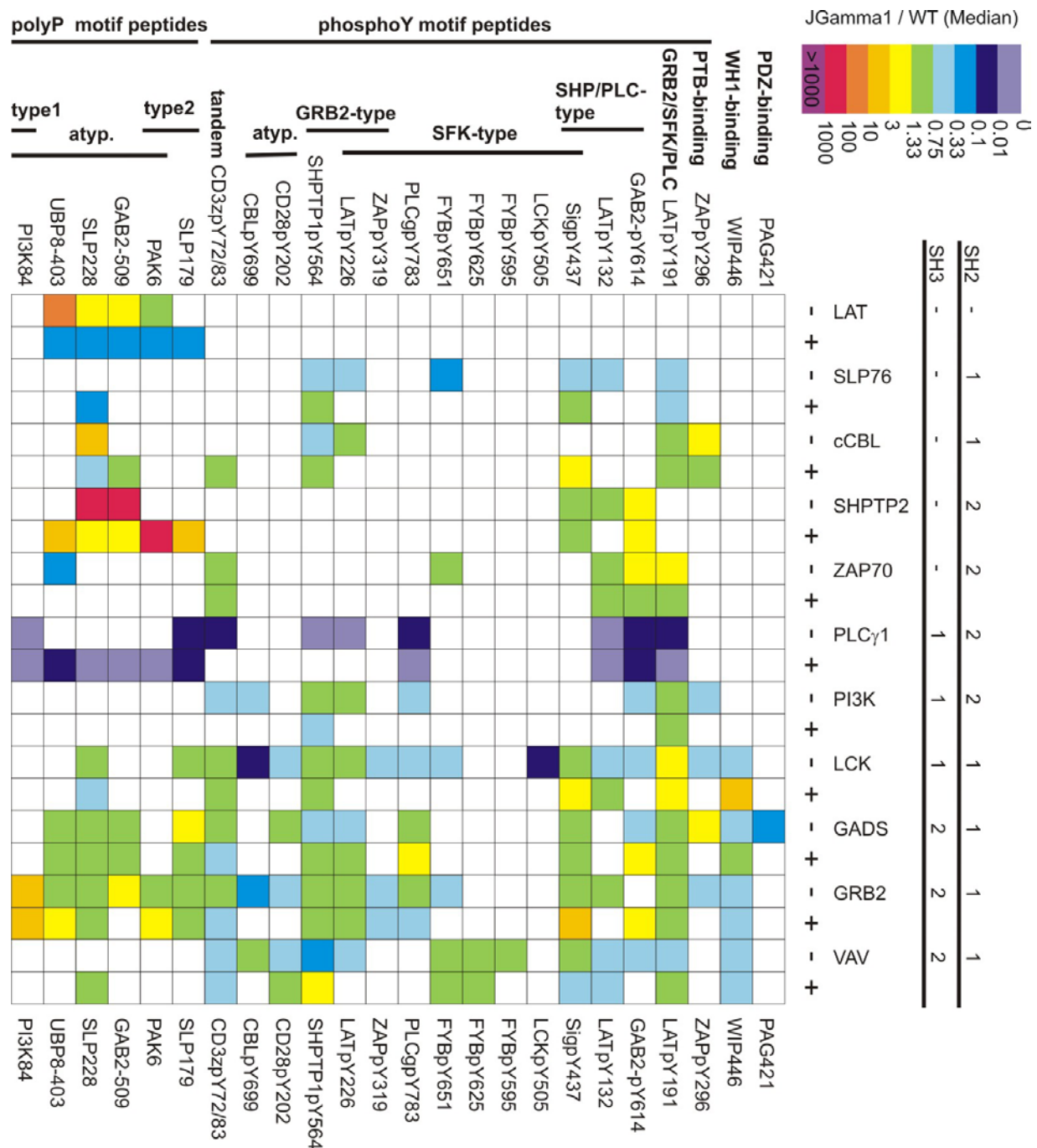
Figure 18: *Changes in protein signal intensity on the peptide microarray between PLCg1 deficient JGamma1 cells and "wildtype" Jurkat cells, expressed as background-corrected ratio JGamma1/WT. Lysates of resting (-) and pervanadate-treated (+) cells were used. The median ratio of 4 experiments is shown, if a minimum of 3 out of 4 experiments produced a signal above threshold.*

5.1.3.4 Stimulus-dependence and time course of protein interactions in T-cell activation

We next employed the peptide arrays to profile the timecourse of protein complex formation in a more physiological model of T-cell activation. Jurkat cells were stimulated for variable times with stimulatory anti-CD3 (clone OKT3), costimulatory anti-CD28 (clone 9.3), or both. On the arrays, distinct and reproducible changes in signal profiles were obtained for PLCγ1, LAT, SLP76 and PI3K (Figure 19). For PLCγ1, signal increases on polyP peptides were strongest after 2 min of CD3-stimulation, and then diminished. Only on SLP228, CD28 stimulation alone induced slight increases in PLCγ1 recruitment. CD3-CD28 costimulation augmented signal increases compared to CD3 stimulation without affecting their kinetics. For LAT, analogous signals were observed for CD3 stimulation, suggesting fast pY-dependent complex-formation with PLCγ1 and corecruitment to the array. For SLP, signal decreases on LATpY peptides were detected upon CD3 stimulation. Interestingly, this decrease was most pronounced after 10 min of stimulation, indicating that recruitment of SLP76 to the LAT complex occurred with slower kinetics than the phosphorylation of LAT and recruitment of PLCγ1. In the presence of antiCD28, signals of detection antibodies from mouse could not be quantified because of high overall backgrounds, accounting for the data points missing for LAT and SLP. For PI3K, no systematic signal changes were observed upon stimulation with CD3 or CD28 alone, whereas costimulation led to a signal decrease. Pervanadate stimulation was conducted in parallel as positiv control, yielding signal changes consistent with the antibody effects. Pervanadate effects were weaker than in the experiments presented above (Figure 16). Antibody stimulation required preincubation on ice, a condition that apparently also affected pervanadate-dependent cell activation.
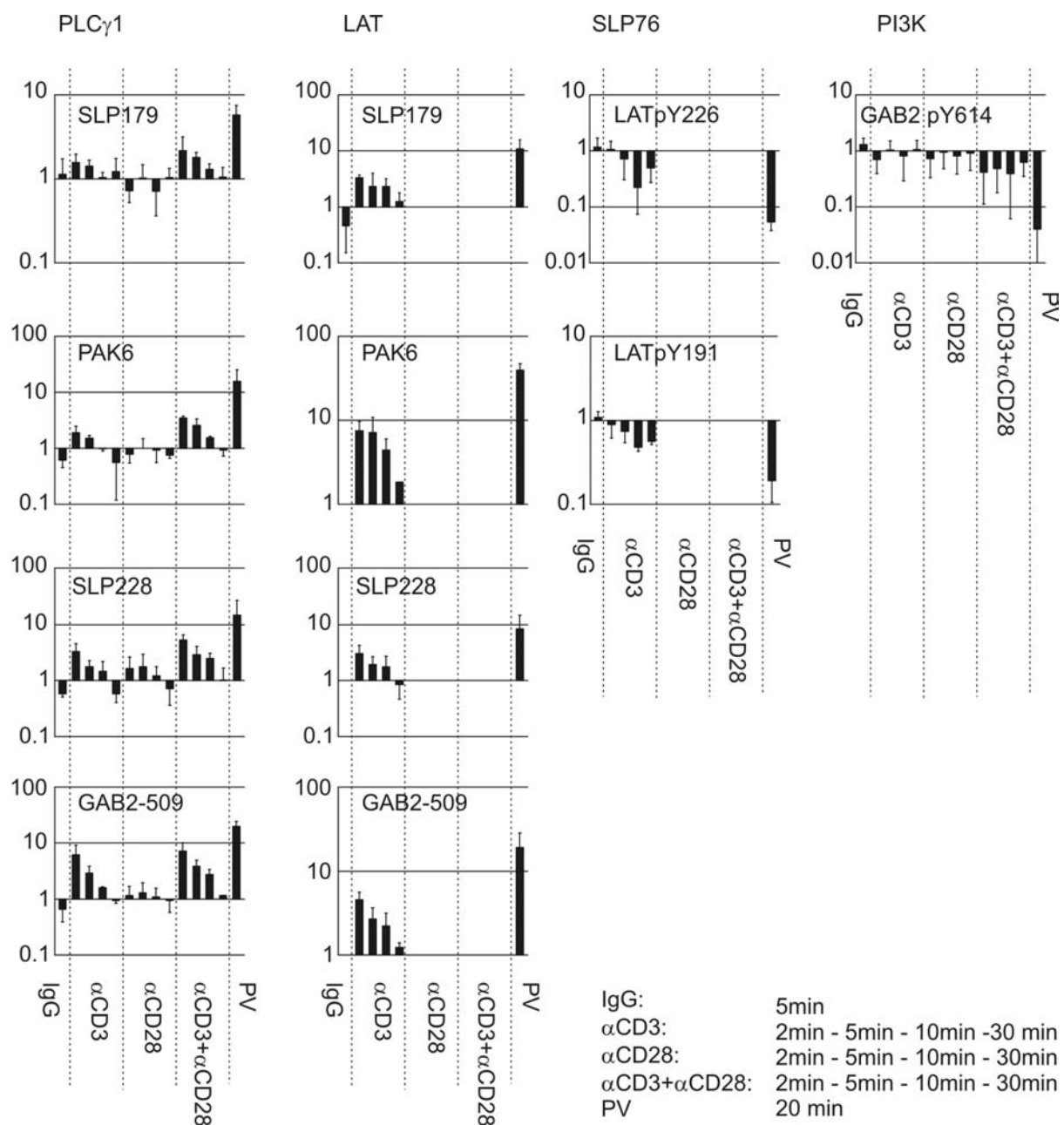
Figure 19: *Signal changes on the peptide microarray following treatment of Jurkat cells with stimulatory antibodies against the TCR/CD3-complex (αCD3) and the CD28 coreceptor (αCD28) for different time points. Ratios of stimulated versus resting cells. In the presence of the stimulation-antibody αCD28, high overall backgrounds forbade quantification of signals of detection antibodies from mouse, accounting for missing data points for LAT and SLP76. Negative control by mock-stimulation with an isotype antibody (IgG), positive control by pervanadate (PV). Signals for the protein indicated on top of each column of graphs, derived from the peptide spot indicated in each graph. Means and mean deviations of the mean of 3 experiments.*

5.1.3.5 Discussion

Signalling processes downstream of transmembrane receptors typically occur in a timeframe of minutes through rearrangement of a given repertoire of signalling components. While signal-induced fast degradation of single components may occur, the levels of most components remain unchanged and expression of further components is still far downstream. However, the molecular interactions of signalling components change significantly. We demonstrate how these changes in interaction can be detected in cell lysates using peptide microarrays.

We have shown previously that changes in the availability of a protein domain involved in a signalling-dependent protein-protein interaction can be detected by a capture peptide probing for the availability of the binding domain (chapter 5.1.1) [149]. This approach was now generalised for the parallel detection of different interactions. In addition, we exploit that proteins directly binding to capture peptides bring along their interaction partners, making microarrays a highly parallel variant of co-purification techniques. In a typical experiment (Figure 19), proteins bound by 24 capture peptides were probed with 8 different antibodies under 16 different conditions, yielding 3072 data points for the analysis of interactions in T-cell signalling using only 10^6 cells per array. In contrast to high throughput tag-based affinity purifications, the array-based approach does not require the introduction of recombinant components into the signalling network. Therefore, the molecular system under scrutiny is not already manipulated before the experiment begins.

On the molecular level, inducible tyrosine phosphorylations trigger the onset of complex formation. Therefore, additional pY sites generated through stimulation compete for SH2-proteins with the pY peptides on the array, while the cellular level of polyP motifs is not changed through stimulation. This may explain a general trend we observed for stimulation-dependent signal changes on the arrays: On pY peptides, signal decreases were dominant, while on polyP peptides signal increases dominated.

Especially on polyP peptides, we detected proteins without a cognate binding motif. Indeed, we were able to dismantle supposed complexes on the arrays in a stepwise and dose dependent manner through competition and titration with peptides corresponding to binding motifs between the proteins in the complex. This finding demonstrates, that detected proteins need not interact directly with the peptide, but may instead be brought along by another protein directly binding the peptide.
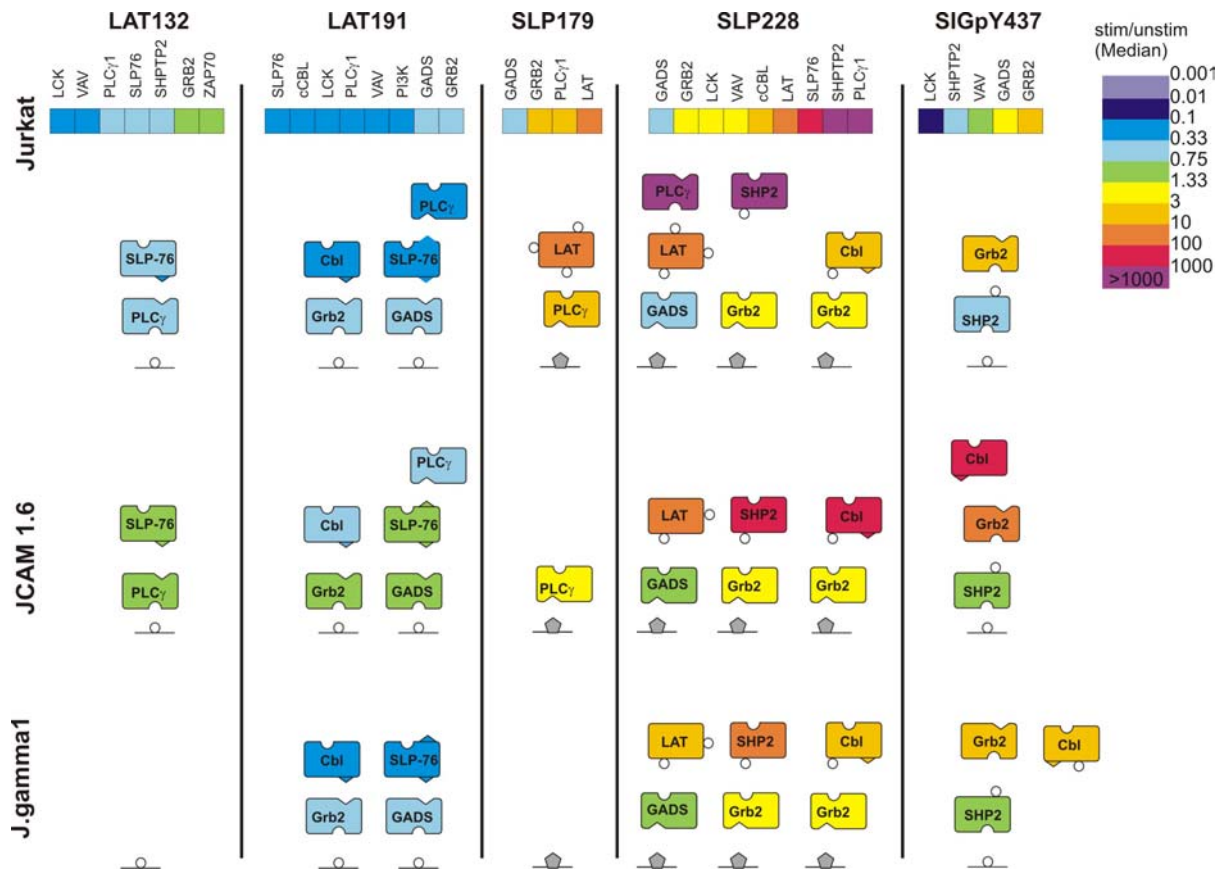
Figure 20: *Schematic diagram for selected proteins detected on the arrays and their supposed hierarchy of binding based on the relative signal change upon pervanadate treatment of cells (represented by the colour of proteins, taken from Figure 16). The immobilised peptides are depicted at the basis of the protein stacks. White circles depict a phosphorylation-dependent binding motif, grey pentangle a polyP motif.*

In lysates of resting cells, we detected the presence of polyP-SH3 domain mediated preformed complex 'nuclei'. For example, on LATpY132, representing a direct binding motif for PLCγ1, we observed stimulation-dependent decreases to the binding of PLCγ1 and SLP76 in Jurkat lysates. In lysates of PLCγ1-deficient Jurkat cells, both proteins were not detectable on LATpY132, suggesting PLCγ1-dependent recruitment of SLP76. For LCK-defective cells, both proteins were detectable, but their signals did not decrease upon stimulation. On LATpY191, corresponding observations were made for the preformed complex of GADS and SLP76. Taken together, these observations suggest that upon stimulation, the preformed complexes contributed to the assembly of larger, phosphotyrosine-dependent signaling complexes.

We realized that complex architectures inferred from the peptide competition experiments were correlated to the different magnitudes of signaling-dependent

signal changes for the different proteins detected on a given peptide. The more distant from the peptide, the more pronounced was the relative signal change for the protein (Figure 17, Figure 20). Assuming a linear chain of protein-protein interactions, this observation can be explained by the potentiation of changes from one level of protein binding to the next: If each of the interactions contributing to a linear complex on the immobilized peptide (peptide-A-B-C) occurred with a different probability after stimulation (peptide-A changing x-fold, A-B changing y-fold, B-C changing z-fold), then the chance to find the outermost protein C on the immobilized peptide would change x*y*z-fold. Per se, x, y, and z may each be larger or smaller that 1. While situations are conceivable where the increases and decreases balance, we found that the relative magnitude of signal changes as described above was a useful indicator of the interaction architectures.

For the interplay of stimulation of TCR/CD3 and CD28 by stimulatory antibodies, our peptide microarrays allowed the analysis of timecourses of protein complex formation in a parallel manner. We demonstrate that the recruitment of SLP to the LAT-signalosome follows a different timecourse than the recruitment of PLCγ1. Recently, an analysis of phosphorylation kinetics in early T-cell signalling showed, that phosphorylaton of LAT-residues Y132 and Y191 reaches maximum levels within two minutes [45]. Our data shows that the arrayed LATpY191 is maximally competed by its cellular counterpart after 10 minutes of stimulation, suggesting that LAT-phosphorylation is not the rate-limiting step for formation of the LAT-signalosome. Co-stimulation with anti-CD28 and anti-CD3 led to more distinct, and additional signal changes concerning PI3K, compared to CD3 stimulation alone. This finding demonstrates the potential of the peptide microarrays for integrated network analysis in systems with multiple stimuli. Likewise, for the analysis of signaling systems missing single proteins, peptide arrays provide a means to uncover effects of molecular links on interaction subsystems.

In conclusion, peptide microarrays provide a tool for the highly parallel analysis of protein-protein interactions in cellular signal transduction, bridging the gap between binding studies with single proteins and complex interactomics experiments. Quantitative analysis of signal changes upon stimulation and competition experiments provide a wealth of information on the functional organisation of protein complexes. This approach will benefit from the use of arrayed peptide libraries derived from the literature as well as by motif prediction [20,14]. In combination with antibody libraries the simultaneous probing for all potential molecular interactions in a signalling network can deepen our understanding of signal transduction in a systems biological view.

5.2   FCS and FCCS for the detection of signalling complexes

Parts of the data presented in this chapter have been published [145,144]

The analysis of protein complexes still mainly relies on cell lysis followed by the application of biochemical techniques. A major advantage compared to intracellular techniques is that complexes of endogenous proteins can be detected, eliminating the need for the generation of fusion proteins and ensuring that complex formation cannot be disturbed by the respective tags. Moreover, in contrast to FRET and BRET, signals are directly correlated with a physical interaction of the proteins.

The characteristic feature of classical biochemical analyses for protein complex analysis is the separation of the protein complex from the remaining cell lysate by affinity purification. Specific binders for one constituent of the complex are coupled to a polymer matrix. Washing of the matrix is necessary during separation, but obviously favours the dissociation of weakly interacting partners. Moreover, the further handling steps for complex detection, e.g. as required for western blotting, are cumbersome and time consuming, limit sample minimisation and complicate automation. Therefore, advances in biochemical methods for the analysis of protein complexes are still urgently needed.

We consequently developed a separation free method for the rapid detection of interactions of endogenous proteins directly in crude cell lysates, combining high detection sensitivity with a minimum of handling steps and consumption of sample and reagents. FCS (Figure 21 A) and FCCS (Figure 21 B) were used for detection.
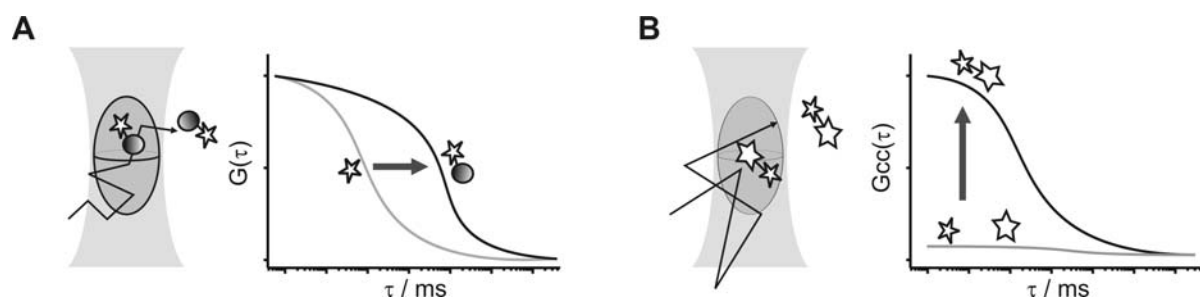

Figure 21: *Schematic of interaction analysis by FCCS and mass-tag FCS. A) Attachment of a mass-tag to a fluorophore-labelled particle slows down the diffusion of the particle, leading to a right shift of the autocorrelation function. B) Two spectrally distinct fluorophores attached to a diffusing particle give rise to a cross-correlation.*

5.2.1 FCS of ZAP70-YFP in cells and lysates

5.2.1.1 Cellular measurements

In initial experiments, we attempted to characterise the stimulation-dependent recruitment of ZAP70-YFP to the TCR/CD3 complex by cellular FCS measurements. We used a cell line expressing ZAP70-YFP at a level of 2.5 times that of endogenous ZAP70 [149]. To induce early steps of T-cell signalling, cells were incubated with sodium pervanadate [142]. This phosphatase inhibitor shifts the balance of kinase and phosphatase activities, inducing the phosphorylation of CD3-subunits and thereby the binding of ZAP70 to the receptor complex at the plasma membrane [152].

Upon pervanadate treatment, relocation of ZAP70-YFP from throughout the cell to the membrane was clearly visible by microscopy[149] (Figure 10, p. 43). FCS was carried out alternatingly in cells with and without addition of pervanadate to the incubation buffer over the duration of 60 min.

When the confocal volume was placed directly on the membrane, a very strong initial bleaching was observed in pervanadate-treated cells, indicating that proteins recruited to the membrane were immobile on the timescale accessible to FCS-measurements (not shown). While those fluorophores clearly corresponded to the ZAP70-YFP recruited to the membrane, in this case cellular FCS did not add significant information to the microscopic image.
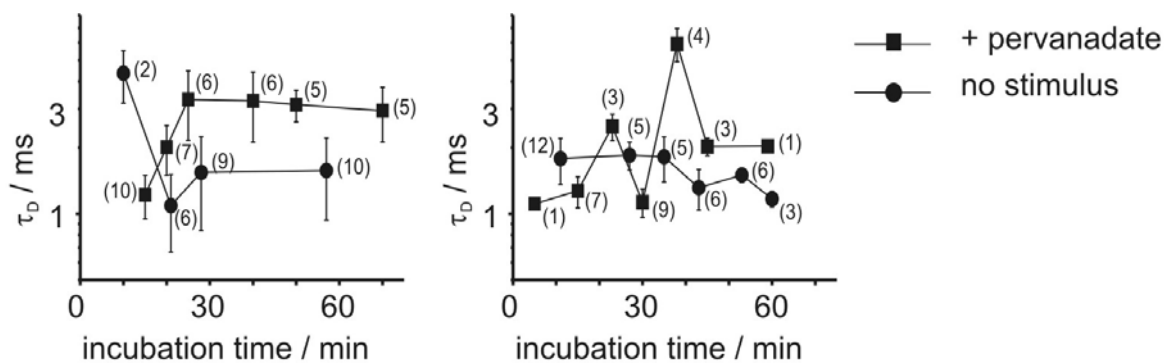
Figure 22: *Intracellular diffusion times of ZAP70-YFP. Panels show independent experiments. Each value is the mean determined from repeated measurements in one individual cell. The number in parenthesis indicates how many of the 15 repeated measurements per cell could be fitted to a function corresponding to Eq. 17. The first measurement was routinely discarded, as it was compromised by bleaching of immobile molecules. Error bars indicate mean deviations from the mean. For pervanadate stimulation, pervanadate was added to the incubation buffer at time 0. Individual cells were measured one after the other, over a total incubation time of 60 minutes.*
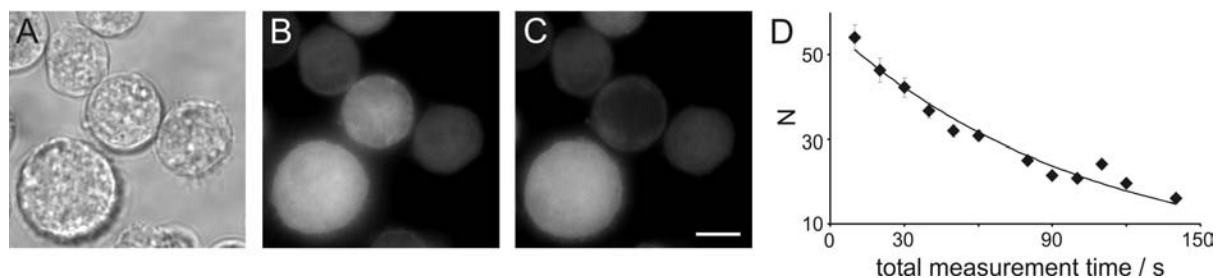
***Figure* 23:** *Decrease of cellular fluorescence during FCS measurements in individual cells. A-C) Transmission and epifluorescence images of cells expressing ZAP70-YFP fusion protein before (B) and after (C) FCS measurement in the central cell. The bar denotes 5 μm. D) The visible decrease in fluorescence was reflected by a decrease in the number N of fluorescent particles derived from curve fits of sequentially recorded intracellular autocorrelation functions. The error bars indicate fitting errors. A monoexponential decay function was fitted to the data points in order to estimate the original N before photobleaching during measurements occurred.*

When the confocal volume was placed in the cytoplasm, the observed diffusion times of ZAP70-YFP did not reproducibly differ between pervandate-treated and resting cells (Figure 22).

As most protein-protein interactions, the association of ZAP70 with CD3 subunits has been originally deduced by co-immunoprecipitations in cell lysates [21,34]). Therefore, our next steps were to investigate, whether FCS could (i) detect complexes of ZAP70-YFP from crude cell lysates and (ii) provide information complementary to co-immunoprecipitation.

To validate lysis, we compared ZAP70-YFP numbers measured in live resting cells and in lysates from resting cells. For intracellular measurements,the confocal volume was placed in a membrane-proximal region of the cell. Transmission and epifluorescence images were taken of the cells before carrying out FCS (Figure 23 A, B). 15 consecutive measurements of 10 s each were conducted. Afterwards, epifluorescence images were taken again, to ensure cells were still in position (Figure 23 C). In cellular FCS, photobleaching was not negligible. Curve fits for the individual autocorrelation curves from 15 measurements according to Eq. 17 revealed a continuous decrease of the number N of ZAP70-YFP molecules. Not all of the 15 autocorrelation curves recorded per cell could be analysed, probably due to microscale-movements of the cell. By plotting N against the total measurement time, the initial number N_0 of particles at measurement time 0 could be inferred from fitting with a monoexponential decay function [156] (Figure 23 D). Using an estimate for the size of the confocal volume (Eq. 6) cytoplasmic concentrations of ZAP70-YFP were calculated. From the images taken of each analysed cell, individual cell

diameters were determined, and total numbers of ZAP70-YFP per cell were calculated assuming spherical cells with homogenous distribution of ZAP70-YFP. On average, $1.7*10^6 \pm 0.5*10^6$ molecules of ZAP70-YFP were found per cell, agreeing well with the number inferred from FCS-measurement in lysate, which was $1.2*10^6 \pm 0.1*10^6$ per cell[149] (see chapter 5.1.1).

5.2.1.2 Measurements in lysates

FCS was carried out in lysates of resting and pervanadate-treated cells. Cells expressing free YFP served as a control. For cells expressing ZAP70-YFP, three parameters changed with pervanadate treatment (Figure 24 A). First, the diffusion coefficient decreased, indicating incorporation of ZAP70-YFP into complexes of higher molecular weight [149].

Second, the number of diffusing fluorescent particles decreased. As the total fluorescence in the lysates remained unchanged, this decrease was not due to a loss of ZAP70-YFP. Third, the brightness of ZAP70-YFP-containing particles (expressed in counts per molecule, cpm) increased.

In comparison, pervanadate had no effect in lysates of control cells expressing free YFP. All results were evaluated for significance by Student's t-test. For lysates of ZAP70-YFP expressing cells, p-values for changes upon pervanadate treatment were $10^{-9} < p < 10^{-6}$. In contrast, for lysates of cells expressing free YFP, p-values were larger by several orders of magnitude and differences were smaller than ± 1 standard deviation. The results were highly reproducible for independent experiments (not shown). Taken together, these changes indicated that signalling complexes containing more than one molecule of ZAP70-YFP were formed. By comparison of the cpm, the average number of ZAP70-YFP molecules per fluorescent particle was estimated to increase from 1 to 1.6 upon pervanadate treatment. As dimerisation of GFP-derivatives occurs with an approximate K_d of 100 µM [75], YFP and YFP-fusion proteins can be safely assumed to be monomeric at the nanomolar concentrations used in FCS.

Approximate average MWs for the diffusing species were calculated (Table 9). The viscosity η of cell lysates was estimated from measurements of free YFP with the known molecular weight of 29kD. Prior to pervanadate treatment, the MW was in the range of 350 kDa. After pervanadate treatment the MW increased to approximately 1500 kDa. These results suggest that ZAP70-YFP was already incorporated into complexes in resting cells.
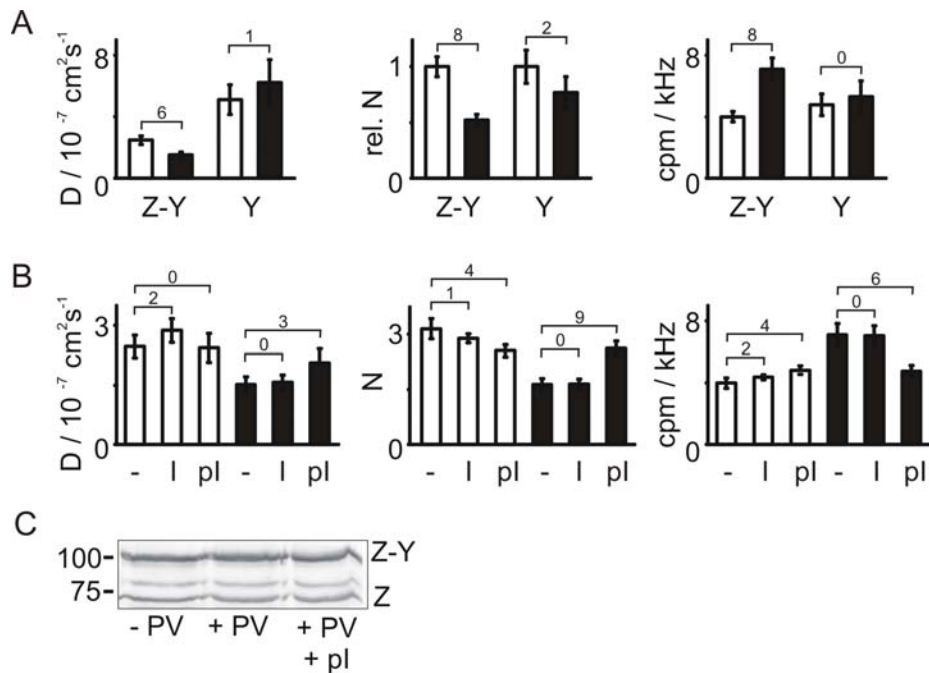
Figure 24: *Detection of protein complexes in crude cell lysates by fluorescence correlation spectroscopy. A) Pervanadate-dependent formation of complexes containing ZAP-70-YFP. Black columns refer to lysates of pervanadate-treated cells, white columns to those of resting cells. Two cell lines were used, expressing ZAP-70-YFP (Z-Y) or free YFP (Y). For ZAP-70-YFP, the diffusion coefficient D (left panel) and the concentration of fluorescent particles (expressed by the number N of particles in the detection volume, center panel) decreased while the particle brightness (expressed in cpm, right panel) increased upon pervanadate treatment. To account for different expression levels of ZAP-70-YFP and free YFP, N was normalised to 1 for the lysates of resting cells. B) Reversion of pervanadate-dependent complex formation by pITAM peptide (pI). pITAM or non-phosphorylated control peptide ITAM (I) were added to a final concentration of 1 μM to lysates of cells expressing ZAP-70-YFP (-, no peptide). Error bars correspond to the standard deviation of 10 repeated measurements of one representative experiment. Numbers x above columns designate $10^{-(x+1)} <$ $p < 10^{-x}$ in Student's t-test. Corresponding data combined from three independent experiments is shown in the supplementary Fig. 1. C) Western blot against ZAP-70 in lysates of untreated (-PV) and pervanadate-treated (+PV) cells expressing ZAP-70-YFP. pITAM (+pI) was used at 1 μM. Equal amounts of total protein were loaded.*

To further exclude a pervanadate-dependent degradation of ZAP70 or unspecific loss of protein due to cell death prior to lysis, lysates were analyzed for total protein content (not shown) and ZAP70-levels (Figure 24 C). Neither was influenced by pervanadate treatment.

ZAP70 is known to bind via its tandem SH2 domain to tyrosine-phosphorylated ITAMs of CD3ϵ and ζ [21,34]. A competitor peptide (also employed on

the peptide arrays, chapter 5.1, p.40) was used to test whether this interaction contributed to forming the observed complexes. This peptide, corresponding to the tyrosine-phosphorylated ITAM1 of CD3ζ (pITAM), partially reversed the effects of pervanadate stimulation. An unphosphorylated control peptide (ITAM) had no effect (Figure 24 B). Again, the level of ZAP70 and ZAP70-YFP was not altered (Figure 24 C). These results confirm the contribution of the tandem SH2 domain of ZAP70 to complex formation.

However, while FCS has proven to be a method suitable for protein complex detection in microliters of cell lysate, the identity of the actual binding partner of ZAP-70-YFP had not been determined. Therefore the next step was to develop an approach for the FCS-based identification of interacting proteins.

Table 9: *Calculation of approximate molecular weights from diffusion times of ZAP70-YFP containing particles (according to Eq. 10, Eq. 12, and Eq. 13). Using the molecular weight and diffusion times of free YFP, the viscosity of the lysates was estimated as 1.8 10^{-3} Pa s.*

Lysate	τ_D / µs	D / 10^{-7} cm^2 s^{-1}	M / kDa
ZAP70-YFP, - PV	256 ± 25	2.4 ± 0.2	353 ± 105
ZAP70-YFP, + PV	419 ± 43	1.5 ± 0.2	1550 ± 473
YFP, - PV	126 ± 19	4.9 ± 0.7	42 ± 19
YFP, + PV	105 ± 20	5.9 ± 1.1	25 ± 14

5.2.2 Detection of signalling complexes in cell lysates by indirect immunolabelling

Antibody-based detection of protein interactions benefits from the large and ever growing repertoire of specific primary antibodies that can be combined to probe for diverse pairs of interacting proteins. However, for monitoring protein-protein interactions by FCS-based techniques, the interaction partners have been in most instances directly covalently labelled, either by chemical conjugation to a fluorophore or by genetic fusion to a fluorescent protein. Although FCS has been used for characterisation of antigen-antibody interactions per se [157,158], to our knowledge only one example exists in which fluorescently labelled primary antibodies have been employed as a labelling tool in FCCS [159].
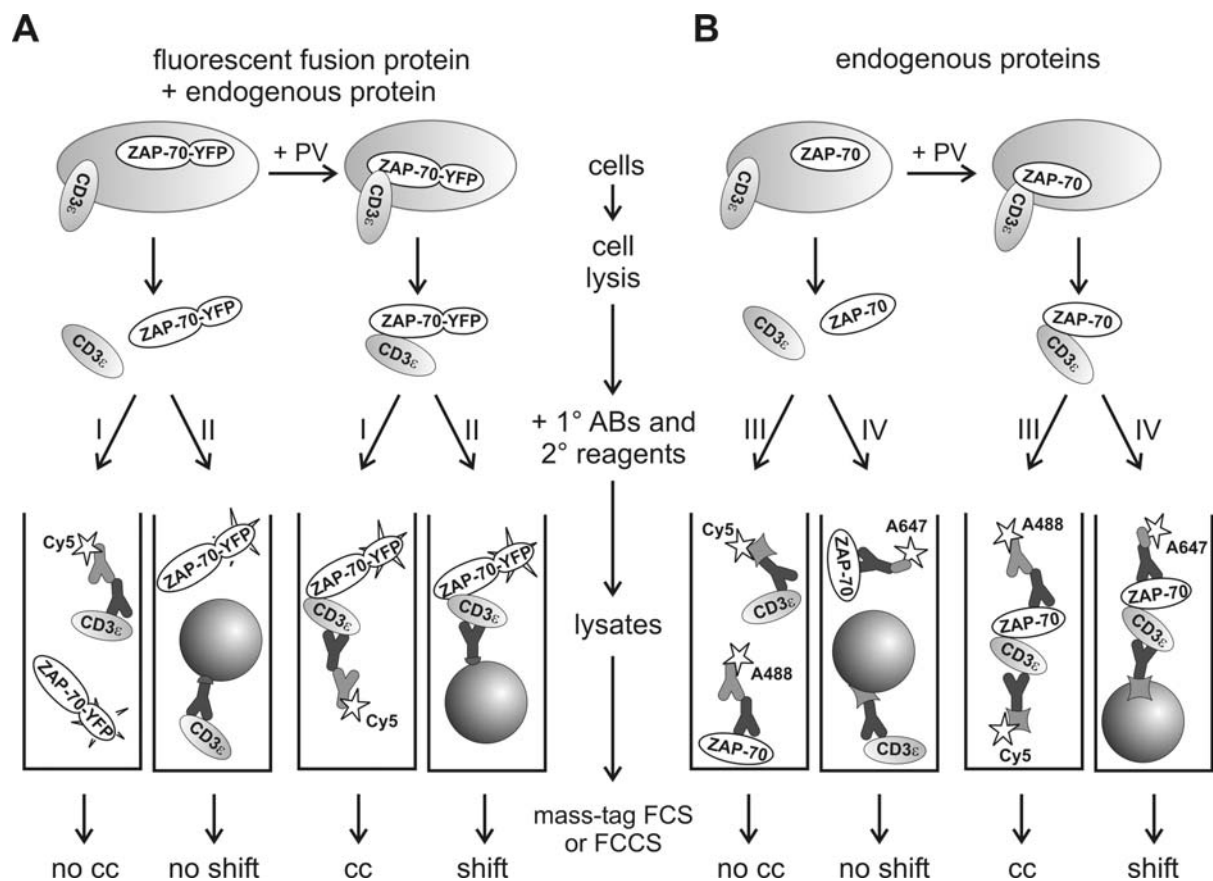
Figure 25: *Detection of complexes by FCCS and mass-tag FCS, exemplified for the pervanadate-induced (+PV) interaction of ZAP-70 with CD3ε. A) For the detection of complexes containing a YFP-fusion protein of ZAP-70, a primary antibody against the possible interaction partner CD3ε and a matching secondary reagent were added to the lysate. This was (I) a Cy5-labelled secondary antibody or (II) a protein G-functionalised microbead. The interaction was detected (I) by the cross-correlation (cc) of YFP and the second fluorophore or (II) by the shift of the autocorrelation function towards longer diffusion autocorrelation times of YFP. B) For the detection of complexes of endogenous proteins, two sets of primary antibodies and matching secondary reagents were used. One secondary reagent introduced a fluorophore, the other one (III) a second fluorophore or (IV) a mass-tag. (A488, A647: fluorophores Alexa488, Alexa647)*

The introduction of an additional binding equilibrium, i. e. that of the antibody to its antigen, is a concern when using this strategy. Moreover, in order to fully exploit the benefit of antibody-based strategies for FCS and FCCS, the detection should be based on indirect immunolabelling to avoid the need for the direct labelling of primary antibodies. However, the presence of even more binding equilibria might compromise the detection of complexes. Here we show that contrary to these expectations, indirect immunolabelling represents a straight-

forward, versatile and specific way to confer properties detectable by FCS or FCCS to proteins in lysates.

Two approaches were followed: labelling of the interaction partners with with two spectrally different fluorophores for FCCS-detection, or, alternatively, labelling of one interaction partner with a fluorophare and the other one with a nanoparticle as mass tag for FCS-detection (Figure 21). Both approaches were initially established for the interaction of ZAP70-YFP with CD3ε and ζ. (Figure 25 A).

5.2.2.1   Mass-tag FCS

FCCS is instrumentally more demanding than FCS, as two lasers for excitation and two detectors are required, and spatial overlap of the detection volumes must be ensured. Additionally, fluorophores with little spectral overlap must be used to avoid FRET and cross-talk. Consequently, we first tested FCS as an alternative to co-immunoprecipiation by indirectly immuno-labelling one protein in a complex with a fluorophore and the other one with a nanoparticle as mass-tag [160].

In single channel FCS, interactions are detected by a shift of the autocorrelation function towards longer autocorrelation times τ, reflecting the smaller diffusion constants of complexes as compared to their constituents alone. Detectable shifts require a substantial mass increase. Binding of antibodies has been employed to analyze molecular complexes by FCS [161], however, for protein complexes the additional molecular weight of a primary antibody may not add sufficiently to the total molecular weight to allow a distinction based on shifts of the diffusional autocorrelation times.

Colloidal paramagnetic nanoparticles of 50 nm diameter functionalised with proteinG or streptavidin were used. First, the influence of the presence of nanoparticles on FCS-measurements was assessed with a simple system, in which no interactions between the diffusing fluorophore rhodamine-6-G and the nanoparticles should occurr. While apparent numbers of fluorophores increased with the concentration of nanoparticles (as seen from the decrease of the autocorrelation amplitude, Figure 26 A), autocorrelation diffusion times τ_D remained constant (Figure 26 B). As changes in τ_D upon mass-increase due to interaction constitute the readout parameter for FCS-based complex analysis, this result demonstrated that shifts in t_D should reflect binding to the n anoparticles and not an artefact caused by changes in the composition of the sample.
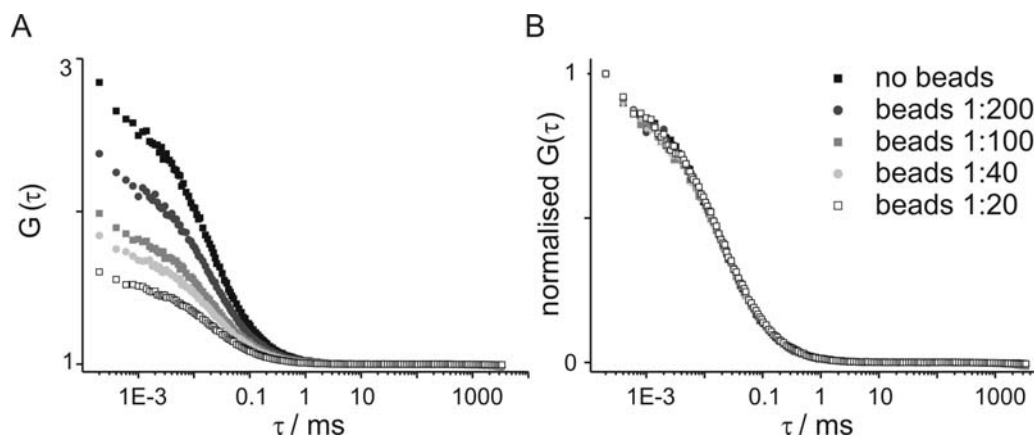
Figure 26: *FCS in solutions with identical concentrations of Rhodamine-6-G and various dilutions of protein G nanoparticles to the stock product. A) Autocorrelation curves and B) standardised autocorrelation curves of 10 measurements each.*
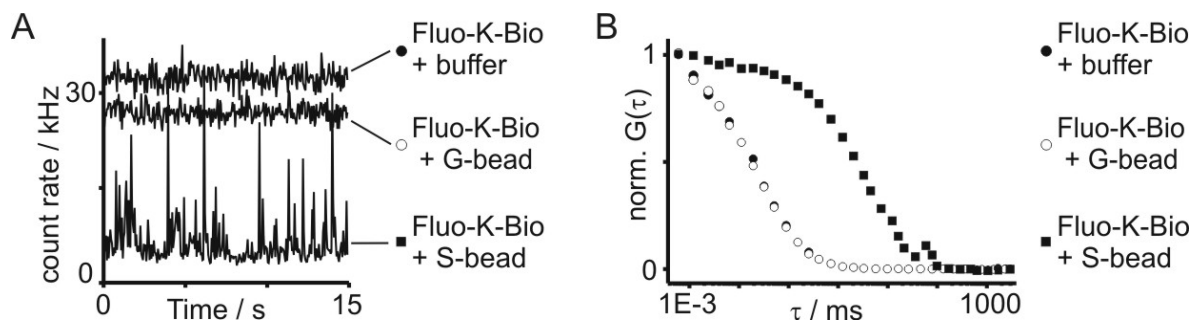
Figure 27: *Lysine functionalised with biotin and fluorescein (Fluo-K-Bio) employed as a fluorescent probe for FCS in the presence of microbeads. A) Count rates of one representative out of ten measurement intervalls of 15 s. B) Normalised autocorrelation curves calculated from ten measurements.*

The effect of nanoparticle-binding on parameters detected by FCS was characterised by a simple positive control. Lysine functionalised with biotin via its N_ε-amino group and with 5(6)-carboxyfluorescein via its N_α-amino group (Fluo-K-Bio) was subjected to FCS measurement either alone or in the presence of streptavidin-functionalised or proteinG-functionalised nanoparticles (Figure 27). Compared to a bead-free solution of Fluo-K-Bio, the addition of beads functionalised with protein G to Fluo-K-Bio led to a slight decrease in the count rate (Figure 27 A) while the autocorrelation curve was not shifted (Figure 27 B). In contrast, addition of beads functionalised with streptavidin led to a strong decrease in the count rate at most timepoints with frequent high peaks during the measurement intervall (Figure 27 A). The autocorrelation curve of Bio-K-Fluo in the presence of streptavidin-beads was shifted strongly towards longer correlation times (Figure 27 B).
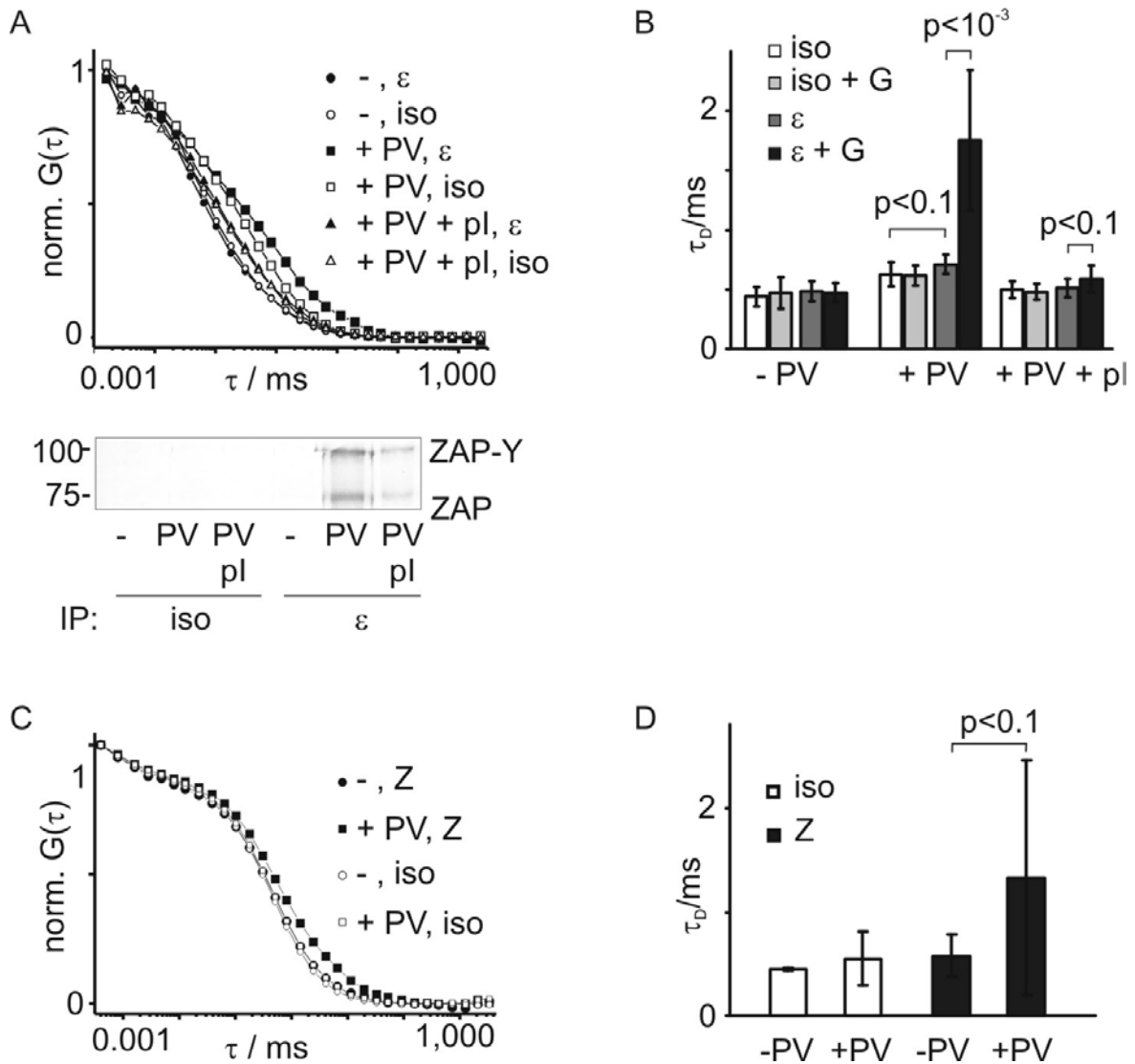
Figure 28: Identification of the constituents of protein complexes in cell lysate by mass-tag FCS. A - B) Interaction of ZAP-70-YFP with CD3ε. Lysates were prepared from resting (-) or pervanadate-treated (+PV) cells. pITAM (pI) was used at a concentration of 2 μM. Lysates were incubated with anti-CD3ε antibody (ε) or a non specific isotype (iso) and protein G beads. A) Normalised average autocorrelation curves from ten repeated measurements of one representative experiment. Western blotting for ZAP-70 in the identical samples. B) Influence of the addition of primary antibodies with and without mass-tag on the relative diffusion time of ZAP-70-YFP-containing particles. Means and standard deviations of ten repeated measurements of one representative experiment are shown. C-D) Mass tag-mediated detection of the interaction of endogenous ZAP-70 and CD3ε. Biotinylated hamster anti-CD3ε antibody, streptavidin-beads, mouse anti-ZAP-70 antibody (Z) and anti-mouse Fab-Alexa647 were added in one step. For negative controls, a non specific mouse isotype antibody (iso) was used. C) Average autocorrelation curves and D) diffusion times τ$_D$ as means and standard deviations from 10 repeated measurements of one representative experiment.

In the first experiments, detection was based on the intrinsic fluorescence of ZAP70-YFP (Figure 25 A, Figure 28 A, B). Incubation with anti-CD3ε antibody and protein G-beads led to a pronounced right-shift of the autocorrelation function in lysates of pervanadate-treated cells, resulting in a significantly ($p<10^{-3}$) increased diffusion autocorrelation time τ_D. Autocorrelation curves from samples containing an isotype antibody instead of anti-CD3ε followed the changes described for ZAP70-YFP (Figure 24 A). Addition of the inhibitory pITAM peptide completely reversed the stimulation dependent increase of τ_D. Alle FCS measurements were carried out in 20 µl sample volume. 130 µl of the same samples were subjected to immunoprecipitation of CD3ε and western blotting for ZAP-70, confirming their pervanadate-induced interaction and a residual interaction after pITAM addition.

We next extended the detection by mass-tags to complexes of endogenous proteins (Figure 25 B, Figure 28 C,D). Biotinylated anti-CD3ε-antibody, streptavidin-conjugated microbeads, anti-ZAP70 antibody and cognate secondary Fab-fragment labelled with Alexa-647 were added to lysates of 3A9 cells. In lysates of pervanadate-treated cells, τ_D of the fluorescent probe was reduced, indicating interaction of ZAP70 with CD3ε. In control samples, an isotype antibody was used instead of anti-ZAP70, and no changes of τ_D were observed upon pervanadate-treatment.

The pervanadate-dependent increase of the diffusion time τ_D was reproducibly detected for the interaction of endogenous ZAP70 and CD3ε. This showed in a proof-of-principle fashion, that FCS and indirect immunolabelling with one fluorophore and one mass tag can be employed to detect signalling-dependent interactions of endogenous proteins from a few microliters of crude cell lysate.

However, the standard deviations of the repeated measurements were always very high (Figure 28 D). This was likely caused by stochastic occurrence of differently sized fluorescent complexes of nanobeads, primary antibodies, target proteins and fluorophore-labelled F(ab) fragments. While the method would still allow binary decisions on whether or not an investigated protein-protein interaction takes place, it would not allow detection of gradual differences. We therefore searched for alternatives for mass-tag-labelling in the correlation spectroscopy based detection of protein-protein interactions.

5.2.2.2 Fluorescence Cross Correlation Spectroscopy

We opted for fluorescence cross correlation spectroscopy (FCCS; Figure 21 B). Again, for first experiments the 3A9 cells expressing ZAP70-YFP at a level 2.5-fold over that of endogenous ZAP70 [149] were used (Figure 25 A). Cells were activated by incubation with the phosphatase inhibitor sodium pervanadate [142]. Lysates were prepared of pervanadate-treated cells and untreated control cells. The YFP moiety of ZAP70-YFP served as one fluorescent probe for FCCS. The presence of CD3ε or ζ in a complex with ZAP70-YFP was probed using cognate monoclonal antibodies and Cy5-labelled secondary antibodies.

In FCCS, the amplitude of the cross-correlation function is a measure of the fraction of particles carrying both fluorophores (Figure 4). For CD3ε, a pronounced cross-correlation between YFP and Cy5 was observed in lysates of pervanadate-treated cells. In lysates of resting cells and of pervanadate-treated cells lacking the anti-CD3ε antibody, no cross-correlations were observed. Analogous changes were observed for the interaction of ZAP70-YFP with CD3ζ. The cross-correlation amplitudes were considerably lower than in the experiments probing for the interaction with CD3ε, likely due to different affinities of the antibodies for their respective targets (Figure 29 A). For changes upon pervanadate treatment, p-values of Student's t-test were $p < 10^{-7}$ for detection of the interaction with CD3ε and $p < 10^{-6}$ for the detection of the interaction with CD3ζ. Control samples were prepared without addition of primary antibody against CD3ε or CD3ζ. All control samples displayed only minimal crosscorrelation amplitudes, irrespective of pervanadate treatment. Student's t-test for comparison of samples with and without primary antibody revealed $10^{-2} < p < 0.5$ for lysates from resting cells, and $10^{-10} < p < 10^{-5}$ for lysates from PV-treated cells (not shown). The results were highly reproducible for independent experiments. Addition of the inhibitory pITAM peptide significantly decreased the cross-correlation amplitude of ZAP70-YFP and indirectly immunolabelled CD3 ε or ζ relative to the value determined in lysates of stimulated cells without addition of peptide.

Addition of an unphosphorylated control peptide was without effect. Both peptides were used at a concentration of 1 µM (Figure 29 A).The inhibitory action of the pITAM peptide was further utilised for titration of complexes with increasing concentrations of peptide. pITAM was present in final concentrations between 0.1 µM and 5 µM in the lysate of PV-treated cells. With increasing pITAM concentration, the cross-correlation amplitude decreased, revealing an IC_{50} of 1 µM pITAM-peptide for the interaction of ZAP-70-YFP and CD3ε (Figure 29 B).
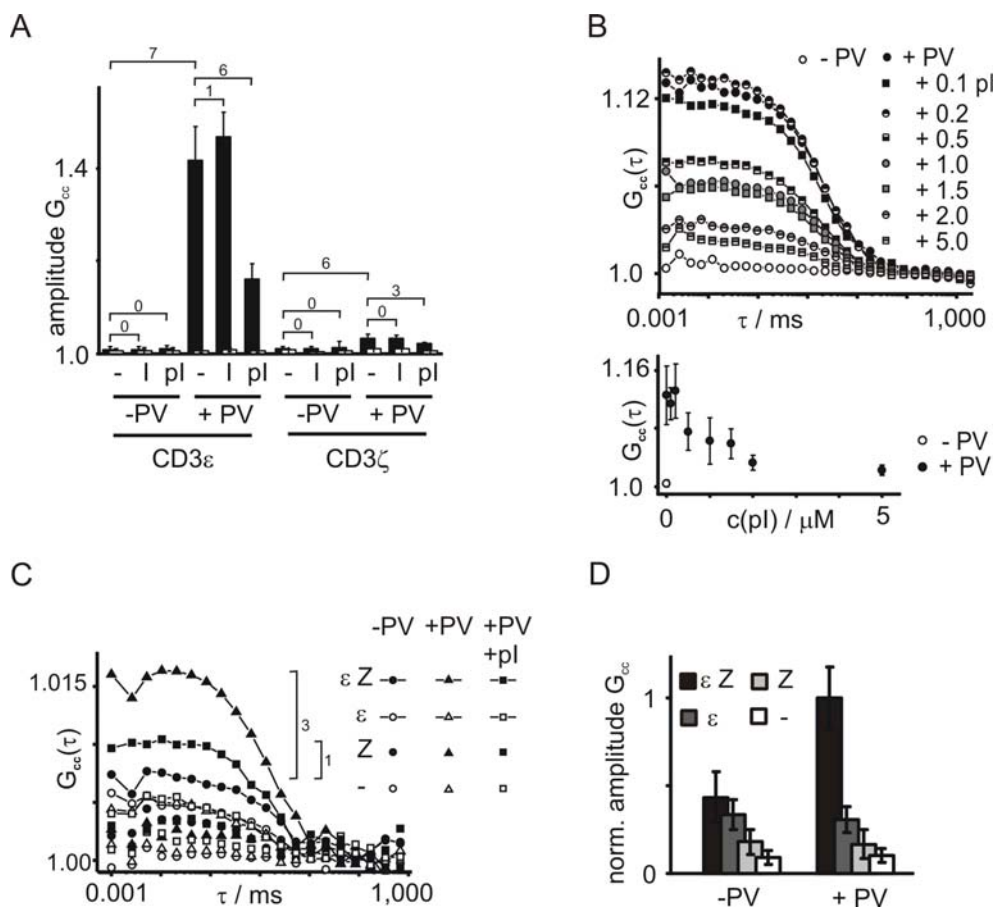
Figure 29: *Identification of the constituents of protein complexes in cell lysates using FCCS. Lysates were prepared from resting (-PV) or pervanadate-treated (+PV) cells. Optionally, ITAM- (I) or pITAM-peptide (pI) was added. A) Cross-correlation amplitudes for the interaction of ZAP-70-YFP with CD3ε or CD3ζ, labelled by addition of anti-CD3ε or -ζ primary and Cy5-conjugated secondary antibodies (black columns). In controls, primary antibodies were omitted (white columns). Means and standard deviations for one representative experiment are shown. Numbers x above columns designate p-values for comparison of samples containing primary antibody ($10^{-(x+1)} < p < 10^{-x}$). B) Cross-correlation curves for the titration of ZAP-70-YFP-CD3ε complexes with pITAM. Average curves from 10 repeated measurements of one representative experiment are shown. C) Interaction of endogenous ZAP-70 and CD3ε, detected by fluorescence cross-correlation of an Alexa488-labelled anti-mouse antibody and streptavidin-Cy5. Primary antibodies were anti-ZAP-70 from mouse (Z) and biotinylated anti-CD3ε from hamster (ε). In controls, either one or both of the primary antibodies were omitted. Average curves from 10 repeated measurements of one representative experiment are shown. Numbers x next to the curves indicate p-values ($10^{-(x+1)} < p < 10^{-x}$) for the comparison of samples containing both antibodies. D) Reproducibility of results from 3 independent experiments as decribed in C). Data sets were internally normalised to the cross-correlation amplitude of the pervanadate-treated sample containing both primary antibodies. Mean values and error propagations of the standard deviations of the single experiments are shown.*

To extend the analysis of molecular complexes by FCCS to complexes containing only unlabelled endogenous proteins, we next employed lysates of untransfected 3A9 cells (Figure 25 B). Lysates were prepared at $5*10^7$ cells/ml. Mouse anti-ZAP70 and hamster anti-CD3ε primary antibodies and matching secondary reagents labelled with distinct fluorophores were directly added to the lysates. (Figure 29 C). As controls, one or both of the primary antibodies were omitted. For the controls containing only one primary antibody, cross-correlations with low amplitudes were detectable independent of pervanadate treatment. These signals were likely due to a slight cross-reactivity of the Alexa488-labelled anti-mouse antibody with the hamster antibody or to an unspecific interaction of Cy5-streptavidin with complexes containing anti-mouse antibodies. In samples containing both primary antibodies, the cross-correlation amplitude for pervanadate-treated cells was significantly higher than the one in resting cells ($p < 10^{-3}$; Figure 29 C). In a sample containing pITAM peptide at a concentration of 2 μM, the pervanadate-dependent increase of the cross-correlation amplitude was partially reverted. The background of cross-correlations of low amplitudes was consistently found in repeated experiments (Figure 29 D).

In a corresponding manner, we probed additional signalling-dependent interactions of endogenous proteins in lysates of resting and stimulated 3A9 cells. Additionally, human Jurkat T leukemia cells were included as a second cell line. In 3A9 cells, the SH2-mediated interactions of GRB2 or PLCγ1 with LAT were detected after pervanadate treatment. By contrast, the GRB2-LAT interaction was not detectable in Jurkat lysates, while the PLCγ1-LAT interaction was detected with similar cross-correlation amplitude compared to the one in 3A9 lysates. Additionally, the SH3-mediated interaction of PLCγ1 with SLP76 was detected in Jurkat lysates in a stimulation-dependent manner (Figure 30). For all pairs of primary and cognate labelled secondary antibodies used in the FCCS-measurements, the autocorrelation functions of the fluorescent labels revealed the presence of slowly diffusing particles, likely corresponding to crosslinked primary and secondary antibodies (not shown).

However, the propensity for formation of crosslinked aggregates varied, depending on the primary antibody used. The mouse IgG2a anti-SLP76 antibody turned out to be especially prone to aggregate with the labelled anti-mouse IgG antibody, resulting in large standard deviations for the detection of the pervanadate-dependent SLP76-PLCγ1 interaction (Figure 30). In this case, the bivalent labelled anti-mouseIgG was replaced with monovalent labelled anti-mouse IgG2a F(ab) fragments, resulting in smaller standard deviations (chapter 4.1.3, Table 7, p. 35).
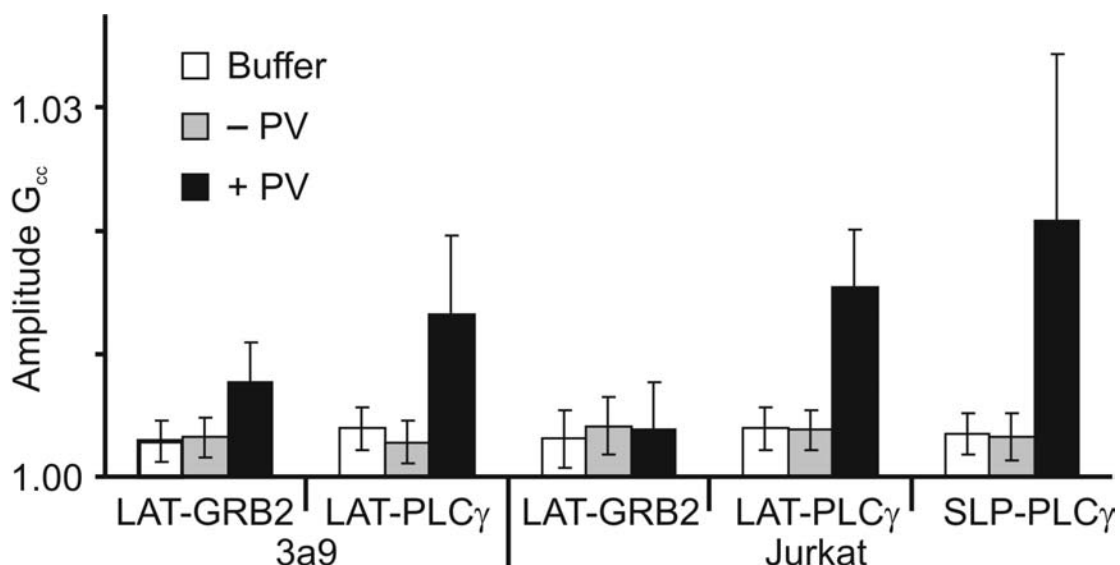
Figure 30: *Further stimulation-dependent interactions of endogenous proteins detected by indirect immunolabelling and FCCS. Lysates of resting or pervanadate-treated Jurkat or 3A9 cells. Per sample, 10^6 cells/20μl lysate were used. Pairs of primary antibodies, one each from mouse and rabbit and species-specific secondary antibodies labelled with Alexa488 or Alexa633 were added in one step. Control samples contained lysis buffer instead of cell lysate. Data from 3 (LAT-GRB2 in Jurkat: 2) independent experiments is presented as mean values with eror bars corresponding to the error propagations of the standard deviations of the single experiments.*

5.2.2.3 Dissection of the LAT-signalosome with interacting peptides

At this point, the FCCS-based detection of protein complexes had proven to be a facile approach for the detection of protein-protein interactions from microlitre volumes of lysates, which could easily be adapted to several interactions. Due to the on-step setup of the samples, the method would lend itself to screening applications, for example in the screening of substances interfering with protein complex formation. For the identification of effective substances for protein complex disruption, the ability to quantitatively compare their activities is mandatory. We therefore intended to further test the FCCS-based protocol for the detection of gradual differences in protein-protein interactions and the determination of IC_{50} values for inhibitors of interactions (The IC_{50} value is the concentration of an inhibitor, at which the signal – in our case the cross-correlation amplitude – observed for the uninhibited system is reduced to 50%).
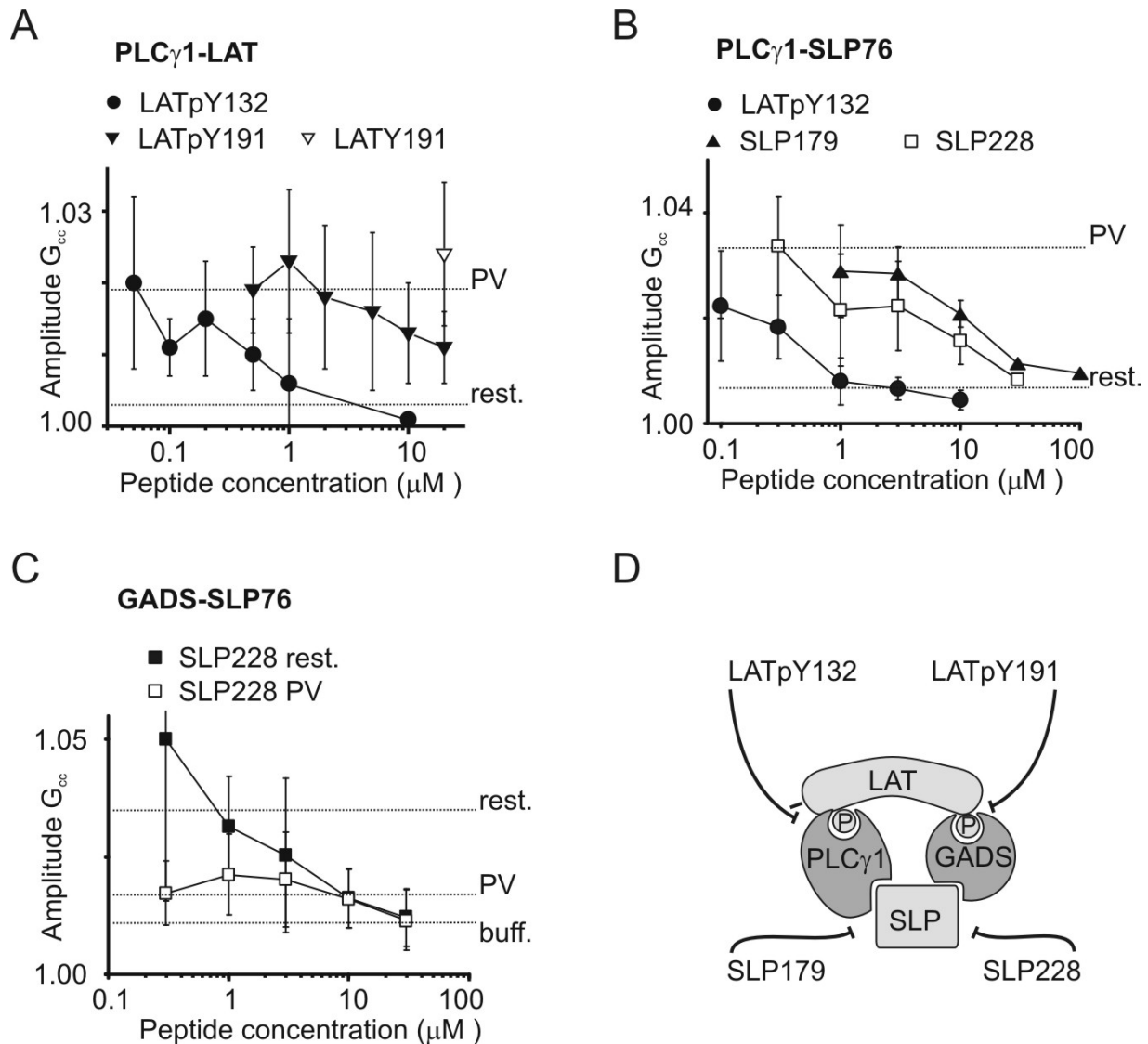
Figure 31: Cross correlation amplitudes for the titration of interactions in the LAT-signalosome with interfering peptides. Lysates of resting (rest.) or pervanadate-treated (PV) Jurkat cells at 10^6 cells/20μl. Dotted lines represent mean cross-correlation amplitudes in samples without peptide addition. Mean values and standard deviations of 10 repeated measurements in one representative experiment A) Titration of LAT-PLCγ1 interaction in lysates of pervanadate-treated cells with peptides LATpY132 and LATpY191 and the unphosphorylated control peptide LAT-Y191. The raw data for this experiment is partially shown in Table 5 (p. 34). B) Titration of SLP76-PLCγ1 interaction in lysates of pervanadate-treated Jurkat cells with peptides LATpY132, SLP228 and SLP179. C) Titration of SLP76-GADS interaction in lysates of resting and pervanadate-treated Jurkat cells with peptide SLP228. D) Schematic of the signalling complex of LAT, SLP-76, PLCγ1, and GADS. The SH2 domain binding binding sites on LAT are mimicked by LATpY132 and LATpY191. The SH3 domain binding sites on SLP76 are mimicked by SLP179 and SLP228.

We picked the interactions of LAT, GADS, SLP76 and PLCγ1 in the LAT-signalosome. As competitors, we chose peptides corresponding to binding motifs of one partner in the protein complexes (Figure 31), which had also been employed on the peptide microarrays (chapter 5.1.3). The phosphotyrosine (pY) motifs of LAT provide docking sites for the SH2 domains of GADS and PLCγ1 [42]. Some level of redundancy of the individual pY residues for binding different signalling proteins has been reported. pY132 was identified as the principal PLCγ1-binding site by in vitro peptide competition experiments [131]. In vivo point mutations on LAT have defined an additional requirement for pY191 for PLCγ1 binding [47]. On the other hand, pY191 was reported to be the preferred binding site for the SH2 domain of GADS [46]. Our own experiments on peptide microarrays including LATpY132 and LATpY191 are in line with these findings (Figure 14 C, p. 51).

The SH2-dependent interaction of LAT and PLCγ1 was disrupted by titration with pY-motif peptides, but not disrupted even by high concentrations of polyP motif peptides (Table 10). The LATpY132 peptide corresponding to the supposed binding site acted more efficiently than the LATpY191 peptide. IC$_{50}$ values of approximately 0.5 μM for LATpY132 and 20 μM for LATpY191 were determined. An unphosphorylated control peptide corresponding to LATY191 had no effect on the cross-correlation amplitude even at high concentrations (Figure 31 A, Table 10). In a previous publication using peptide concentrations of up to 10 μM and immunoprecipitation in combination with western blot for detection, no effect of the pY191 peptide on the LAT-PLCγ1 interaction had been detected [131]. The relative activities of both peptides as we observed them are consistent with a direct binding of PLCγ1 to pY132 and an auxiliary function of pY191. pY191 has also been implicated in binding of the adapter protein GADS, and therefore instead of directly binding to PLCγ1 may contribute to stabilising the tetrameric core signalosome of LAT, GADS, SLP76 and PLCγ1 [131,47,132] (Figure 31).

The interaction of SLP76 and PLCγ1 was only detected after pervanadate treatment and was sensitive to titration with polyP peptide SLP179 (IC$_{50}$ = 25 μM), the supposed direct competitor for the interaction [49]. The polyp peptide SLP228 (supposed to compete for the GADS-SH3 binding to SLP76) disrupted the SLP76-PLCγ1 interaction with an IC$_{50}$ of 10 μM. In the peptide microarray experiments using these peptides, we detected PLCγ1 from resting cells on SLP179, but not on SLP228. Only after pervanadate-treatment, PLCγ1 was found on SLP228 (Figure 14 C) and could be detached from this spot by titration with LATpY132 and LATpY191 (Figure 17 C, p. 57). This suggests that the inhibitory action of SLP228 seen in the FCCS-experiment probing the SLP76-PLCγ1 interaction was caused by destabilising

the LAT-signalosome between SLP76 and GADS – and subsequent dissociation of SLP76 – rather than by direct interference at the SLP76-PLCγ1 binding site.

Moreover, the pY motif peptide LATpY132 disrupted the SLP76-PLCg1 interaction with an IC_{50} of 0.5 µM, exactly as found for the LAT-PLCγ1 interaction. This strongly suggests, (i) that the mode of action for LATpY132 on this SH3-mediated interaction is indirect and (ii) that the SLP76-PLCγ1 interaction plays merely a stabilising role in the LAT-signalosome and is not sufficient to hold PLCγ1 in place.

By contrast, the SH3-mediated interaction between SLP76 and GADS is constitutive, and was already detected in lysates of resting cells. It could be disrupted by SLP228 with an IC_{50} of 5 µM. pY peptides had no effect on the SLP-GADS interaction in resting cells. Upon activation of cells with pervanadate, cross-correlation amplitudes for the SLP-GADS interaction decreased relative to the resting state, but could still be further suppressed by titration with SLP228. The decreased cross-correlation amplitude may have been caused by poor accessibility of GADS for the antibody upon recruitment of GADS into larger complexes. Correspondingly, FCCS was not able to detect GADS in complex with LAT.

Table 10: *IC_{50} values for the titration of the interactions in the LAT-signalosome with interfering peptides. no effect: For up to 30 µM of the respective peptide, no systematic titration-dependent decrease of the cross-correlation amplitude was observed. DMF was employed at 1% (v/v) in the lysate, corresponding to the DMF concentration at 30 µM peptide.*

	LAT-PLCγ1 stim. dependent	PLCγ1-SLP stim. dependent	SLP-GADS constitutive	GADS-LAT not detectable
LATpY132	IC_{50} 0.5 µM	IC_{50} 0.5 µM	no effect	n.d.
SLP179	no effect	IC_{50} 25 µM	no effect	n.d.
SLP228	no effect	IC_{50} 10 µM	IC_{50} 5 µM	n.d.
LATpY191	IC_{50} 20 µM	n.d.	no effect	n.d.
DMF control	no effect	no effect	no effect	n.d.

5.2.2.4 Discussion

FCCS and FCS were employed for detecting interactions of endogenous signalling proteins after indirect immunolabelling in microliter volumes of crude cell lysates. To our knowledge, this is the first report of the FCS-based detection of molecular complexes by indirect immunolabelling of both components. In the vast majority of previous reports applying FCS or FCCS, the binding partners were either expressed as fluorescent fusion proteins or chemically labelled, thereby requiring dedicated experimental designs and limiting the application of these techniques to the detection of selected molecular interactions.

Especially for the screening of substances that interfere with complex formation, crude cell lysates containing endogenous proteins only are highly preferable over reconstituted systems. First, posttranslational modifications are formed in the physiological context. Second, the formation of some complexes may depend on further proteins in an activation-dependent manner [162]. The screening of inhibitors that interfere with such interactions would therefore require the *in vitro* reconstitution of highly complex signalling machineries. In our case, inhibitors of interactions that depend on the phosphorylation of tyrosine residues were compared for their ability to interfere with the interactions constituting the LAT-signalosome in T-cell signalling.

In comparison to co-immunoprecipitation and western blotting, one of the assets of our approach also defines its limitations: The enrichment and purification of complexes is an intrinsic characteristic of co-immunoprecipitation. The FCCS-based method omits enrichment and washing steps by employing antibodies under equilibrium binding conditions directly in crude cell lysates. Furthermore, in western blotting, the determination of relative molecular weights provides additional information on the specificity of the reagents and the presence of protein isoforms. As this intrinsic control is missing in FCCS, it is advisable to use well-characterised antibodies known to be specific for their target.

There may be situations in which the detection of complexes is not possible by FCCS. Complexes of low abundance proteins may escape detection, because they cannot be sufficiently enriched. Rare complexes of high abundance proteins may escape detection, because uncomplexed proteins bind a major part of the antibodies. On the other hand, rare complexes of high abundance proteins may also be prone to dissociation when the unbound fraction is removed from equilibrium by washing steps in conventional enrichment techniques. Working under equilibrium conditions using FCCS may therefore still be beneficial in these cases. Similar limitations apply

if one of the two partners in a protein complex is significantly more abundant than the other.

As our approach for labelling and FCS respectively FCCS detection is conceptually very straightforward, it may seem surprising that it has not been described before. Indirect immunolabelling may have been shunned in FCS and FCCS based on two assumptions.

First, cross-linking of primary antibodies and multivalent secondary reagents (like whole antibodies or streptavidin) may lead to the formation of large fluorescent aggregates which compromise the evaluation of autocorrelation functions. In our FCCS experiments, some antibody aggregation was obvious from the contribution of slowly diffusing components to the autocorrelation function of the fluorescent label of the secondary antibody. However, this contribution did not interfere with the detection of complex formation, as the cross-correlation amplitude was only dependent on the inducible interaction of the examined proteins. Moreover, for primary antibodies especially prone to aggregate with whole bivalent secondary IgG-antibodies, monovalent secondary F(ab) fragments could be used. One should note that in contrast to the FCCS measurements, in the mass-tag strategy large aggregates of analytes and beads are generated intentionally as a readout. Therefore, all reagents that may cause aggregates by themselves must be avoided in combination with mass-tags. Consequently, we used fluorescently labelled monovalent F(ab)-fragments instead of bivalent secondary antibodies.

Second, the detection of a protein complex by indirect immunolabelling depends on the presence of five molecular interactions (Figure 25, p. 71), each with its own binding equilibrium. One should therefore assume that only a minor fraction of the protein complexes is simultaneously labelled with both fluorescent reagents. The calculation of fractions of bound versus unbound molecules in antibody-antigen complexes allows an estimation of the range of dissociation constants K_d and binding partner concentrations allowing FCCS detection:

The dissociation constant K_d can be written as:

$$K_d = \frac{[Ag] \cdot [Ab]}{[AgAb]} = \frac{([Ag_{tot}] - [AgAb]) \cdot ([Ab_{tot}] - [AgAb])}{[AgAb]} \qquad \text{Eq. 18}$$

with [Ag], [Ab], [AgAb] designating the equilibrium concentrations of free antigen, free antibody and antigen-antibody complex, and [Ag_{tot}], [Ab_{tot}] designating the total concentration of both binding partners. Eq. 18 can be resolved for [AgAb], resulting in a quadratic equation with K_d, [Ag_{tot}] and [Ab_{tot}] as parameters. The requirement to use approximately 10 nM (1.5 µg/ml assuming an IgG with a MW of

150kD) of labelled secondary reagent for FCCS-detection imposes constraints on the optimisation of the relative concentrations of binding partners.

With respect to protein complex detection by FCCS as described above, $[Ab_{tot}]$ = 10nM is the concentration of an antibody in the sample, and both its K_d for binding its target and the concentration of the target in the lysate are unknown. Table 11 lists various combinations of K_d and $[Ag_{tot}]$ in the range that can be expected for the experimental setup described above, and resulting concentrations of [AgAb], and fractions of bound antibody and bound antigen. A number of conclusions can be drawn within the framework given by Table 11:

(i) For detection of protein interaction by indirect immunolabelling and FCCS, an excess of unlabelled antigen is as deleterious as an excess of unbound antibody. With any given dissociation constant, the most advantageous situation will arise if antigen and antibody are equimolar. The same line of reasoning applies to the relative concentrations of primary and secondary antibodies. Antibody concentrations of 10 nM are routinely used; therefore the ideal target protein concentration is likewise 10 nM. With typical lysate concentrations of $5*10^7$ cells/ml lysis buffer, this corresponds to 120,000 copies of the target protein per cell. This is well in the range of our own analysis for ZAP70 (confer p. 40) and published data for various proteins from the MAP kinase cascade [163].

(ii) As a consequence the only parameter that can be changed considerably in order to optimise the fraction of doubly labelled particles, is the concentration of the cell lysate. As Table 11 suggests, we observed that decreasing the concentration of the target proteins by preparing lysates of lower cell density in some cases was crucial to reach a higher fraction of doubly labelled complexes (shown in [145]).

(iii) The dissociation constants of the antibodies determine the fractions of labelled, and therefore detectable, proteins. Unfortunately, most commercial antibodies are not characterised with respect to their dissociation constants. However, the ideal working concentration for FCCS of 10 nM (1.5 µg/ml) is in the range generally used for many other antibody-based techniques, indicating that dissociation constants of antibodies are usually low enough to yield results at these concentrations. Even if all five dissociation constants involved in giving rise to the doubly labelled species monitored (Figure 25) are in the range between 10^{-8}M and 10^{-9}M, doubly labelled fractions on the order of a few percent can be expected. Indeed, we have found that indirect immunolabelling as described in this protocol affords fractions of doubly labelled particles on the order of a few percent of total labels in the samples. These are sufficient for a reliable detection by FCCS.

Table 11: *Model calculation for bound fractions of molecules in an antibody (Ab) – antigen (Ag) interaction, depending on total concentrations of binding partners [Ag$_{tot}$], [Ab$_{tot}$] and the dissociation constant K$_d$ of the interaction.The last column "fraction[5]" lists the likelihood, that 5 interactions with the given parameters coincide, as is the case for FCCS-detection by indirect immunolabelling. Bold type distinguishes situations where [Ag$_{tot}$] = [Ab$_{tot}$], which are advantageous with respect to detection by FCS or FCCS.*

K$_d$ / M	[Ag$_{tot}$] / M	[Ab$_{tot}$] / M	[AgAb] /M	[AgAb]/ [Ag$_{tot}$] = fraction of bound Ag	[AgAb]/ [Ab$_{tot}$] = fraction of bound Ab	fraction [5]
	1.00E-07	1.00E-08	9.01E-09	0.09	0.90	
1.00E-08	**1.00E-08**	**1.00E-08**	**3.82E-09**	**0.38**	**0.38**	**0.008**
	1.00E-09	1.00E-08	4.88E-10	0.49	0.05	
	1.00E-07	1.00E-08	9.89E-09	0.10	0.99	
1.00E-09	**1.00E-08**	**1.00E-08**	**7.30E-09**	**0.73**	**0.73**	**0.207**
	1.00E-09	1.00E-08	9.01E-10	0.90	0.09	
	1.00E-07	1.00E-08	9.99E-09	0.10	1.00	
1.00E-10	**1.00E-08**	**1.00E-08**	**9.05E-09**	**0.90**	**0.90**	**0.590**
	1.00E-09	1.00E-08	9.89E-10	0.99	0.10	
	1.00E-07	1.00E-08	1.00E-08	0.10	1.00	
1.00E-11	**1.00E-08**	**1.00E-08**	**9.69E-09**	**0.97**	**0.97**	**0.859**
	1.00E-09	1.00E-08	9.99E-10	1.00	0.10	

Contrary to what may be expected from the potential limitations listed above, little optimisation was required in the cases for which we have measured cross-correlations. All antibodies that we successfully used were from commercial sources with no prior selection for exceptionally high affinity. In general, primary antibodies validated for immunoprecipitation also performed well in the FCS and FCCS experiments.

The simplicity of our protocol and the general availability of reagents significantly extends the applicability of FCS and FCCS in the detection of protein complexes. With growing collections of highly specific antibodies the method is applicable to a basically unlimited array of interactions. Table 12 tentatively compares FCCS-based detection of interactions with existent approaches for large-scale interaction screens. In comparison to other approaches for the scanning of protein-protein interactions, FCCS as presented here is notable for its potential to pick up the interaction of endogenous, untagged proteins from microlitre amounts

of sample in a simple "mix, incubate, and measure" protocol. FCCS-based scanning for protein-protein interactions relies on a library of antibodies. In contrast, established methods may require the construction of extensive libraries of fusion-proteins. Due to the confocal detection volume and the nanomolar sensitivity of FCCS, minimal amounts of sample and reagents are needed. Moreover, the straightforward protocol avoids sample loss during prolonged handling and allows for easy automation.

Table 12: Comparison of the FCCS-based technique to other techniques employed for scanning of protein-protein interactions

	2-Hybrid	**Tandem Affinity Purification + Mass Spectrometry** [164]	**Whole Interactome Scanning Experiment** [11]	**FCCS or mass-tag FCS**
Physical basis for screening	libraries of bait & prey fusion proteins	library of tandem-tagged proteins	arrayed library of peptides	library of antibodies
Whose interaction is detected?	2 overexpressed exogenous proteins	tagged exogenous protein with endogenous proteins	endogenous protein with arrayed peptides	unmodified endogenous proteins
Interaction detected where?	in living cells	from lysate, after purification	from lysate, after washing the array	in crude lysate at equilibrium
Additional features	usually pairwise constitutive inter-actions; modifications for detection of con-stitutive interactions [165]	unbiased detection mode, no selection of affinity reagents for detection necessary		pairwise constitutive and inducible interactions mix and measure: one-step protocol

6 Summary

The aim of this thesis was to develop methods for the parallel analysis of complexes of endogenous proteins, and to employ them in the context of T-cell signal transduction. As a general rule, all efforts to monitor a system lead to the introduction of changes into this system. The dissection of protein-protein interactions in cellular signalling requires the introduction of detectable features to distinguish proteins from one another. Two basic options exist: Either a label (in the broadest sense) is introduced into the intact cells – this allows to follow signalling processes in a live, but manipulated cellular system. Alternatively, signalling is induced in unmanipulated cells, which are then disrupted – this allows to introduce labels after the signalling processes of interest have taken place in their unperturbed physiological context. We opted for the second possibility, as the labelling of proteins in lysates is more versatile and therefore more amenable to parallelisation compared to the labelling of proteins in life cells. Two approaches were developed, one based on peptide microarrays, the other one on fluorescence correlation and cross correlation spectroscopy.

We show that peptide microarrays provide a robust and quantitative means for detecting signalling-dependent changes of molecular interactions. Recruitment of a protein into a complex upon stimulation of a cell leads to the masking of an otherwise exposed binding site. In cell lysates this masking can be detected by reduced binding to a microarray carrying a peptide that corresponds to the binding motif of the respective interaction domain. Compared to established techniques, the method provides a significant shortcut to the detection of molecular interactions. This approach was first exemplified for the binding of ZAP70 to a bis-pY-motif of the activated T-cell receptor via its tandem SH2 domain. Binding of ZAP70 to the microarray was either detected by virtue of the intrinsic fluorescence of a ZAP70-YFP fusion protein or by indirect immunofluorescence. In both cases, the activation-dependent recruitment of ZAP70 into signalling complexes reduced the microarray-bound signal. This reduction in signal provided quantitative information on the change of the fraction of available binding sites and, through combination with FCS and western blotting, even on the number of available and occupied ZAP70 tandem-SH2 domains per cell.

We then extended the concept by using arrays comprising 15 SH2 domain-binding pY motif peptides, 6 SH3 domain-binding polyP motif peptides, 1 PTB-binding peptide, 1 WH1-binding peptide and 1 PDZ-binding peptide. Lysates of resting or stimulated Jurkat cells were incubated on these arrays and the binding of two signalling proteins per array was detected by two-colour indirect

immunofluorescence. With 16 arrays per slide incubated in parallel, this approach yields 768 data points on protein-protein interactions in cellular signalling per experiment, or multiples of this number if several slides are incubated in parallel. In addition to changes caused by the masking of binding sites, we found that also recruitment of proteins into complexes leads to signal changes. This endows the arrays with properties of co-purification methods, but in a highly parallel and miniaturised fashion. Competition with peptides corresponding to interaction motifs dismantled complexes on the arrays in a stepwise and dose dependent manner and provided detailed information on the architecture of signalling complexes. For stimulation of Jurkat cells through receptor crosslinking with anti-CD3 and/or anti-CD28 antibodies, the timecourse of the changes in the pattern of molecular interactions could be monitored. Experiments with Jurkat cell derivatives lacking either an upstream signalling kinase or a protein involved in a central signalling complex demonstrate that the peptide arrays provide a means to dissect functional interdependences in cellular signalling networks.

FCCS and FCS were used to detect interactions of endogenous signalling proteins using simple "mix, incubate, and measure" protocols in microliter volumes of crude cell lysates. Both binding partners of interest were targeted by indirect immunolabelling. Using 384-well plates, measurements were conducted in as little as 20 μl crude cell lysate per sample, corresponding to $0.2 - 1 * 10^6$ cells. Matched pairs of primary antibodies against the interaction partners and labelled secondary reagents were all added to the crude cell lysates in one step. The indirect labelling of two constituents of a complex enabled the specific and sensitive detection of signalling-dependent complex formation. FCCS, using two spectrally different fluorophores as labels, proved superior to FCS, using one fluorophore and one mass-tag. The one-step addition of reagents and separation-free detection minimise the number of manipulations required for complex detection and make the protocol readily compatible with automation. So far, we have applied the method for detecting the signalling-dependent formation of molecular complexes in T-cell signal transduction. Moreover, we demonstrate that IC_{50} values for substances interfering with protein-protein interactions can be determined. Competition experiments with peptides disrupting interactions constituting a central protein complex in T-cell signalling, the LAT-signalosome, revealed the relative importance of the individual interactions in stabilising the complex.

We therefore conclude, that the FCCS-based approach on protein complex detection is well suited for the parallel detection of a set of protein-protein interactions within a cellular signalling network, in applications relating to systems biology. Data sets on the evolution of interactions over time in response to different

stimuli may be generated with comparably little effort. Here, the ability to work with systems containing only endogenous proteins is especially advantageous, as overexpression of fusion-proteins with detection tags may favor the formation of protein complexes and distort signalling pathways. Another application might be the screening for inhibitory substances of protein-protein interactions. Inhibitors can be ranked by determining their IC_{50} values through titration. Especially for interactions depending on signalling-dependent posttranslational modifications, an approach based on endogenous proteins in their native cellular context is preferable over reconstituted systems. With a growing body of experience, one may envision future applications in the screening for new interactions and the generation of interaction maps using libraries of antibodies.

7 Zusammenfassung

Ziel dieser Doktorarbeit war, im Kontext der T-Zell-Signaltransduktion Methoden zur parallelen Analyse von Komplexen endogener Proteine zu entwickeln. Generell gilt, dass jeder Versuch, ein System zu beobachten, bereits Veränderungen in diesem System hervorruft. Die Aufklärung von Protein-Protein-Interaktionen im zellulären Signalgeschehen verlangt die Einführung von detektierbaren Merkmalen, um Proteine voneinander zu unterscheiden. Dafür gibt es zwei grundlegende Möglichkeiten: Entweder wird eine Markierung (im weitesten Sinne) in die intakten Zellen eingebracht – dies erlaubt das Verfolgen von Signalvorgängen in einem lebenden, jedoch bereits veränderten System. Alternativ wird das Signalgeschehen in unveränderten Zellen induziert, die dann lysiert werden – dies erlaubt die Einführung von Markierungen, nachdem die zu untersuchenden Signalvorgänge in ihrem unveränderten physiologischen Kontext abgelaufen sind. Wir entschieden uns für die zweite Möglichkeit, da die Markierung von Proteinen in Lysaten flexibler einsetzbar und daher einfacher parallelisierbar ist als die Markierung von Proteinen in lebenden Zellen. Zwei Herangehensweisen wurden entwickelt, die eine basierend auf Peptidmikroarrays, die andere basierend auf Fluoreszenz-Korrelations- und Kreuzkorrelations-Spektroskopie (FCS / FCCS).

Wir zeigen, dass Peptidmikroarrays einen einfachen Weg zur quantitativen Detektion signalabhängiger Protein-Protein-Interaktionen eröffnen. Die Einbeziehung eines Proteins in einen Proteinkomplex führt zur Maskierung einer andernfalls frei zugänglichen Bindungsstelle. In Zelllysaten lässt sich solch eine Maskierung detektieren, da sie auf einem Mikroarray, der ein zu der maskierten Bindungsstelle passendes Peptid-Bindemotiv trägt, zu verminderter Anbindung des Proteins führt. Im Vergleich zu bestehenden Techniken stellt diese Methode eine deutliche Vereinfachung der Detektion molekularer Interaktionen dar. Dieser Ansatz wurde zunächst beispielhaft validiert anhand der Bindung der Tandem-SH2-Domänen von ZAP70 an ein bis-pY-Motiv des aktivierten T-Zell-Rezeptors. Die Bindung von ZAP70 an ein entsprechendes Peptid auf dem Mikroarray wurde entweder durch die intrinsische Fluoreszenz eines ZAP70-YFP Fusionsproteins, oder durch indirekte Immunfluoreszenzfärbung detektiert. In beiden Fällen reduzierte die aktivierungsabhängige Einbeziehung von ZAP70 in Signalproteinkomplexe das Fluoreszenzsignal auf dem Mikroarray. Diese Signalreduktion enthielt quantitative Information über die Änderung des Anteils verfügbarer Bindungsstellen und, kombiniert mit FCS und Western Blotting, über die Anzahl verfügbarer und maskierter ZAP70-Tandem-SH2-Domänen pro Zelle.

Anschließend wurde dieser Ansatz ausgeweitet, indem Mikroarrays mit 15 verschiedenen SH2-Domänen-bindenden pY-Motiv-Peptiden, sechs SH3-Domänen-bindenden polyP-Motiv-Peptiden, und je einem PTB-, WH1- und PDZ-Domänen-bindenden Peptid zum Einsatz kamen. Lysate ruhender oder stimulierter Jurkat-Zellen wurden auf diesen Arrays inkubiert und die Bindung von zwei Signaltransduktionsproteinen per Array anschließend durch indirekte Immunfluoreszenz mit zwei verschiedenen Fluorophoren detektiert. Mit der parallelen Inkubation von 16 Mikroarrays pro Objektträger liefert ein Experiment 768 Datenpunkte zu Protein-Protein-Interaktionen in der zellulären Signaltransduktion - oder Vielfache dieser Zahl, wenn mehrere Objektträger parallel inkubiert werden. Zusätzlich zu den durch Maskierungseffekte hervorgerufenen Änderungen fanden wir, dass auch die Einbeziehung von Proteinen in Komplexe zu Signaländerungen führt. Dies verleiht den Mikroarrays Eigenschaften von Ko-Aufreinigungsmethoden, aber in hoch-paralleler und miniaturisierter Art und Weise. Kompetitionen mit Peptiden, die den Bindemotiven innerhalb der Komplexe entsprachen, ermöglichten die schrittweise und konzentrationsabhängige Zerlegung der Komplexe auf den Arrays und lieferten somit detaillierte Informationen zur Komplexarchitektur. Nach Stimulation von Jurkat-Zellen durch Rezeptor-Kreuzvernetzung durch anti-CD3 und/oder anti-CD28 Antikörper ließ sich der Zeitverlauf von Änderungen im Muster molekularer Interaktionen beobachten. Experimente mit Jurkat-Zellen, denen entweder eine aktive Kinase der frühen Signaltransduktion oder ein in viele Komplexe involviertes Protein fehlten, demonstrierten weiterhin, dass Peptidarrays funktionale Zusammenhänge in zellulären Signalnetzwerken zeigen.

FCS und FCCS wurden genutzt, um Interaktionen endogener Signaltransduktions-Proteine in einfachen „Misch, inkubier und miss"-Protokollen in Mikro-litervolumina von Zelllysat zu detektieren. Beide hinsichtlich ihrer Bindung zu untersuchenden Proteine wurden indirekt immunmarkiert. Die Messungen wurden in Multititerplatten mit 384 Probenkammern in jeweils lediglich 20 µl Lysat pro Ansatz, entsprechend $0,2 - 1,0 * 10^6$ Zellen, durchgeführt. Abgestimmte Paare von Primärantikörpern gegen die Bindungspartner und markierten Sekundärreagenzien wurden in einem Schritt zu den Zelllysaten gegeben. Diese indirekte Markierung zweier Komplexbestandteile ermöglichte die spezifische und sensitive Detektion von signalabhängiger Proteinkomplexbildung. FCCS unter Nutzung von zwei spektral unterschiedlichen Fluorophoren als Markierung erwies sich dabei als überlegen gegenüber der FCS mit einem Fluorophor und einem Nanopartikel als Massen-markierung. Die Zugabe aller Reagenzien in einem Schritt und die von Trennungs-schritten unabhängige Detektion minimieren die Zahl notwendiger Handhabungs-schritte und machen die Methode kompatibel für die Automatisierung. Bisher haben

wir die Methode für die Detektion signalabhängiger Proteinkomplexe in der T-Zell-Signaltransduktion eingesetzt. Daneben demonstrierten wir die Bestimmung von IC_{50}-Werten für Inhibitoren der Komplexbildung. Titrationsexperimente mit Peptiden, die die individuellen Interaktionen in einem zentralen Komplex der T-Zell-Signaltransduktion kompetieren, zeigten die relative Bedeutung der einzelnen Interaktionen für die Stabilisierung des gesamten Komplexes.

Wir folgern daher, dass unser FCCS-basierter Ansatz zur Detektion von Proteinkomplexen gut geeignet ist, um mehrere Interaktionen innerhalb eines zellulären Signalnetzwerkes parallel zu verfolgen, beispielsweise in system-biologischen Fragestellungen. Datensätze zur Entwicklung von Interaktionen über die Zeit und in Antwort auf unterschiedliche Stimuli könnten so mit vergleichsweise wenig Aufwand generiert werden. In diesem Zusammenhang ist es besonders vorteilhaft, in Systemen mit ausschließlich endogenen Proteinen arbeiten zu können, da die Überexpression von Fusionsproteinen mit Detektionsmarkierungen die Bildung von Proteinkomplexen favorisieren und das zelluläre Signalgeschehen verzerren könnte. Eine weitere Anwendung kann die Reihenuntersuchung potentieller Inhibitoren von Protein-Protein-Interaktionen sein. Inhibitorkandidaten ließen sich dabei anhand ihres durch Titrationen ermittelten IC_{50}-Wertes ver-gleichend beurteilen. Vor allem für Interaktionen, die auf posttranslationalen Modifikationen beruhen, ist ein auf endogenen Proteinen in ihrem natürlichen zellulären Kontext basierender Ansatz einem rekonstituierten System vorzuziehen. Mit wachsender Erfahrung mit der Methode ist auch vorstellbar, sie zukünftig für die Neuidentifikation von Interaktionen mit Hilfe von Antikörper-Bibliotheken einzusetzen.

8 References

1. Minton, A. P. Implications of macromolecular crowding for protein assembly. *Curr. Opin. Struct. Biol.* **10**, 34 (2000).

2. Chothia, C. Proteins. One thousand families for the molecular biologist. *Nature* **357**, 543 (1992).

3. Aloy, P. and Russell, R.B. Ten thousand interactions for the molecular biologist. *Nat. Biotechnol.* **22**, 1317 (2004).

4. Warner, G. J., Adeleye, Y.A., & Ideker, T. Interactome networks: the state of the science. *Genome Biol.* **7**, 301 (2006).

5. Rual, J. F. et. al. Towards a proteome-scale map of the human protein-protein interaction network. *Nature* **437**, 1173 (2005).

6. Stelzl, U. et. al. A human protein-protein interaction network: a resource for annotating the proteome. *Cell* **122**, 957 (2005).

7. Hunter, T. Signaling--2000 and beyond. *Cell* **100**, 113 (2000).

8. Gavin, A. C. et. al. Functional organization of the yeast proteome by systematic analysis of protein complexes. *Nature* **415**, 141 (2002).

9. Pawson, T. and Nash, P. Assembly of cell regulatory systems through protein interaction domains. *Science* **300**, 445 (2003).

10. Linding, R. et. al. Protein disorder prediction: implications for structural proteomics. *Structure* **11**, 1453 (2003).

11. Landgraf, C. et. al. Protein Interaction Networks by Proteome Peptide Scanning. *PLoS Biol.* **2**, E14 (2004).

12. Otte, L. et. al. WW domain sequence activity relationships identified using ligand recognition propensities of 42 WW domains. *Protein Sci.* **12**, 491 (2003).

13. Wiedemann, U. et. al. Quantification of PDZ domain specificity, prediction of ligand affinity and rational design of super-binding peptides. *J. Mol. Biol.* **343**, 703 (2004).

14. Neduva, V. et. al. Systematic discovery of new recognition peptides mediating protien interaction networks. *PLoS Biol.* **3**, e405 (2005).

15. Pereira-Leal, J. B. and Teichmann, S.A. Novel specificities emerge by stepwise duplication of functional modules. *Genome Res.* **15**, 552 (2005).

16. Wange, R. L. and Huang, Y. T cell receptor signaling: Beyond complex complexes. *J. Biol. Chem.* **279**, 28827 (2004).

17. Mayer, B. J., Hamaguchi, M., & Hanafusa, H. A novel viral oncogene with structural similarity to phospholipase C. *Nature* **332**, 272 (1988).

18. Sadowski, I., Stone, J.C., & Pawson, T. A noncatalytic domain conserved among cytoplasmic protein-tyrosine kinases modifies the kinase function and transforming activity of Fujinami sarcoma virus P130gag-fps. *Mol. Cell. Biol.* **6**, 4396 (1986).

19. Waksman, G., Shoelson, S.E., Pant, N., Cowburn, D., & Kuriyan, J. Binding of a high affinity phosphotyrosyl peptide to the Src SH2 domain: Crystal structures of the complexed and peptide-free forms. *Cell* **72**, 779 (1993).

20. Puntervoll, P. et. al. ELM server: a new resource for investigating short functional sites in modular eukaryotic proteins. *Nucl. Acids Res.* **31**, 3625 (2003).

21. Ottinger, E. A., Botfield, M.C., & Shoelson, S.E. Tandem SH2 domains confer high specificity in tyrosine kinase signaling. *J. Biol. Chem.* **273**, 729 (1998).

22. Lim, W. A., Richards, F.M., & Fox, R.O. Structural determinants of peptide-binding orientation and of sequence specificity in SH3 domains. *Nature* **372**, 375 (1994).

23. Bedford, M. T. et. al. Arginine methylation inhibits the binding of proline-rich ligands to Src homology 3, but not WW, domains. *J. Biol. Chem.* **275**, 16030 (2000).

24. Acuto, O. and Michel, F. CD28-mediated co-stimulation: a quantitative support for TCR signalling. *Nat. Rev. Immunol.* **3**, 939 (2003).

25. Mustelin, T. and Tasken, K. Positive and negative regulation of T-cell activation through kinases and phosphatases. *Biochem. J.* **371**, 15 (2003).

26. Veillette, A., Bookman, M.A., Horak, E.M., & Bolen, J.B. The CD4 and CD8 T cell surface antigens are associated with the internal membrane tyrosine-protein kinase p56lck. *Cell* **55**, 301 (1988).

27. Shaw, A. S. et. al. Short related sequences in the cytoplasmic domains of CD4 and CD8 mediate binding to the amino-terminal domain of the p56lck tyrosine protein kinase. *Mol. Cell. Biol.* **10**, 1853 (1990).

28. Barber, E. K., Dasgupta, J.D., Schlossman, S.F., Trevillyan, J.M., & Rudd, C.E. The CD4 and CD8 antigens are coupled to a protein-tyrosine kinase (p56lck) that phosphorylates the CD3 complex. *Proc. Natl. Acad. Sci U. S. A.* **86**, 3277 (1989).

29. D'Oro, U. and Ashwell, J.D. Cutting edge: the CD45 tyrosine phosphatase is an inhibitor of Lck activity in thymocytes. *J. Immunol.* **162**, 1879 (1999).

30. Irles, C. et. al. CD45 ectodomain controls interaction with GEMs and Lck activity for optimal TCR signaling. *Nat. Immunol.* **4**, 189 (2003).

31. Bergman, M. et. al. The human p50csk tyrosine kinase phosphorylates p56lck at Tyr-505 and down regulates its catalytic activity. *EMBO J.* **11**, 2919 (1992).

32. Brdicka, T. et. al. Phosphoprotein associated with glycosphingolipid-enriched microdomains (PAG), a novel ubiquitously expressed transmembrane adaptor protein, binds the protein tyrosine kinase csk and is involved in regulation of T cell activation. *J. Exp. Med.* **191**, 1591 (2000).

33. Isakov, N. et. al. ZAP-70 binding specificity to T cell receptor tyrosine-based activation motifs: the tandem SH2 domains of ZAP-70 bind distinct tyrosine-based activation motifs with varying affinity. *J. Exp. Med.* **181**, 375 (1995).

34. Wange, R. L., Malek, S.N., Desiderio, S., & Samelson, L.E. Tandem SH2 domains of ZAP-70 bind to T cell antigen receptor zeta and CD3 epsilon from activated Jurkat T cells. *J. Biol. Chem.* **268**, 19797 (1993).

35. Mege, D. et. al. Mutation of tyrosines 492/493 in the kinase domain of ZAP-70 affects multiple T-cell receptor signaling pathways. *J. Biol. Chem.* **271**, 32644 (1996).

36. Neumeister, E. N. et. al. Binding of ZAP-70 to phosphorylated T-cell receptor zeta and eta enhances its autophosphorylation and generates specific

binding sites for SH2 domain-containing proteins. *Mol. Cell. Biol.* **15**, 3171 (1995).

37. Pelosi, M. et. al. Tyrosine 319 in the interdomain B of ZAP-70 is a binding site for the Src homology 2 domain of Lck. *J. Biol. Chem.* **274**, 14229 (1999).

38. Lupher, J., Songyang, Z., Shoelson, S.E., Cantley, L.C., & Band, H. The Cbl Phosphotyrosine-binding Domain Selects a D(N/D)XpY Motif and Binds to the Tyr292 Negative Regulatory Phosphorylation Site of ZAP-70. *J. Biol. Chem.* **272**, 33140 (1997).

39. Meng, W., Sawasdikosol, S., Burakoff, S.J., & Eck, M.J. Structure of the amino-terminal domain of Cbl complexed to its binding site on ZAP-70 kinase. *Nature* **398**, 84 (1999).

40. UniProtKB/Swiss-Prot database entry P22681: CBL_HUMAN, http://www.expasy.org/uniprot/P22681 (2006)

41. Wang, H. Y. et. al. Cbl promotes ubiquitination of the T cell receptor zeta through an adaptor function of Zap-70. *J. Biol. Chem.* **276**, 26004 (2001).

42. Zhang, W., Sloan-Lancaster, J., Kitchen, J., Trible, R.P., & Samelson, L.E. LAT: the ZAP-70 tyrosine kinase substrate that links T cell receptor to cellular activation. *Cell* **92**, 83 (1998).

43. Wardenburg, J. B. et. al. Phosphorylation of SLP-76 by the ZAP-70 protein-tyrosine kinase is required for T-cell receptor function. *J. Biol. Chem.* **271**, 19641 (1996).

44. Zhang, W., Trible, R.P., & Samelson, L.E. LAT Palmitoylation: Its Essential Role in Membrane Microdomain Targeting and Tyrosine Phosphorylation during T Cell Activation. *Immunity* **9**, 239 (1998).

45. Houtman, J. C. D., Houghtling, R.A., Barda-Saad, M., Toda, Y., & Samelson, L.E. Early Phosphorylation Kinetics of Proteins Involved in Proximal TCR-Mediated Signaling Pathways. *J. Immunol.* **175**, 2449 (2005).

46. Zhang, W. et. al. Association of Grb2, Gads, and phospholipase C-gamma 1 with phosphorylated LAT tyrosine residues. Effect of LAT tyrosine mutations on T cell angigen receptor-mediated signaling. *J. Biol. Chem.* **275**, 23355 (2000).

47. Zhu, M., Janssen, E., & Zhang, W. Minimal requirement of tyrosine residues of linker for activation of T cells in TCR signaling and thymocyte development. *J. Immunol.* **170**, 325 (2003).

48. Liu, S. K., Fang, N., Koretzky, G.A., & Jane McGlade, C. The hematopoietic-specific adaptor protein Gads functions in T-cell signaling via interactions with the SLP-76 and LAT adaptors. *Curr. Biol.* **9**, 67 (1999).

49. Yablonski, D., Kadlecek, T., & Weiss, A. Identification of a Phospholipase C-{gamma}1 (PLC-{gamma}1) SH3 Domain-Binding Site in SLP-76 Required for T-Cell Receptor-Mediated Activation of PLC-{gamma}1 and NFAT. *Mol. Cell. Biol.* **21**, 4208 (2001).

50. Dombroski, D. et. al. Kinase-independent functions for Itk in TCR-induced regulation of Vav and the actin cytoskeleton. *J. Immunol.* **174**, 1385 (2005).

51. Reynolds, L. F. et. al. Vav1 transduces T cell receptor signals to the activation of the Ras/ERK pathway via LAT, Sos, and RasGRP1. *J. Biol. Chem.* **279**, 18239 (2004).

52. Li, N. et. al. Guanine-nucleotide-releasing factor hSos1 binds to Grb2 and links receptor tyrosine kinases to Ras signalling. *Nature* **363**, 85 (1993).

53. Ravichandran, K. S. et. al. Interaction of Shc with the zeta chain of the T cell receptor upon T cell activation. *Science* **262**, 902 (1993).

54. Database: PROSITE - Protein families and domains, www.expasy.org/prosite/ (2006)

55. Database: UniProt Knowledgebase (Swiss-Prot and TrEMBL) - Protein knowledgebase, www.expasy.org/sprot/ (2006)

56. Liu, Y. et. al. Regulation of protein kinase Ctheta function during T cell activation by Lck-mediated tyrosine phosphorylation. *J. Biol. Chem.* **275**, 3603 (2000).

57. Roose, J. P., Mollenauer, M., Gupta, V.A., Stone, J., & Weiss, A. A diacylglycerol-protein kinase C-RasGRP1 pathway directs Ras activation upon antigen receptor stimulation of T cells. *Mol. Cell. Biol.* **25**, 4426 (2005).

58. Sun, Z. et. al. PKC-theta is required for TCR-induced NF-kappaB activation in mature but not immature T lymphocytes. *Nature* **404**, 402 (2000).

59. Bubeck Wardenburg, J. et. al. Regulation of PAK activation and the T cell cytoskeleton by the linker protein SLP-76. *Immunity* **9**, 607 (1998).

60. da Silva, A. J. et. al. Cloning of a novel T-cell protein FYB that binds FYN and SH2-domain-containing leukocyte protein 76 and modulates interleukin 2 production. *Proc. Natl. Acad. Sci. U. S. A.* **94**, 7493 (1997).

61. Martin-Cofreces, N. B. et. al. Role of Fyn in the Rearrangement of Tubulin Cytoskeleton Induced through TCR. *J. Immunol.* **176**, 4201 (2006).

62. Shim, E. K. et. al. Association of the Src homology 2 domain-containing leukocyte phosphoprotein of 76 kD (SLP-76) with the p85 subunit of phosphoinositide 3-kinase. *FEBS Lett.* **575**, 35 (2004).

63. King, P. D. et. al. Analysis of CD28 cytoplasmic tail tyrosine residues as regulators and substrates for the protein tyrosine kinases, EMT and LCK. *J. Immunol.* **158**, 580 (1997).

64. Holdorf, A. D. et. al. Proline residues in CD28 and the Src homology (SH)3 domain of Lck are required for T cell costimulation. *J. Exp. Med.* **190**, 375 (1999).

65. Holdorf, A. D., Lee, K.H., Burack, W.R., Allen, P.M., & Shaw, A.S. Regulation of Lck activity by CD4 and CD28 in the immunological synapse. *Nat. Immunol.* **3**, 259 (2002).

66. Garcon, F. et. al. The SH3 domain of Tec kinase is essential for its targeting to activated CD28 costimulatory molecule. *Eur. J. Immunol.* **34**, 1972 (2004).

67. Pages, F. et. al. Binding of phosphatidylinositol-3-OH kinase to CD28 is required for T-cell signalling. *Nature* **369**, 327 (1994).

68. Schneider, H., Cai, Y.C., Prasad, K.V., Shoelson, S.E., & Rudd, C.E. T cell antigen CD28 binds to the GRB-2/SOS complex, regulators of p21ras. *Eur. J. Immunol.* **25**, 1044 (1995).

69. Scharenberg, A. M. et. al. Phosphatidylinositol-3,4,5-trisphosphate (PtdIns-3,4,5-P3)/Tec kinase-dependent calcium signaling pathway: a target for SHIP-mediated inhibitory signals. *EMBO J.* **17**, 1961 (1998).

70. Saito, T. and Yamasaki, S. Negative feedback of T cell activation through inhibitory adapters and costimulatory receptors. *Immunol. Rev.* **192**, 143 (2003).

71. Parry, R. V. et. al. Ligation of CD28 stimulates the formation of a multimeric signaling complex involving grb-2-associated binder 2 (gab2), SRC homology phosphatase-2, and phosphatidylinositol 3-kinase: evidence that negative regulation of CD28 signaling requires the gab2 pleckstrin homology domain. *J. Immunol.* **176**, 594 (2006).

72. Lock, L. S., Royal, I., Naujokas, M.A., & Park, M. Identification of an atypical Grb2 carboxyl-terminal SH3 domain binding site in Gab docking proteins reveals Grb2-dependent and -independent recruitment of Gab1 to receptor tyrosine kinases. *J. Biol. Chem.* **275**, 31536 (2000).

73. Lakowicz, J. R. Principles of fluorescence spectroscopy; Kluwer Academic / Plenum Publishers, New York (1999)

74. Atkins, P. W. and de Paula, J. Atkin's Physical Chemistry; Oxford University Press, Oxford (2006)

75. Tsien, R. Y. The green fluorescent protein. *Annu. Rev. Biochem.* **67**, 509 (1998).

76. Griesbeck, O., Baird, G.S., Campbell, R.E., Zacharias, D.A., & Tsien, R.Y. Reducing the environmental sensitivity of yellow fluorescent protein. Mechanism and applications. *J. Biol. Chem.* **276**, 29188 (2001).

77. Nagai, T. et. al. A variant of yellow fluorescent protein with fast and efficient maturation for cell-biological applications. *Nat. Biotechnol.* **20**, 87 (2002).

78. Shaner, N. C. et. al. Improved monomeric red, orange and yellow fluorescent proteins derived from Discosoma sp. red fluorescent protein. *Nat. Biotechnol.* **22**, 1567 (2004).

79. Wilhelm, S., Gröbler, B., Gluch, M., and Heinz, H. Die konfokale Laser Scanning Mikroskopie. Carl Zeiss Jena (2003)

80. Rigler, R., Mets, Ü., Widengren, J., & Kask, P. Fluorescence correlation spectroscopy with high count rate and low background: analysis of translational diffusion. *Eur. Biophys. J.* **22**, 169 (1993).

81. Brock, R. Fluorescence correlation spectroscopy in cell biology. In: Fluorescence spectroscopy in biology; Springer, Berlin-Heidelberg (2005)

82. Schwille, P. and Haustein, E. Fluorescence Correlation Spectroscopy - An Introduction to its Concepts and Applications. In: Biophysics Textbook Online; Biophysical Society, Bethesda, Maryland (2003)

83. Schwille, P., Meyer-Almes, F.J., & Rigler, R. Dual-color fluorescence cross-correlation spectroscopy for multicomponent diffusional analysis in solution. *Biophys. J.* **72**, 1878 (1997).

84. Schwille, P., Kummer, S., Heikal, A.A., Moerner, W.E., & Webb, W.W. Fluorescence correlation spectroscopy reveals fast optical excitation-driven intramolecular dynamics of yellow fluorescent proteins. *Proc. Natl. Acad. Sci. U. S. A.* **97**, 151 (2000).

85. Elson, E. L. and Magde, D. Fluorescence correlation spectroscopy. I. Conceptual Basis and Theory. *Biopolymers* **13**, 1 (1974).

86. Applications Manual: LSM510 - ConfoCor2, Fluorescence Correlation Spectroscopy. Carl Zeiss, Advanced Imaging Microscopy (2001)

87. Winter, R. and Noll, F. Methoden der biophysikalischen Chemie; B.G. Teubner, Stuttgart (1998)

88. Clegg, R. M. Fluorescence resonance energy transfer. *Curr. Opin. Biotechnol.* **6**, 103 (1995).

89. Moore, K. J. et. al. Single Molecule Detection Technologies in Miniaturized High Throughput Screening: Fluorescence Correlation Spectroscopy. *J. Biomol. Screen.* **4**, 335 (1999).

90. Jahnz, M. and Schwille, P. An ultrasensitive site-specific DNA recombination assay based on dual-color fluorescence cross-correlation spectroscopy. *Nucleic Acids Res.* **33**, e60 (2005).

91. Maertens, G., Vercammen, J., Debyser, Z., & Engelborghs, Y. Measuring protein-protein interactions inside living cells using single color fluorescence correlation spectroscopy. Application to human immunodeficiency virus type 1 integrase and LEDGF/p75. *FASEB J.* **19**, 1039 (2005).

92. Kim, S. A., Heinze, K.G., Waxham, M.N., & Schwille, P. Intracellular calmodulin availability accessed with two-photon cross-correlation. *Proc. Natl. Acad. Sci. U. S. A.* **101**, 105 (2004).

93. Meissner, O. and Haberlein, H. Lateral mobility and specific binding to GABA(A) receptors on hippocampal neurons monitored by fluorescence correlation spectroscopy. *Biochemistry* **42**, 1667 (2003).

94. Pramanik, A., Olsson, M., Langel, U., Bartfai, T., & Rigler, R. Fluorescence correlation spectroscopy detects galanin receptor diversity on insulinoma cells. *Biochemistry* **40**, 10839 (2001).

95. Saito, K., Ito, E., Takakuwa, Y., Tamura, M., & Kinjo, M. In situ observation of mobility and anchoring of PKCbetaI in plasma membrane. *FEBS Lett.* **541**, 126 (2003).

96. Pick, H. et. al. Monitoring expression and clustering of the ionotropic 5HT3 receptor in plasma membranes of live biological cells. *Biochemistry* **42**, 877 (2003).

97. Chen, Y., Wei, L.N., & Muller, J.D. Unraveling protein-protein interactions in living cells with fluorescence fluctuation brightness analysis. *Biophys. J.* **88**, 4366 (2005).

98. Kogure, T. et. al. A fluorescent variant of a protein from the stony coral Montipora facilitates dual-color single-laser fluorescence cross-correlation spectroscopy. *Nat. Biotech.* **24**, 577 (2006).

99. Thews, E. et. al. Cross Talk Free Fluorescence Cross-Correlation Spectroscopy in Live Cells. *Biophys. J.* **89**, 2069 (2005).

100. Bacia, K., Majoul, I.V., & Schwille, P. Probing the endocytic pathway in live cells using dual-color fluorescence cross-correlation analysis. *Biophys. J.* **83**, 1184 (2002).

101. Remy, I. and Michnick, S.W. Clonal selection and in vivo quantitation of protein interactions with protein-fragment complementation assays. *Proc. Natl. Acad. Sci U. S. A.* **96**, 5394 (1999).

102. Hu, C. D. and Kerppola, T.K. Simultaneous visualization of multiple protein interactions in living cells using multicolor fluorescence complementation analysis. *Nat. Biotechnol.* **21**, 539 (2003).

103. Mahajan, N. P. et. al. Bcl-2 and Bax interactions in mitochondria probed with green fluorescent protein and fluorescence resonance energy transfer. *Nat. Biotechnol.* **16**, 547 (1998).

104. Heding, A. Use of the BRET 7TM receptor/ -arrestin assay in drug discovery and screening. *Expert Rev. Mol. Diagn.* **4**, 403 (2004).

105. Ramsay, G. DNA chips: state-of-the art. *Nat. Biotechnol.* **16**, 40 (1998).

106. Schena, M. et. al. Microarrays: biotechnology's discovery platform for functional genomics. *Trends Biotechnol.* **16**, 301 (1998).

107. Cheung, V. G. et. al. Making and reading microarrays. *Nat. Genet.* **21**, 15 (1999).

108. Bertone, P. and Snyder, M. Advances in functional protein microarray technology. *FEBS J.* **272**, 5400 (2005).

109. Hultschig, C. et. al. Recent advances of protein microarrays. *Curr. Opin. Chem. Biol.* **10**, 4 (2006).

110. Zhu, H. et. al. Global analysis of protein activities using proteome chips. *Science* **293**, 2101 (2001).

111. Silzel, J. W., Cercek, B., Dodson, C., Tsay, T., & Obremski, R.J. Mass-sensing, multianalyte microarray immunoassay with imaging detection. *Clin. Chem.* **44**, 2036 (1998).

112. Ekins, R. P. Ligand assays: from electrophoresis to miniaturized microarrays. *Clin. Chem.* **44**, 2015 (1998).

113. Kusnezow, W. et. al. Kinetics of antigen binding to antibody microspots: Strong limitation by mass transport to the surface. *Proteomics* **6**, 794 (2005).

114. Pellois, J. P. et. al. Individually addressable parallel peptide synthesis on microchips. *Nat. Biotechnol.* **20**, 922 (2002).

115. Frank, R. The SPOT-synthesis technique. Synthetic peptide arrays on membrane supports--principles and applications. *J. Immunol. Methods* **267**, 13 (2002).

116. He, M. and Taussig, M.J. DiscernArray(TM) technology: a cell-free method for the generation of protein arrays from PCR DNA. *J. Immunol. Methods* **274**, 265 (2003).

117. Ramachandran, N. et. al. Self-Assembling Protein Microarrays. *Science* **305**, 86 (2004).

118. Miller, J. C. et. al. Antibody microarray profiling of human prostate cancer sera: antibody screening and identification of potential biomarkers. *Proteomics* **3**, 56 (2003).

119. Saviranta, P. et. al. Evaluating Sandwich Immunoassays in Microarray Format in Terms of the Ambient Analyte Regime. *Clin. Chem.* **50**, 1907 (2004).

120. Cho, R. J. et. al. Transcriptional regulation and function during the human cell cycle. *Nat. Genet.* **27**, 48 (2001).

121. Anderson, K., Potter, A., Baban, D., & Davies, K.E. Protein expression changes in spinal muscular atrophy revealed with a novel antibody array technology. *Brain* **126**, 2052 (2003).

122. Wingren, C. and Borrebaeck, C.A. High-throughput proteomics using antibody microarrays. *Expert Rev. Proteomics.* **1**, 355 (2004).

123. Huang, R. P. Cytokine protein arrays. *Methods Mol. Biol.* **264**, 215 (2004).

124. Qin, S. et. al. Development of a reverse capture autoantibody microarray for studies of antigen-autoantibody profiling. *Proteomics* **6**, 3199 (2006).

125. Lueking, A. et. al. Profiling of Alopecia Areata Autoantigens Based on Protein Microarray Technology. *Mol. Cell. Proteomics* **4**, 1382 (2005).

126. Robinson, W. H. et. al. Autoantigen microarrays for multiplex characterization of autoantibody responses. *Nat. Med.* **8**, 295 (2002).

127. Nielsen, U. B., Cardone, M.H., Sinskey, A.J., MacBeath, G., & Sorger, P.K. Profiling receptor tyrosine kinase activation by using Ab microarrays. *Proc. Natl. Acad. Sci U. S. A.* **100**, 9330 (2003).

128. Gaide, O. et. al. CARMA1 is a critical lipid raft-associated regulator of TCR-induced NF-kappa B activation. *Nat. Immunol.* **3**, 836 (2002).

129. Goda, S., Quale, A.C., Woods, M.L., Felthauser, A., & Shimizu, Y. Control of TCR-mediated activation of beta 1 integrins by the ZAP-70 tyrosine kinase interdomain B region and the linker for activation of T Cells adapter protein. *J. Immunol.* **172**, 5379 (2004).

130. Nicoll, G. et. al. Identification and characterization of a novel siglec, siglec-7, expressed by human natural killer cells and monocytes. *J. Biol. Chem.* **274**, 34089 (1999).

131. Paz, P. E. et. al. Mapping the Zap-70 phosphorylation sites on LAT (linker for activation of T cells) required for recruitment and activation of signalling proteins in T cells. *Biochem. J.* **356**, 461 (2001).

132. Lin, J. and Weiss, A. Identification of the minimal tyrosine residues required for linker for activation of T cell function. *J. Biol. Chem.* **276**, 29588 (2001).

133. Harkiolaki, M. et. al. Structural basis for SH3 domain-mediated high-affinity binding between Mona/Gads and SLP-76. *EMBO J.* **22**, 2571 (2003).

134. Zettl, M. and Way, M. The WH1 and EVH1 Domains of WASP and Ena/VASP Family Members Bind Distinct Sequence Motifs. *Curr. Biol.* **12**, 1617 (2002).

135. Itoh, K. et. al. Cutting edge: negative regulation of immune synapse formation by anchoring lipid raft to cytoskeleton through Cbp-EBP50-ERM assembly. *J. Immunol.* **168**, 541 (2002).

136. Bokoch, G. M. et. al. Interaction of the Nck adapter protein with p21-activated kinase (PAK1). *J. Biol. Chem.* **271**, 25746 (1996).

137. Cai, Y. C. et. al. Selective CD28pYMNM mutations implicate phosphatidylinositol 3-kinase in CD86-CD28-mediated costimulation. *Immunity* **3**, 417 (1995).

138. Marengere, L. E. et. al. Proto-oncoprotein Vav interacts with c-Cbl in activated thymocytes and peripheral T cells. *J. Immunol.* **159**, 70 (1997).

139. Irvin, B. J., Williams, B.L., Nilson, A.E., Maynor, H.O., & Abraham, R.T. Pleiotropic contributions of phospholipase C-gamma1 (PLC-gamma1) to T-cell antigen receptor-mediated signaling: reconstitution studies of a PLC-gamma1-deficient Jurkat T-cell line. *Mol. Cell. Biol.* **20**, 9149 (2000).

140. Straus, D. B. and Weiss, A. Genetic evidence for the involvement of the lck tyrosine kinase in signal transduction through the T cell antigen receptor. *Cell* **70**, 585 (1992).

141. Köhler, K. et. al. Chemical genetics when timing is critical: A pharmacological concept for the maturation of T cell contacts. *ChemBioChem* **6**, 152 (2005).

142. Secrist, J. P., Burns, L.A., Karnitz, L., Koretzky, G.A., & Abraham, R.T. Stimulatory effects of the protein tyrosine phosphatase inhibitor, pervanadate, on T-cell activation events. *J. Biol. Chem.* **268**, 5886 (1993).

143. Laemmli, U. K. Cleavage of structural proteins during the assembly of the head of bacteriophage T4. *Nature* **227**, 680 (1970).

144. Stoevesandt, O. and Brock, R. One-step analysis of protein complexes in microliters of cell lysate using indirect immunolabeling & fluorescence cross-correlation spectroscopy. *Nat. Protocols,* in press (2006).

145. Stoevesandt, O., Köhler, K., Fischer, R., Johnston, I.C., & Brock, R. One-step analysis of protein complexes in microliters of cell lysate. *Nat. Methods* **2**, 833 (2005).

146. Hummel, W. Entwicklung von Peptid-Mikroarrays zur parallelen Analyse der aktivierungsabhängigen Änderung molekularer Wechselwirkungen in der T-Zell-Signaltransduktion. Diplomarbeit, Fakultät für Biologie, Universität Tübingen (2005)

147. Wolf, S. Analyse molekularer Wechselwirkungen in der T-Zell-Signaltransduktion mit synthetischen Peptiden. Diplomarbeit, Fakultät für Biologie, Universität Tübingen (2005)

148. Elbs, M. and Brock, R. Determination of binding constants on microarrays with confocal fluorescence detection. *Anal. Chem.* **75**, 4793 (2003).

149. Stoevesandt, O. et. al. Peptide Microarrays for the Detection of Molecular Interactions in Cellular Signal Transduction. *Proteomics* **5**, 2010 (2005).

150. Espejo, A., Cote, J., Bednarek, A., Richard, S., & Bedford, M.T. A protein-domain microarray identifies novel protein-protein interactions. *Biochem. J.* **367**, 697 (2002).

151. Chan, A. C., Iwashima, M., Turck, C.W., & Weiss, A. ZAP-70: a 70 kd protein-tyrosine kinase that associates with the TCR zeta chain. *Cell* **71**, 649 (1992).

152. Sloan-Lancaster, J. et. al. Regulation of ZAP-70 intracellular localization: visualization with the green fluorescent protein. *J. Exp. Med.* **186**, 1713 (1997).

153. Thompson, N. L. Fluorescence Correlation Spectroscopy. In: Topics in Fluorescence Spectroscopy; Plenum Press, New York (2002)

154. Schramm, W. and Paek, S.H. Modeling of immunosensors under nonequilibrium conditions. II. Experimental determination of performance characteristics. *Anal. Biochem.* **196**, 326 (1991).

155. Freeburn, R. W. et. al. Evidence That SHIP-1 Contributes to Phosphatidylinositol 3,4,5-Trisphosphate Metabolism in T Lymphocytes

and Can Regulate Novel Phosphoinositide 3-Kinase Effectors. *J. Immunol.* **169**, 5441 (2002).

156. Weidemann, T. et. al. Counting Nucleosomes in Living Cells with a Combination of Fluorescence Correlation Spectroscopy and Confocal Imaging. *J. Mol. Biol.* **334**, 229 (2003).

157. Scheffler, S., Sauer, M., & Neuweiler, H. Monitoring Antibody Binding Events in Homogeneous Solution by Single-Molecule Fluorescence Spectroscopy. *Z. Phys. Chem.* **219**, 665 (2005).

158. Tetin, S. Y., Swift, K.M., & Matayoshi, E.D. Measuring antibody affinity and performing immunoassay at the single molecule level. *Anal. Biochem.* **307**, 84 (2002).

159. Vamosi, G. et. al. IL-2 and IL-15 receptor {alpha}-subunits are coexpressed in a supramolecular receptor cluster in lipid rafts of T cells. *Proc. Natl. Acad. Sci U. S. A.* **101**, 11082 (2004).

160. Schaertl, S., Meyer-Almes, F.J., Lopez-Calle, E., Siemers, A., & Kramer, J. A Novel and Robust Homogeneous Fluorescence-Based Assay Using Nanoparticles for Pharmaceutical Screening and Diagnostics. *J. Biomol. Screen.* **5**, 227 (2000).

161. Kobayashi, T., Okamoto, N., Sawasaki, T., & Endo, Y. Detection of protein-DNA interactions in crude cellular extracts by fluorescence correlation spectroscopy. *Anal. Biochem.* **332**, 58 (2004).

162. Sasahara, Y. et. al. Mechanism of Recruitment of WASP to the Immunological Synapse and of Its Activation Following TCR Ligation. *Mol. Cell* **10**, 1269 (2002).

163. Schoeberl, B., Eichler-Jonsson, C., Gilles, E.D., & Muller, G. Computational modeling of the dynamics of the MAP kinase cascade activated by surface and internalized EGF receptors. *Nat. Biotechnol.* **20**, 370 (2002).

164. Brajenovic, M., Joberty, G., Kuster, B., Bouwmeester, T., & Drewes, G. Comprehensive Proteomic Analysis of Human Par Protein Complexes Reveals an Interconnected Protein Network. *J. Biol. Chem.* **279**, 12804 (2004).

165. Lemmens, I. et. al. Heteromeric MAPPIT: a novel strategy to study modification-dependent protein-protein interactions in mammalian cells. *Nucl. Acids Res.* **31**, e75 (2003)

9 Publications

Original publications

Stoevesandt O., Elbs M., Köhler K., Lellouch A. C., Fischer R., André T., Brock R., Peptide microarrays for the detection of molecular interactions in cellular signal transduction. *Proteomics* **5**, 2010 (2005)

Köhler K., Lellouch A.C., Vollmer S., **Stoevesandt O.,** Hoff A, Peters L., Rogl H., Malissen B., Brock R. Chemical inhibitors when timing is critical: a pharmacological concept for the maturation of T cell contacts. *Chembiochem* **6**, 152 (2005)

Stoevesandt O., Fischer R., Köhler K., Johnston I.C.D., Brock R., One-step analysis of protein complexes in microliters of cell lysate. *Nat. Methods* **2**, 833 (2005)

Stoevesandt O., Brock R., One-step analysis of protein complexes in microliters of cell lysate using indirect immunolabeling & fluorescence cross-correlation spectroscopy. *Nat. Protocols*, in press

Manuscripts in preparation

Stoevesandt O., Köhler K., Wolf S., André T., Hummel W., Brock R., Peptide microarrays for the dissection of protein interaction networks.

Fischer R., Hufnagel H.-J., Bächle D., **Stoevesandt O**., Jung G., Brock R., A doubly labeled penetratin analogue as a ratiometric sensor for intracellular proteolytic stability.

Meine akademischen Lehrer in Tübingen und Amherst waren:

K. Albert, E. O. Bayer, H. Bisswanger, K. W. Bock, P. Bohley, R. Brock, K. Eisele, M. Fitzgerald-Hayes, K. Fröhlich, G. Gauglitz, F. Götz, G. Häfelinger, H.-P. Hagenmaier, B. Hamprecht, M. Hanack, S. Helms, W. Hoch, G. Jung, I. Kaltashov, L. M. Gierasch, W. Göpel, H. Günzl, G. Klein, E. Lindner, L. Margulis, C. Martin, E. Martz, D. Mecke, W. Nakel, H. Oberhammer, W. Pfeiffer, H. Pommer, K. Poralla, H. Probst, H.-G. Rammensee, K. Reutter, R. Rosenstein, K. Rotondi, M. Schwarz, S. Stoeva, J. Strähle, J. F. Swain, W. Voelter, J. Voigt, K. Wegmann, U. Weser, K.-H. Wiesmüller, W. Wohlleben, C. Ziegler, R. Zimmermann.

Curriculum Vitae

Oda Milena Sibylle Stoevesandt
* 9. September 1976, Hannover

1983 - 1987	Kerschensteiner-Grundschule, Schweinfurt
1987 - 1996	Alexander-von-Humboldt-Gymnasium, Schweinfurt
Juni 1996	Abitur (1,0)

Okt. 1996 – Juli 2002	Studium der Biochemie, Eberhard-Karls-Universität Tübingen, Stipendium für besonders Begabte nach dem Bayerischen Begabtenförderungsgesetz
Feb. 1999	Vordiplom („sehr gut")
Aug. 1999 – Aug. 2000	Auslandsstudium, University of Massachusetts at Amherst (USA)
Aug. 2000 – Mai 2001	Praktikum und anschließend Tätigkeit als wissenschaftliche Hilfskraft am Max-Planck-Institut für Entwicklungsbiologie Tübingen in der Arbeitsgruppe von PD Dr. Werner Hoch
Nov. 2001 – Juli 2002	Diplomarbeit am Zentrum für Medizinische Forschung der Universität Tübingen, betreut von Prof. Dr. H.-G. Rammensee, angeleitet von Prof. Dr. G. Klein: „E-Cadherin- und β-Catenin-vermittelte Prozesse in der humanen Erythropoese"
Juli 2002	Diplom in Biochemie („sehr gut")

Nov. 2002 – Aug. 2006	Wissenschaftliche Angestellte am Interfakultären Institut für Zellbiologie der Universität Tübingen; im Rahmen dieser Tätigkeit dort von
Nov. 2002 – Mai 2006	Doktorarbeit betreut von Prof. Dr. H.-G. Rammensee, angeleitet von PD Dr. R. Brock: „Parallele und miniaturisierte Analyse von Protein-Protein-Interaktionen in der T-Zell-Signaltransduktion mittels Fluoreszenz-Kreuz-korrelations-Spektroskopie und Peptidmikroarrays"

seit Aug. 2006	Wissenschaftliche Angestellte am Babraham Institute (Cambridge, GB), Betreuung des EU FP6 Projektes „ProteomeBinders"